

852
LA-10297-PR
Progress Report

logged in 7/23/85
KS

Los Alamos National Laboratory is operated by the University of California for the United States Department of Energy under contract W-7405-ENG-36

*Research and Development Related to
the Nevada Nuclear Waste Storage
Investigation*

April 1—June 30, 1985

Los Alamos Los Alamos National Lab
Los Alamos, New Mexico

HYDROLOGY DOCUMENT NUMBER 235

The four most recent reports in this series, unclassified, are LA-9846-PR, LA-10006-PR, LA-10032-PR, and LA-10154-PR.

This report was prepared by the Los Alamos National Laboratory as part of the Nevada Nuclear Waste Storage Investigations managed by the Nevada Operations Office of the US Department of Energy. Based upon their applicability to the investigations, some results from the Radionuclide Migration Project, managed by the Nevada Operations Office of the US Department of Energy, are included in this report.

Prepared by Lia Mitchell, Group INC-7

DISCLAIMER

This report was prepared as an account of work sponsored by an agency of the United States Government. Neither the United States Government nor any agency thereof, nor any of their employees, makes any warranty, express or implied, or assumes any legal liability or responsibility for the accuracy, completeness, or usefulness of any information, apparatus, product, or process disclosed, or represents that its use would not infringe privately owned rights. Reference herein to any specific commercial product, process, or service by trade name, trademark, manufacturer, or otherwise, does not necessarily constitute or imply its endorsement, recommendation, or favoring by the United States Government or any agency thereof. The views and opinions of authors expressed herein do not necessarily state or reflect those of the United States Government or any agency thereof.

Research and Development Related to the Nevada Nuclear Waste Storage Investigations

April 1—June 30, 1984

Compiled by

R. S. Rundberg, A. E. Ogard, and D. T. Vaniman

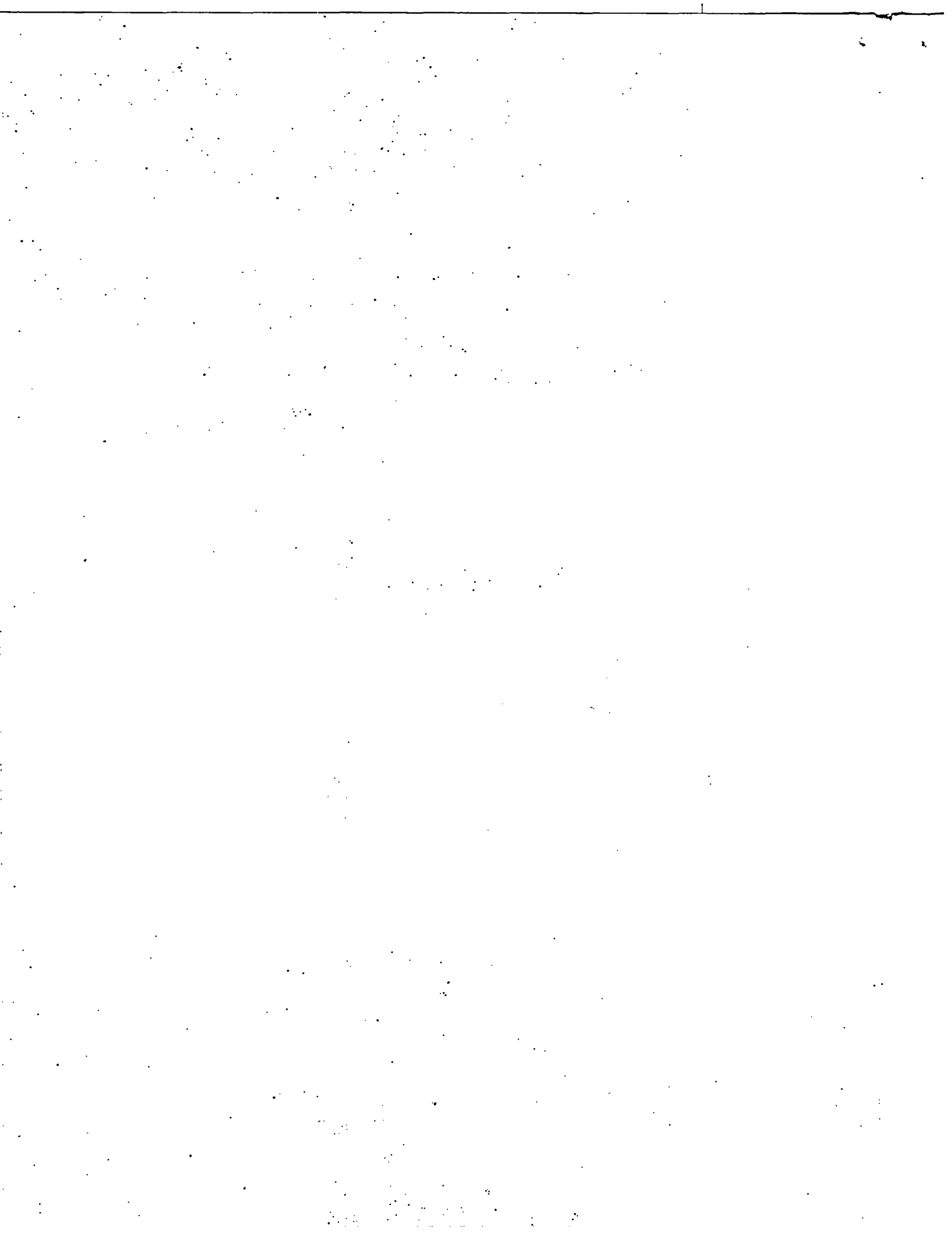
Contributors

B. P. Bayhurst	S. S. Levy
D. L. Bish	A. J. Mitchell
J. D. Blacic	E. J. Mroz
N. W. Bower	T. W. Newton
L. F. Brown	H. Nitsche*
D. E. Broxton	A. E. Norris
F. M. Byers, Jr.	E. Nuttall**
F. Caporuscio	A. E. Ogard
B. A. Carlos	P. Q. Oliver
M. R. Cisneros	P. D. Palmer
B. M. Crowe	D. M. Roy†
D. B. Curtis	R. S. Rundberg
W. R. Daniels	V. L. Rundberg
C. J. Duffy	K. W. Thomas
N. Edelstein*	J. L. Thompson
L. S. Hersman	B. J. Travis
D. E. Hobart	D. T. Vaniman
S. W. Hodson	R. J. Vidale
J. F. Kerrisk	P. L. Wanek
S. D. Knight	K. Wolfsberg
F. O. Lawrence	

*Materials and Molecular Research Division, Lawrence Berkeley Laboratory, Berkeley, CA 94720.

**Chemical-Nuclear Engineering Department, University of New Mexico, Albuquerque, NM 87131.

†Materials Research Laboratory, Pennsylvania State University, University Park, PA 16802.



CONTENTS

ABSTRACT	1
EXECUTIVE SUMMARY	2
I. INTRODUCTION	9
II. GEOCHEMISTRY	9
A. Groundwater Chemistry	9
1. Redox State of Water from Well UE-25b#1 Pumping Test	9
2. Biodegradation of Drilling Fluids	17
B. Natural Isotope Chemistry	19
C. Hydrothermal Geochemistry	24
1. Thermodynamics of Zeolites	24
2. Natural Analogues	28
D. Solubility Determinations	37
1. Waste-Element Solubilities	37
2. Zeolite Formation from Water with High Calcium and Magnesium Content	42
3. Effect of Aqueous Complexes on Sorption Behavior	43
4. Actinide Chemistry in Near-Neutral Solutions	46
5. Determination of Solubilities and Complexation of Waste Radionuclides Pertinent to Geologic Disposal at the Nevada Test Site	48
E. Sorption and Precipitation	54
1. Batch Sorption Experiments of Uranium, Tin, and Thorium	54
2. Long-Term Sorption Experiments on Technetium and Neptunium	54
3. Neptunium Sorption Isotherm Measurements	56
4. Effect of Groundwater Composition on the Sorptive Properties of Tuff	60
F. Dynamic Transport Processes	65
A Kinetic Effect in Actinide Sorption	65

G.	Retardation Sensitivity Analysis	70
1.	Field Studies	70
2.	Analysis of Laboratory Measurements of Colloids	71
3.	Comparison of TRACR3D with Analytical Solutions	72
H.	Applied Diffusion	75
III.	MINERALOGY-PETROLOGY OF TUFF	76
A.	Petrographic Stratigraphy of the Topopah Spring Member	76
B.	Studies of Natural Alteration at Yucca Mountain . .	81
C.	Sulfur Analyses within the Topopah Spring Member . .	82
D.	Mineralogy/Petrology along Transport Pathways away from the Host Rock	82
E.	Reports	85
IV.	TECTONICS AND VOLCANISM	85
V.	TUFF LABORATORY PROPERTIES	86
VI.	SEALING MATERIALS EVALUATION	90
A.	Objectives	90
B.	Elevated-Temperature Reaction Experiments	91
C.	Intermediate-Temperature Reaction Experiments . . .	93
D.	Discussion	93
	REFERENCES	96

RESEARCH AND DEVELOPMENT RELATED TO THE NEVADA NUCLEAR
WASTE STORAGE INVESTIGATIONS

April 1--June 30, 1984

Compiled by

R. S. Rundberg, A. E. Ogard, and D. T. Vaniman

Contributors

B. P. Bayhurst	S. S. Levy
D. L. Bish	A. J. Mitchell
J. D. Blacic	E. J. Mroz
N. W. Bower	T. W. Newton
L. F. Brown	H. Nitsche
D. E. Broxton	A. E. Norris
F. M. Byers, Jr.	E. Nuttall
F. Caporuscio	A. E. Ogard
B. A. Carlos	P. Q. Oliver
M. R. Cisneros	P. D. Palmer
B. M. Crowe	D. M. Roy
D. B. Curtis	R. S. Rundberg
W. R. Daniels	V. L. Rundberg
C. J. Duffy	K. W. Thomas
N. Edelstein	J. L. Thompson
L. S. Hersman	B. J. Travis
D. E. Hobart	D. T. Vaniman
S. W. Hodson	R. J. Vidale
J. F. Kerrisk	P. L. Wanek
S. D. Knight	K. Wolfsberg
F. O. Lawrence	

ABSTRACT

This report summarizes the contribution of the Los Alamos National Laboratory to the Nevada Nuclear Waste Storage Investigations for the third quarter of FY 1984.

EXECUTIVE SUMMARY

This report summarizes some of the technical contributions from the Los Alamos National Laboratory to the Nevada Nuclear Waste Storage Investigations (NNWSI) project managed by the Nevada Operations Office of the US Department of Energy (DOE) during the period April 1 through June 30, 1984. The report is not a detailed technical document but does indicate the status of the investigations being performed at Los Alamos.

GEOCHEMISTRY

The objective of this work is to determine the geochemical properties of Yucca Mountain tuff and groundwater. These properties will be used as a basis for predicting the migration of radionuclides to the accessible environment and for assessing the geochemical response of a potential repository site in Yucca Mountain in the southwest portion of the Nevada Test Site to the emplacement of a repository.

Groundwater Chemistry

The changes in oxidation-reduction potential (Eh) that were measured in the pumping test of Well UE-25b/#1 have been modeled using the Nernst equation for the oxidation-reduction couples that may be present in this groundwater. Couples that were considered were $\text{Fe}^{+2} - \text{Fe}^{+3}$, $\text{NO}_3^- - \text{NO}_2^-$, and $\text{Mn}^{+2} - \text{Mn}$ solid. The various measures of the oxidation-reduction potential gave conflicting quantitative information about the equilibrium conditions. Because the pumping system may be mixing waters from several zones even when packers are used, a single oxidation-reduction couple may not be indicative of the actual system. The measurement itself may be an overall "average" of the system.

Natural Isotope Chemistry

Soil samples from four locations on or adjacent to Yucca Mountain were analyzed for chloride concentrations to determine the suitability of the sites for measuring rainfall infiltration during the past 25 years by the ^{36}Cl tracer technique. Three of the four locations appeared to have chloride concentrations in which the expected depth profile for vertical infiltration has been modified by flooding or, in the case of the Yucca Mountain crest

site, by moderate precipitation events. The site in Yucca Wash appears to have a characteristic chloride profile favorable for ^{36}Cl measurements. Another field trip to Yucca Mountain is planned to locate ^{36}Cl sampling sites closer to the Exploratory Shaft site than Yucca Wash.

Hydrothermal Geochemistry

A model has been developed for the free energy of the analcime solid solution. The model is an ideal one; that is, it assumes no excess enthalpy of mixing. The excess entropy of mixing is assumed to be due to the configurational entropy of end member mixing, of aluminum-silicon mixing on the T1 sites, and of sodium vacancy mixing on the sodium sites. This model has been found to be consistent with much of the data existing for analcime, but points out that few, if any of these data are unambiguous. Measurements which can be used to evaluate this model are generally uncertain because all of the important parameters were not measured. For this reason, this study is proving very important to the planning of experiments to develop thermodynamic models for other zeolites.

Natural Analogues

A repository for storage of radioactive waste in felsic tuff has been proposed at Yucca Mountain in the southwest corner of the Nevada Test Site. Because the waste will generate heat in the near-field environment, nine hot spring occurrences in felsic rock were examined to study the effect of heated groundwater on the physical and chemical properties of the rock. Both water chemistry and bulk rock mineralogy were determined. Changes were noted that may prove relevant to the near-field environment of a radioactive waste repository: (1) Some of the rocks that had been exposed to hot water appeared to be more porous and friable than their unexposed counterparts and (2) it appeared that acid systems had been formed by many but not all of the springs at some stage in their evolution.

Solubility Determinations

The solubilities of six waste elements (uranium, plutonium, americium, strontium, radium, and technetium) in waters from Wells J-13, UE-25p#1, and USW H-3 have been calculated with the EQ3 chemical equilibrium computer program and the current thermodynamic data base. Data recently received from

Lawrence Livermore National Laboratory for technetium were added to the data base for these calculations.

Recent observations of zeolite compositions from Wells UE-25b#1 and UE-25p#1 show that these zeolites do not exhibit the progression from calcium-rich to sodium-rich compositions with increasing depth that has been observed in other drill holes. Reaction path calculations done with EQ3/6 indicate that the zeolite compositions are consistent with the higher calcium content of water from these wells.

Transport calculations of the effect of aqueous complex formation on sorption by ion exchange have been done using the one-dimensional transport model CHEMTRN. The results indicate that with strontium, for which less than 15% of the aqueous strontium is complexed in waters from Yucca Mountain, the extent of complex formation would not have a significant effect on transport.

Work is continuing on determination of formation constants of Pu(IV) with carbonate and of the solubility product of hydrous plutonium oxide. Tentative conclusions of the Pu(IV)-carbonate work are that at least three different complexes of Pu(IV) with carbonate are present under the conditions of these experiments and that a mixed citrate-carbonate complex may exist.

An experimental examination of the stability of complexes of Am(III) with carbonate has been started. This effort will use the same technique employed with plutonium, the competition of carbonate and citrate ions for Am(III).

Sorption and Precipitation

Batch sorption studies with Well J-13 groundwater have continued this quarter for uranium, tin, technetium, neptunium, and thorium. The desorption ratios for uranium were lower than expected but may be explained by the experimental errors associated with small sorption measurements. The tin ratios were as expected. The technetium and neptunium studies are part of a long-term sorption experiment (15 months) studying the changes in R_d for these two elements with time. No changes have been observed over the nine months of the experiment. Thorium sorption ratios do not correlate with pH or mineralogy of the tuff samples studied and range from ~140 to 1230 ml/g. Neptunium isotherm measurements were completed using CO₂-controlled atmospheric conditions to maintain the pH near 7. There is little, if any, effect of neptunium concentration on the measured sorption ratio.

Because the groundwater composition may vary between the repository and the accessible environment, studies are in progress to determine what effect various compositions have on the measured sorption ratio. The groundwater currently being investigated is from Well UE-25p#1 from a depth of 1298 to 1792 m. This water has a much higher salt content than Well J-13 groundwater. Sorption ratios for tin were higher in the Well UE-25p#1 water than in Well J-13 water. It is suspected that precipitation of tin occurs in this higher ionic strength water. Future studies will include additional tuff samples, more radionuclides, and water from Well USW H-3.

Dynamic Transport Processes

An apparent kinetic effect, observed in the sorption experiments of plutonium and americium in which the actinide solution was flowing through columns of crushed tuff, was later confirmed in batch sorption experiments terminated at varying times. In column experiments, the kinetic effect is manifested by a significant fraction of the input activity passing through the column with the solvent front. In batch experiments, the kinetic effect results in very marked increases in the sorption ratio (activity on the rock versus activity in the water) as contact times are extended from hours to days to weeks. It is not clear whether the kinetic effect is due to speciation changes in the dissolved actinide, colloidal transport, time dependence of the sorption process itself, or some other phenomenon. It is important that the underlying cause of this kinetic effect be discovered if we are to predict the extent of actinide transport from an underground nuclear waste repository.

A program to numerically invert autocorrelated photon spectroscopy data was developed. The code, which uses regularization and a positivity constraint, will enable a detailed study of particle size distributions. This advance will greatly enhance the ability of NNWSI to address the question of colloid or particulate transport.

Two additional 2-m crushed-tuff columns have been prepared each containing Well USW G-2-339 tuff, a montmorillonite-containing tuff, for use in anion exclusion studies and actinide transport studies. These long columns will provide long residence times to access actinide adsorption kinetics in a dynamic system.

The fractured tuff columns are continuing to be eluted with cationic tracers, and the results are in the process of being interpreted with matrix diffusion models. New solid rock core columns are being prepared in an effort to find cores permeable enough to enable transport experiments in a reasonable time frame.

Retardation Sensitivity Analysis

Investigation of colloid transport is proceeding on several fronts.

- (1) Examination of field studies that involved radiocolloid migration. Two field studies of heavy element radionuclide migration carried out at Los Alamos have been identified and assessed for relevance to the NNWSI project.
- (2) Analysis of lab measurements of colloids. Personnel in INC Division are using a laser system to measure colloid size distributions. We are assisting in the analysis. Inverse mathematical techniques are being adapted to analyze the particle size distributions. The Fredholm integral equation of the first kind that represents the laser scattering process can be solved using the Tihonov regularization method.
- (3) Modeling of colloid transport. To verify the colloid transport model in TRACR3D, a simple, one-dimensional calculation has been made to compare with an analytic solution.

Applied Diffusion

Three analytical techniques were evaluated for measuring low concentrations of bromide ions in groundwater on a routine basis for use in the diffusion field experiment and for monitoring tagged water in the Exploratory Shaft mining operations. The three techniques were ion chromatography with an ultraviolet detector, ion chromatography with a potentiostatic detector, and neutron activation analysis. Ion chromatography with an ultraviolet detector appears to be the most suitable analysis technique for bromide concentrations as low as 50 $\mu\text{g}/\text{l}$, which are likely to be encountered if bromide is used as a tracer in measurements of diffusivity under field conditions.

Mineralogy-Petrology

Data on petrographic stratigraphy within the Topopah Spring Member reveal several features that may provide stratigraphic subdivisions within this otherwise very homogeneous rock unit. The importance of being able to determine stratigraphic position within the Topopah Spring Member arises because of the need to identify which level of the Topopah Spring is being worked during repository construction. A knowledge of variability within the Topopah is also important for extrapolation of experimental results from the exploratory shaft to other parts of the exploration block at Yucca Mountain.

Using the broader subdivisions of upper lithophysal, middle nonlithophysal, lower lithophysal, and lower nonlithophysal, researchers have found that petrographic criteria allow distinctions between the two lithophysal and between the nonlithophysal zones. These criteria include the abundance of xenoliths and quartz phenocrysts in the lower nonlithophysal zone and the greater abundance of silica-filled microvesicles in the upper lithophysal zone. Of greater importance for internal stratigraphy, it has been found that the abundance of cryptocrystalline groundmass texture is a measure of proximity to the base within either nonlithophysal zone.

Other petrologic studies during this quarter have indicated alteration temperatures of 91 to 95°C for the original formation of quartz, heulandite, and smectite above the basal vitrophyre of the Topopah Spring Member. The possibility of acid sulfate alteration within the Topopah was also investigated, and the low total sulfur contents (46 to 137 ppm) suggest that this possibility is remote. Studies of zeolite formations show that despite local and regional variability in exchangeable cation composition (calcium, sodium, and potassium), the silicon-to-aluminum ratios of Yucca Mountain clinoptilolites remain fairly uniform and, therefore, suggest relative uniformity of sorptive behavior.

Tectonics and Volcanism

Field work was completed of the geology and tectonic setting of sites of Quaternary volcanism in southern Death Valley. Major and trace element data are entered into a data base system on the VAX 11/780 for all basaltic rocks of the Nevada Test Site (NTS). A manuscript entitled "Volcanic Hazard Assessment for Disposal of High-Level Radioactive Waste" was accepted by the National Research Council for publication in a special symposium volume.

Tuff Laboratory Properties

Long-term creep deformation experiments have been completed on Calico Hills zeolitized tuff samples and have just been initiated on samples of welded devitrified tuff of the Topopah Spring Member. Analysis of the Calico Hills data shows that hydration/dehydration strains are large and strongly time-dependent. Compressive stresses (hydration) of 20 to 60 MPa are attainable, and tensile stresses (dehydration) can exceed the strength of any rock within the thermal field of a repository. Creep deformation of zeolitized samples is characterized by "steady state" strain rate, which offers hope that predictive models of mechanical strength can be formulated that will be valid over the long time extrapolations required for performance assessment.

Sealing Materials Evaluation

Cement samples which are high in silica have been tested. These compositions were selected to maximize formation of the silicate minerals tobermorite and gyrolite resulting in a less porous, less permeable material. Samples of this material have been subjected to elevated pressure, temperature conditions in the presence of water for extended periods of time. Reaction at 200°C showed extensive development of tobermorite with lesser gyrolite. Reactions at 150 and 90°C showed development of calcite and lesser tobermorite. The fluid compositions in these experiments have also been determined and will be used to make estimates of the probable dissolution rates of fault seals at Yucca Mountain.

I. INTRODUCTION

This report summarizes some of the technical contributions from the Los Alamos National Laboratory to the NNWSI project managed by the Nevada Operations Office of the US DOE during the period April 1 through June 30, 1984. The report is not a detailed technical document but does indicate the status of the investigations being performed at Los Alamos.

II. GEOCHEMISTRY

A. Groundwater Chemistry (A. E. Ogard, J. Kerrisk, and L. E. Hersman)

1. Redox State of Water from Well UE-25b#1 Pumping Test. The oxidation-reduction potential (Eh) is one of the more important properties of groundwater because of its effect on speciation and solubility. The lower the Eh of a solution the lower the oxidation state and solubilities of waste elements tend to be.

During the Well UE-25b#1 pumping test¹ five different kinds of measurements were made that relate to the redox state of the water: potentials of platinum electrode (Eh) and sulfide electrode (Es), dissolved oxygen content, total NO_3^- and NO_2^- content, total iron content, and total manganese content. All five measurements gave the same qualitative indication, that after the second day of the test the water became more oxidizing as pumping continued. However, the five different measurements gave different quantitative indications of the redox state of the water. The lack of equilibrium among various redox couples in natural waters is common.^{2,3} Although it may never be possible to characterize the redox state of Yucca Mountain water by a single value of Eh, this work is aimed at characterizing the redox state of those couples that may influence the redox state of dissolved radionuclides. The following paragraphs discuss the results from the five redox-related measurements made during the Well UE-25b#1 pumping test.¹

Platinum electrode and sulfide electrode potentials (Eh and Es) measured during the test were similar, starting at about -20 mV on day 2 and increasing monotonically to about 170 mV on day 28 (see Fig. 1). Under equilibrium conditions values of Eh in this range would indicate reducing conditions, possibly controlled by the $\text{Fe}^{3+}/\text{Fe}^{2+}$ redox couple, with no measurable dissolved oxygen.

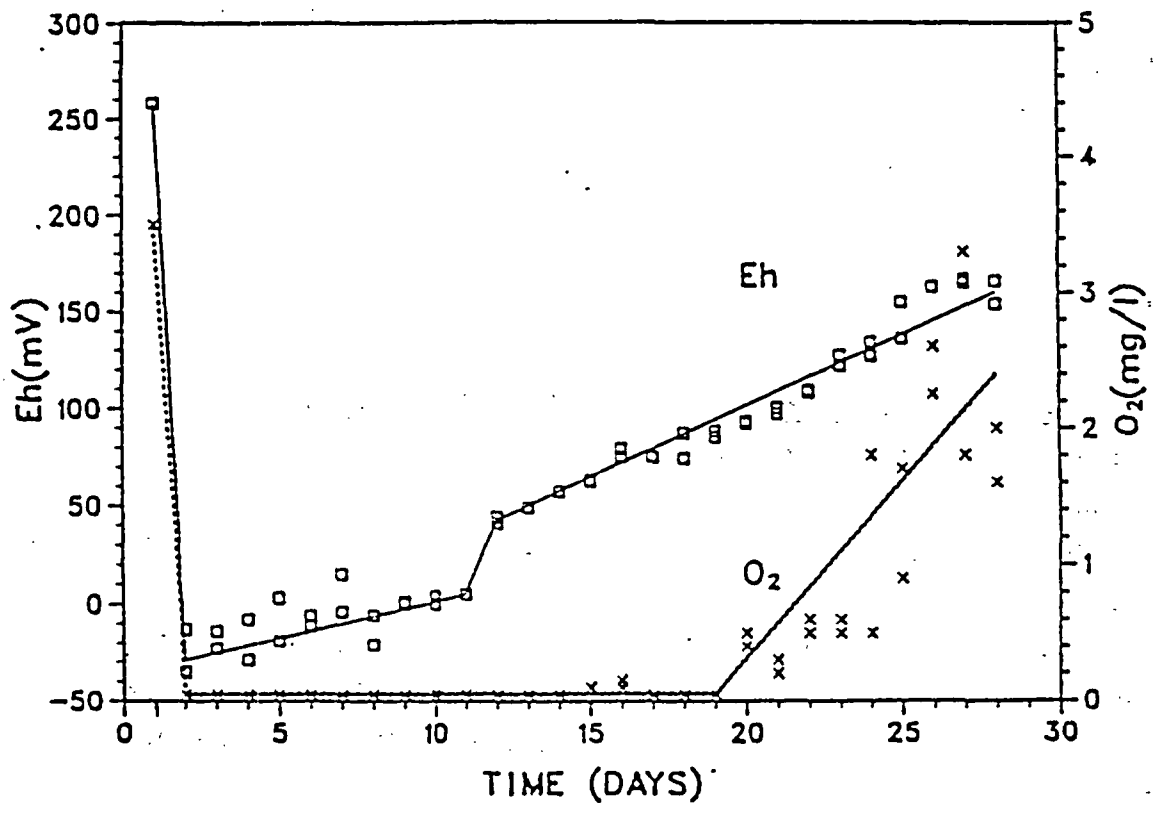


Fig. 1. The Eh and dissolved O₂ from Well UE-25b#1 pumping test (from LA-9577-PR).

Dissolved oxygen was below the detection limit (0.1 mg/l) from days 2 through 19 of the pumping test except for indications at the detection limit on days 15 and 16 (see Fig. 1). From days 20 through 28 the dissolved oxygen content increased from the detection limit to the range of 2 to 3 mg/l. Any level of dissolved oxygen above the detection limit would indicate an equilibrium Eh of ~700 mV. Values of Eh measured with a platinum electrode in natural waters with dissolved oxygen present are normally below the equilibrium level, being in the 300 to 500 mV range.⁴ This range of Eh (300 to 700 mV) is well above the values of Eh measured in Well UE-25b#1 water when dissolved oxygen was present (80 to 170 mV).

Measured values of total NO_3^- and NO_2^- allow a value of Eh associated with the $\text{NO}_3^-/\text{NO}_2^-$ redox couple to be calculated. Both NO_3^- and NO_2^- were detected from days 1 through 19 (see Fig. 2); the Eh associated with the measured concentrations was ~ 400 mV. From day 20 through the end of the pumping test the NO_2^- content was below the detection limit (0.1 mg/l); only NO_3^- was detected. An Eh can no longer be calculated from only one concentration; however, the presence of only NO_3^- indicates that the water became more oxidizing.

Only total iron content of the water was measured so an Eh associated with the $\text{Fe}^{3+}/\text{Fe}^{2+}$ couple cannot be calculated. However, at the pH of Well UE-25b#1 water essentially all dissolved iron would exist as Fe^{2+} or its complexes.⁴ The total iron content of the water decreased from ~ 1 mg/l at day 2 to less than 0.1 mg/l at day 28 (see Fig. 3). This decrease was most likely associated with oxidation of Fe^{2+} to Fe^{3+} and precipitation of some solid containing ferric iron. Because both the decreasing total iron content and the increasing Eh of the water during the pumping test were signs of oxidation, an attempt was made to relate the two variables. Figure 4 shows a plot of \log_{10} (total iron) as a function of Eh. Although there is considerable scatter, a straight line (the solid line) can be drawn through the data. Two other lines, describing the solubility of iron as controlled by amorphous $\text{Fe}(\text{OH})_3$ and siderite (FeCO_3) in this water are also shown; the EQ3 chemical equilibrium computer program was used to calculate these solubilities. Solubilities of other iron oxides such as goethite [$\text{FeO}(\text{OH})$] and magnetite (Fe_3O_4) are much lower. If Fe^{2+} is being oxidized to Fe^{3+} , which precipitates, an equation (unbalanced) of the form



can be written for the reaction. The Eh and Fe^{2+} concentration for this reaction are related as

$$\text{Eh} = E^\circ - \left(\frac{0.059}{n}\right)\log_{10}[\text{Fe}^{2+}] ,$$

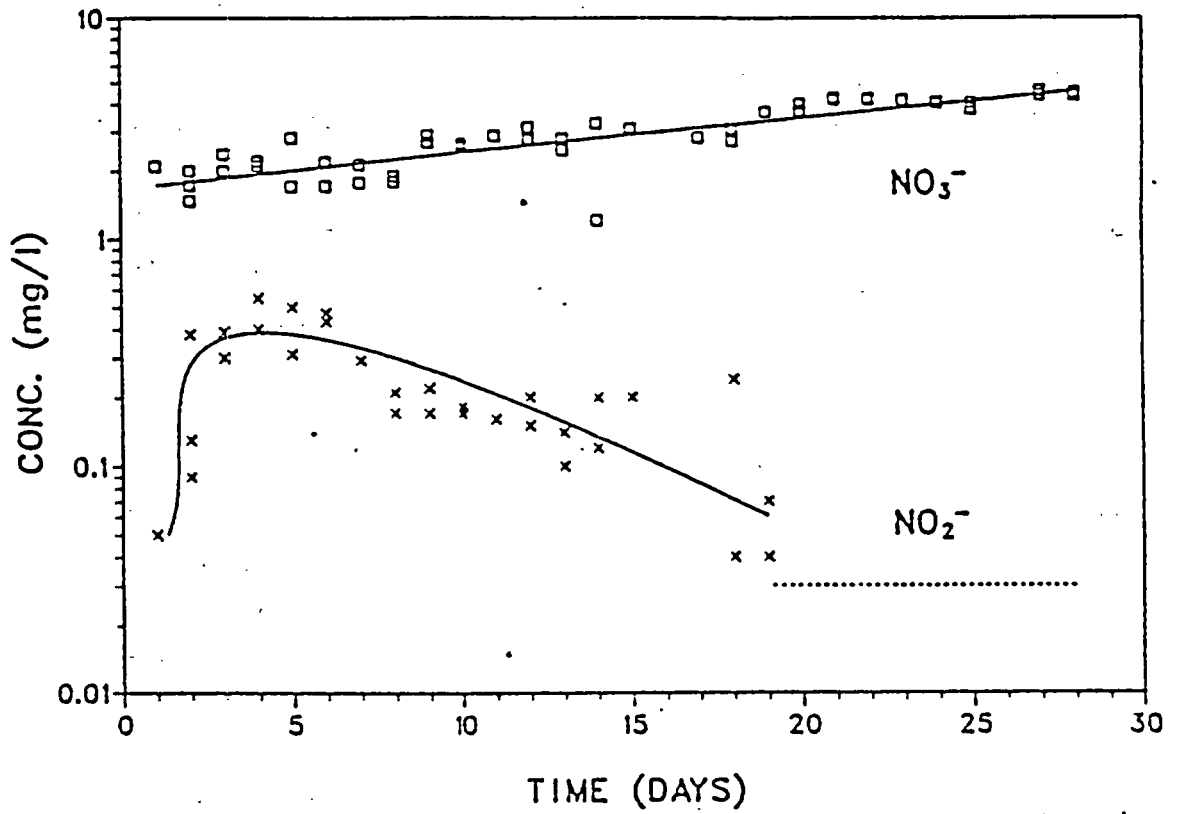


Fig. 2. Total NO_3^- and NO_2^- content of water from Well UE-25b#1 pumping test (from LA-9577-PR).

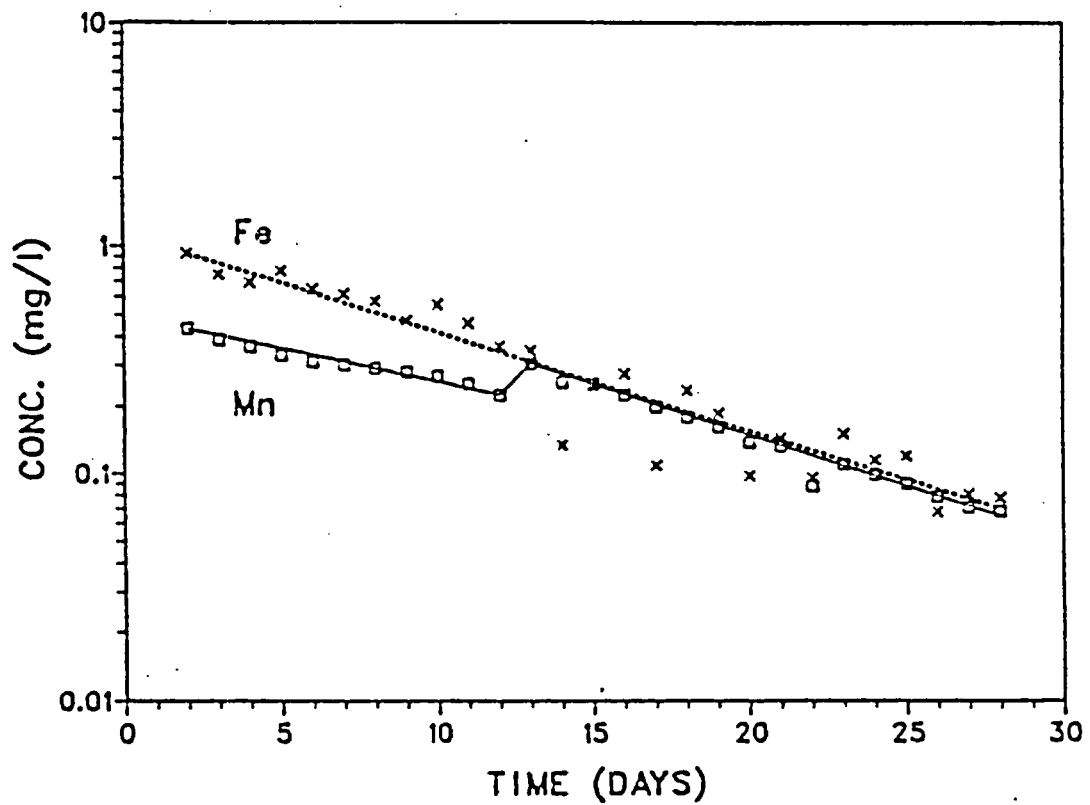


Fig. 3. Total iron and manganese contents of water from Well UE-25b#1 pumping test (from LA-9577-PR).

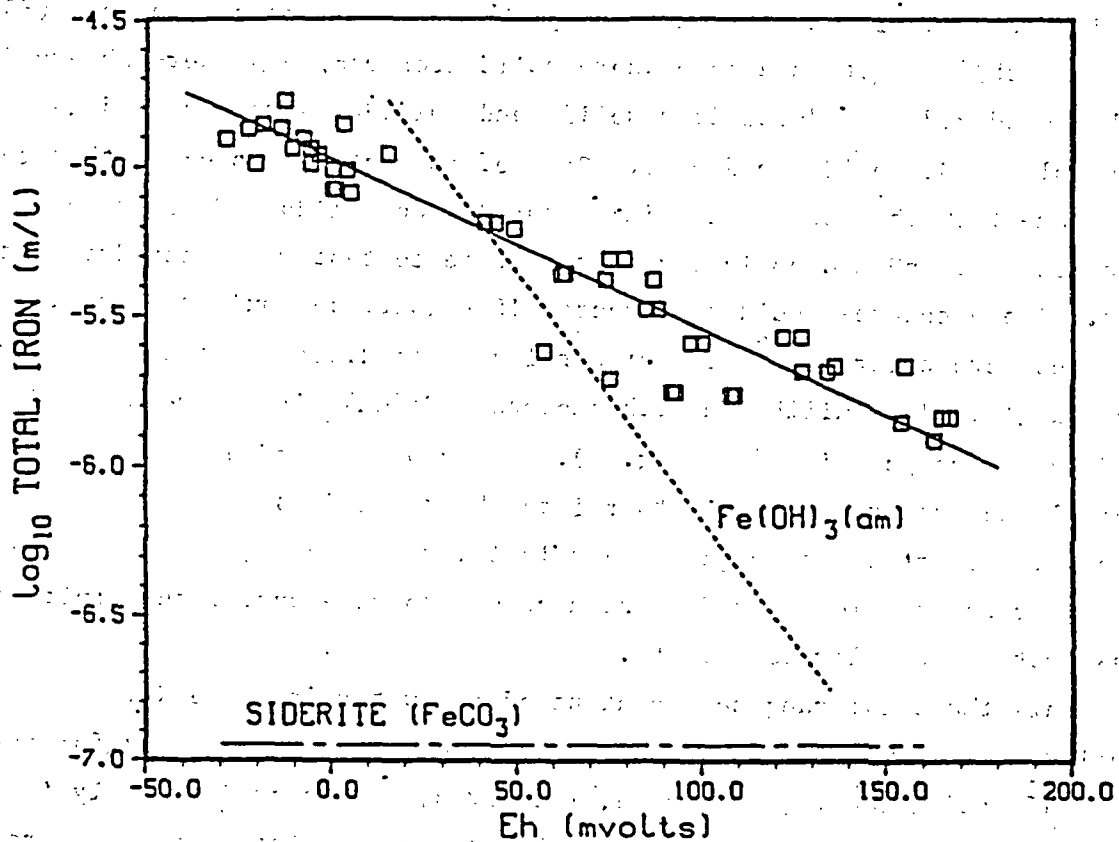
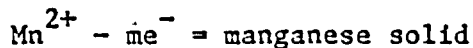


Fig. 4. Plot of total iron content as a function of Eh for water from Well UE-25b#1 pumping test.

where E' incorporates terms involving E° for the reaction, pH, and activity coefficients. If the Fe^{2+} concentration is assumed equal to the total dissolved iron content of the water, this equation defines a straight line between $\log_{10}(\text{total iron})$ and Eh, as shown in Fig. 4. From the slope of the solid line in Fig. 4, the value of n can be calculated as $1/3$. Unfortunately, a value of $1/3$ for n does not correspond to a known iron oxide. If the solid oxide were $\text{Fe}(\text{OH})_3$ or hematite (Fe_2O_3), n would be 1; if the oxide were magnetite (Fe_3O_4), n would be $2/3$. Thus, there does not appear to be an equilibrium relation between the iron content of the water and the measured Eh.

The source of dissolved ferrous iron in the water from the Well UE-25b#1 pumping test is also uncertain. The packed-off section of the hole (853 to 914 m depth)¹ is within a zone where solid iron compounds were observed to be highly oxidized.⁵ Reduced iron solids and sulfides were observed deeper in this hole (1036 to 1219 m depth). Some of the water sampled in this test may have come from the zone containing reduced iron solids. However, essentially no decrease in pH and no increase in sulfate content were seen during the test. These changes would be expected if significant oxidation of iron sulfides were occurring.² The higher levels of dissolved total iron are approximately in equilibrium with amorphous $\text{Fe}(\text{OH})_3$ if the measured Eh is used in the calculation (see Fig. 4). An Eh of -100 mV or less would have to control the iron redox couple to relate the total dissolved iron content to iron oxide (hemetite or magnetite) solubility. However, in this range of Eh, sulfide concentrations would be high enough to make pyrite the limiting solid phase with a very low solubility.

Only the total manganese content of the water from the Well UE-25b#1 pumping test was measured. Although an Eh cannot be calculated for the $\text{Mn}^{4+}/\text{Mn}^{2+}$ redox couple, manganese, like iron, exists predominantly in the reduced state in solution.⁴ The total manganese content decreased from ~0.4 mg/l on day 2 to less than 0.1 mg/l on day 28 (see Fig. 3). There was a perturbation between days 12 and 13 that seemed to divide the data into two sections. It came at about the same time as a sharp increase in Eh (see Fig. 1). An attempt was also made to relate the decreasing total manganese content of the water with the increasing Eh. Figure 5 shows a plot of \log_{10} (total manganese) as a function of Eh. The solid lines through the two groups of data have the same slope. If Mn^{2+} is being oxidized and precipitates, an equation (unbalanced) of the form



can be written, and the Eh of this reaction can be related to the Mn^{2+} concentration as

$$\text{Eh} = E'' - \left(\frac{0.059}{m}\right) \log_{10} [\text{Mn}^{2+}]$$

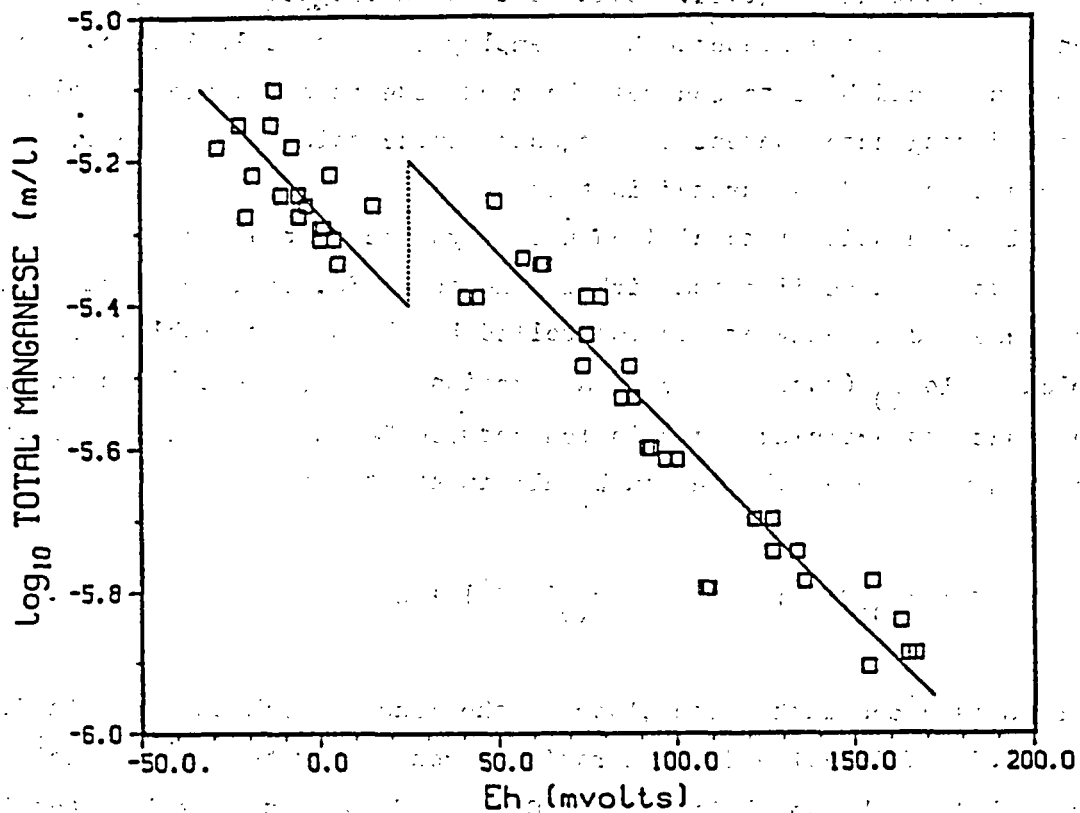


Fig. 5. Plot of total manganese content as a function of Eh for water from Well UE-25b#1 pumping test.

The variable E'' incorporates E° for the reaction, pH, and activity coefficients. If the Mn^{2+} concentration is assumed equal to the total dissolved manganese content, the slope of the solid lines in Fig. 5 can be used to determine m . A value of about 1/3 is obtained for m in this manner. As with iron, this does not correspond to a reaction forming any known manganese oxide. For example, if the solid oxide were hausmannite (Mn_3O_4), m would be 2/3; if the solid were pyrolusite (MnO_2), m would be 2. Thus, the total manganese content of the water does not appear to be in equilibrium with the measured Eh. Manganese solubility would be limited in this water by the solid rhodochrosite ($MnCO_3$). However, the calculated solubility (from an EQ3 calculation) would be about an order of magnitude greater than the largest

manganese content observed. Solubility with respect to manganese oxides is even greater if the measured Eh is employed in the calculation. An Eh of 200 to 400 mV would have to control the manganese redox couple to relate the observed manganese content to manganese oxide solubility. Thus, manganese appears to be undersaturated in this water.

Although neither total iron nor manganese contents of Well UE-25b#1 water appear to be in equilibrium with the measured Eh, it is possible that iron and manganese redox behavior are controlled by the same variable. Figure 6 shows a plot of \log_{10} (total iron) as a function of \log_{10} (total manganese). From the equations defining the relation between Eh and total concentration for iron and manganese, the Eh can be eliminated to give

$$\log_{10}[\text{Fe}^{2+}] = \left(-\frac{n}{m}\right)\log_{10}[\text{Mn}^{2+}] + C,$$

where C is a constant. The slope of the line through the data in Fig. 6 is $\left(\frac{n}{m}\right) = 1.5$. This value for the ratio is constant with $n = 1$ [total iron controlled by the solubility of $\text{Fe}(\text{OH})_3$ or Fe_2O_3] and $m = 2/3$ (total manganese controlled by the solubility of hausmannite). Thus, it is possible that both iron and manganese are being oxidized by the same process, a process that does not appear to be in equilibrium with the measured Eh.

In summary, the various measures of the redox state of the water from the Well UE-25b#1 pumping test give conflicting quantitative information. However, they all indicate that the water, after initially being reduced, became more oxidizing as the test progressed. A possible mechanism for this result is that the test actually sampled water from more than one zone, that is, water with different redox characteristics. Mixing different waters during pumping could result in kinetic control of the concentrations of species involved in redox reactions. Equilibrium considerations would only control the extent to which reactions would occur. The oxidizing agent had to be strong enough to oxidize Fe^{2+} , Mn^{2+} , and NO_2^- . Dissolved oxygen, which was observed during the latter third of the test, is the most likely candidate. The possibility also exists that biodegradation of drilling fluids in the near vicinity of the well resulted in depletion of the oxygen content of the water. Continued pumping then brought fresh, oxygenated water to the pump.

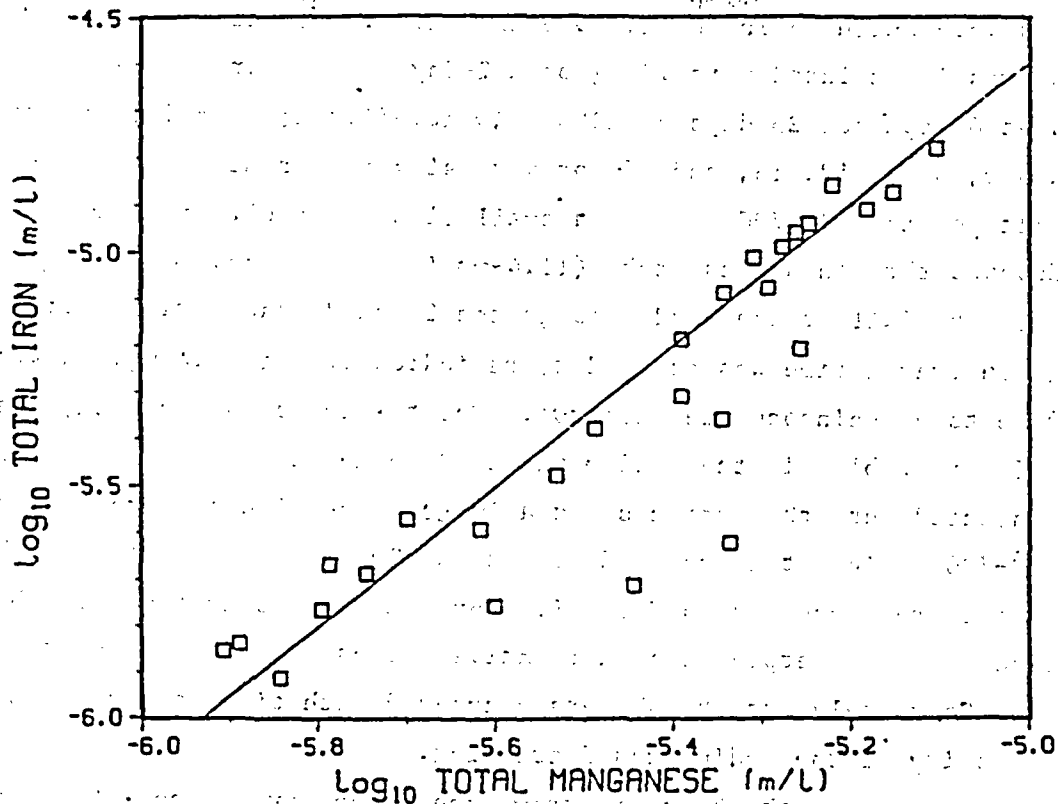


Fig. 6. Plot of total iron content as a function of total manganese content of water from Well UE-25b/#1 pumping test.

Calculations similar to these will be done with the compositional results of waters from Well USW H-3 and from the soon-to-be-pumped Well USW H-6. By so doing, we hope to get some insight into the controlling reactions of the oxidation-reduction potential (Eh) of the water.

2. Biodegradation of Drilling Fluids. The purpose of this research is to determine if microbial activity can change the groundwater composition and consequently influence the mobility of waste elements, especially multivalent elements such as plutonium. We are interested in those microorganisms capable of utilizing drilling fluids as growth substrates because drilling fluids are used extensively in the drilling of wells and geology holes for characterization of Yucca Mountain at the Nevada Test Site.

A long-term experiment investigating viscosity changes of two of the drilling fluids, ASP-700 and Turco 5622, was recently completed. Five

bacterial species were grown individually in the ASP-700 medium, while two species were cultured in the Turco 5622 medium. For each unknown, 180 ml of medium was inoculated with 18 ml of a 2-day old culture. These flasks were mixed at 60 rpm for 25 days at 22°C. Twenty-five ml of media were withdrawn on days 0, 3, 7, 12, 18, and 25 for viscosity measurements. To measure the viscosity of the ASP-700 medium, a small glass bead (2.9 mm diam., 0.0303 g) was dropped through a glass tube (11.4-mm i.d. by 20 cm) containing the medium. The fall of the bead through the 20-cm distance was timed, and any change in travel time was assumed to be indicative of a change in viscosity relative to an uninoculated control. For the Turco 5622 medium, the rate of rise of air bubbles in the medium was used to measure viscosity. Air bubbles were injected into the medium using a 10- μ l, precision syringe, and as with the ASP-700 medium, the travel distance was 20 cm. The results of this experiment are expressed in Table I. Any increase, over time, in the values reported can be interpreted as a relative increase in the viscosity of the medium. Conversely, as the numbers decreased with time, one can assume that the viscosity of the medium was decreasing.

Apparently, as the bacteria grew, the viscosity of the ASP-700 medium decreased. This was true for all five species tested, and these results contradict those results reported.⁶ At this time, no explanation can be given to account for this discrepancy. Following an initial decrease, the viscosity of the Turco 5622 medium tended to increase with time until day 25 where the values were similar to day 0. These results suggest that more than one constituent of the Turco 5622 medium was being acted upon by the microorganisms, which in turn, had varying effects on viscosity.

Experiments are now being conducted to determine if these drilling fluids are available for anaerobic biodegradation. One sample of the Turco 5622 medium was placed in a 1.0- μ serum bottle fitted with a one-way glass valve. Prior to autoclaving, the medium was reduced by boiling it in an oxygen-free environment and by adding cysteine as a reducing agent. The media was then autoclaved, cooled under an atmosphere of oxygen-free gas, and inoculated with 10 ml of an anaerobic culture. The bottles were then sealed and will be incubated at room temperature for approximately 3 months. Gas production will be monitored periodically by connecting the serum bottles to Warburg manometers and measuring the displacement of manometric fluid.

TABLE I
THE EFFECTS OF BACTERIAL GROWTH ON THE RELATIVE VISCOSITY
OF ASP-700 AND TURCO 5622 MEDIUM^a

Day	Species Number						
	ASP-700					Turco 5622	
	9.A.2.b	9.A.3	9.A.5	11.A.2.a	11.A.2.b	1.A	6.A
0	0.93	0.93	0.91	0.92	0.90	1.32	1.24
3	0.94	0.99	0.96	0.94	0.95	1.01	0.98
7	0.91	0.98	0.92	0.91	0.92	--	1.25
12	0.92	0.99	0.95	0.90	0.90	1.33	1.19
18	0.72	0.75	0.74	0.71	0.70	1.51	1.75
25	0.80	0.84	0.86	0.75	0.75	1.33	1.21

^aResults are expressed as a ratio of the unknown value divided by the control value.

B. Natural Isotope Chemistry (K. Wolfsberg, A. E. Norris, H. W. Bentley, and S. K. Gifford)

Water infiltration at Yucca Mountain during the past 25 years can be traced by measuring the penetration of ³⁶Cl that occurred as global fallout from high-yield nuclear tests in the Pacific Ocean area. Soil samples were collected in February from four locations on or adjacent to Yucca Mountain. These samples have been analyzed for chloride concentrations to help determine the sites and the sampling protocols that will be used to obtain the material required for the ³⁶Cl analyses.

The four sites sampled in February were the crest of Yucca Mountain (36° 52'N, 116° 28'W), a bulldozer trench in Coyote Wash (36° 51'N, 116° 27'W), a trench in Yucca Wash (YW-6, 36° 52'N, 116° 25'W), and a trench in Fortymile Canyon (FW-3, 36° 49'N, 116° 24'W). The latitude and longitude co-ordinates are approximate. The chloride contents of the soil samples are listed in Table II and are plotted in Figs. 7 through 10. The ordinate values of the chloride concentrations are plotted on a linear scale in the first two figures, but on a logarithmic scale in the last two.

TABLE II
 CHLORIDE CONCENTRATION IN SOIL SAMPLES
 FROM YUCCA MOUNTAIN LOCATIONS

<u>Sample Identification^a</u>	<u>Depth (meters below land surface)</u>	<u>mg Cl⁻/kg soil</u>
YC-1	0.0000-0.1016	9.51
YC-2	0.1016-0.2032	17.64
YC-3	0.2032-0.2540	10.49
YC-4	0.3048-0.4572	24.6
CW-13	0.0000-0.1270	45.3
CW-12	0.1524-0.3048	20.6
CW-11	0.3556-0.4318	5.3
CW-10	0.4572-0.5588	4.2
CW-9	0.6096-0.7112	5.6
CW-8	0.9144-1.0668	2.0
CW-7	1.2446-1.4224	6.2
CW-6	1.6002-1.7526	14.1
CW-5	2.1336-2.2860	46.1
CW-4	2.5908-2.7432	6.8
CW-3	3.0480-3.2004	8.1
CW-2	3.3528-3.5052	24.9
CW-1	3.8100-3.9624	5.4
YW6-13	0.0000-0.1524	3.5
YW6-12	0.1778-0.2540	416.2
YW6-11	0.2032-0.3048	152.0
YW6-10	0.3556-0.4318	25.0
YW6-9	0.4318-0.4826	156.9
YW6-8	0.5080-0.6350	92.9
YW6-7	0.5334-0.6858	159.4
YW6-6	0.7620-0.9144	46.5
YW6-5	0.9906-1.0922	62.4

TABLE-II (cont)

<u>Sample Identification</u> ^a	<u>Depth</u> <u>(meters below land surface)</u>	<u>mg Cl⁻/kg soil</u>
YW6-4	1.2192-1.3716	1457.9
YW6-3	1.3716-1.5240	1865.3
YW6-2	1.6510-1.8288	781.4
YW6-1	2.1336-2.2352	1378.8
FW3-7	0.0000-0.1524	2.6
FW3-6	0.1524-0.2286	2.6
FW3-5	0.3048-0.4572	2.7
FW3-4	0.6096-0.7620	11.3
FW3-3	0.9144-1.1176	161.0
FW3-2	1.2954-1.4478	187.3
FW3-1	1.5240-1.6764	140.4

^aThe two-letter codes designate the following:

YC = crest of Yucca Mountain

CW = Coyote Wash bulldozer trench

YW = Yucca Wash trench

FW = Fortymile Canyon trench

Both the low chloride concentrations in the samples taken from the crest of Yucca Mountain and the maximum chloride concentration for this data set, which occurs at the bedrock surface, are what one would expect from recent leaching. The shallow depth to bedrock (0.46 m) is such that even a moderate precipitation event could flush the section. The low chloride content at the bedrock surface indicates that a drain exists for infiltrating water.

The chloride data from the Coyote Wash samples can be interpreted in terms of active, but not recent, flushing of chlorides. There may be a significant horizontal component to recharge at the location sampled, which is not unexpected for a wash such as this one. The relatively high chloride concentrations at the surface may be attributable to surface vegetation, which holds rainfall infiltration within the shallow root zone.

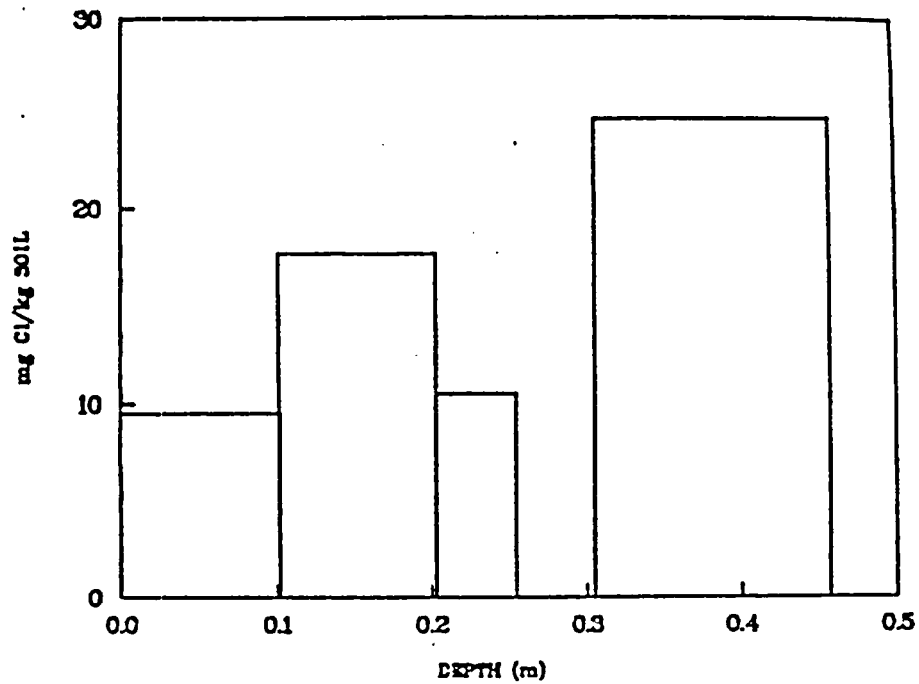


Fig. 7. Chloride distribution on Yucca Mountain crest.

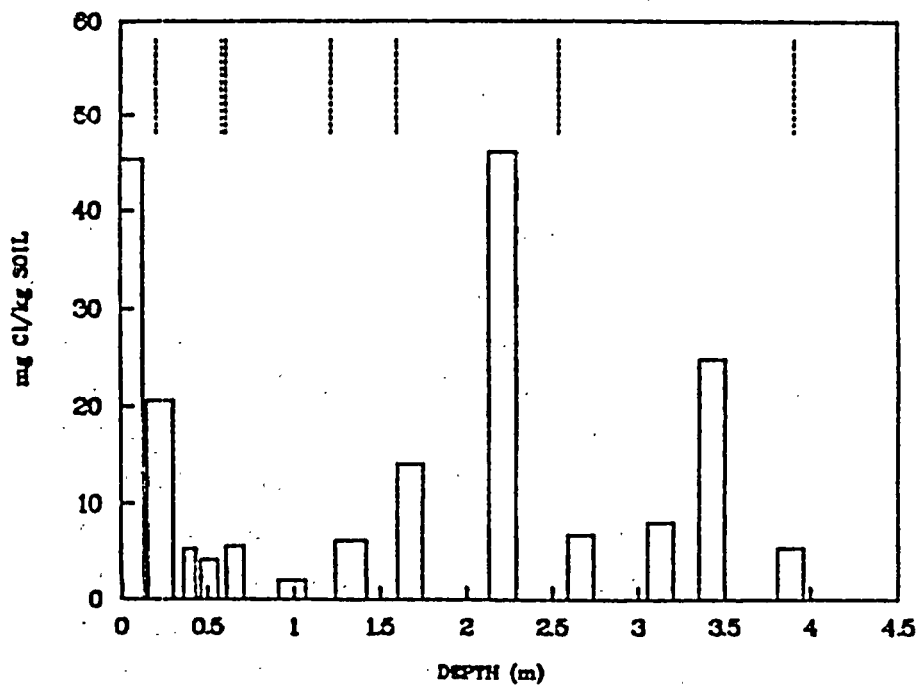


Fig. 8. Chloride distribution in trench CW.

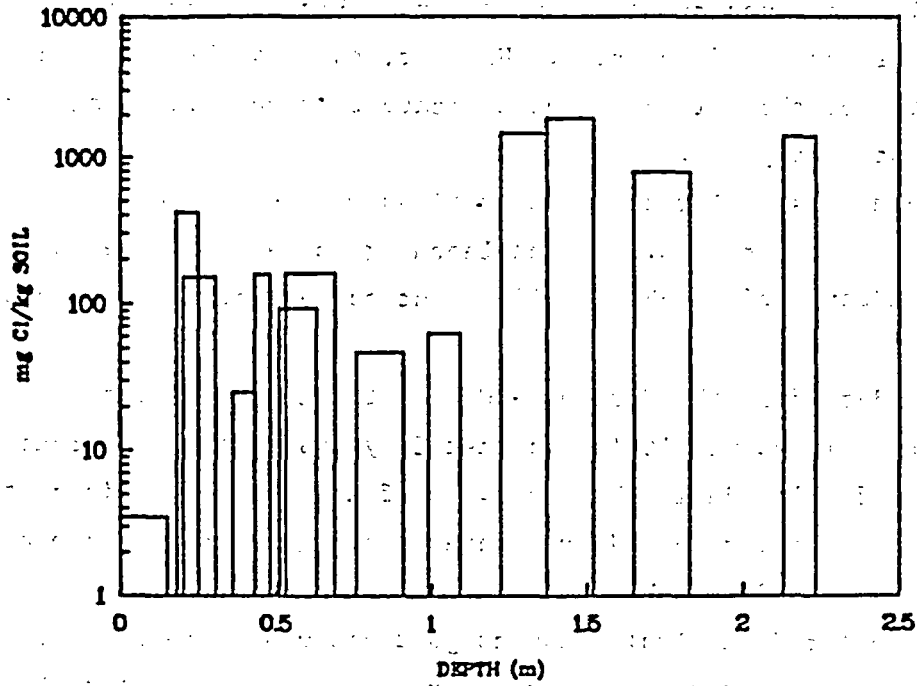


Fig. 9. Chloride distribution in Trench YW-6.

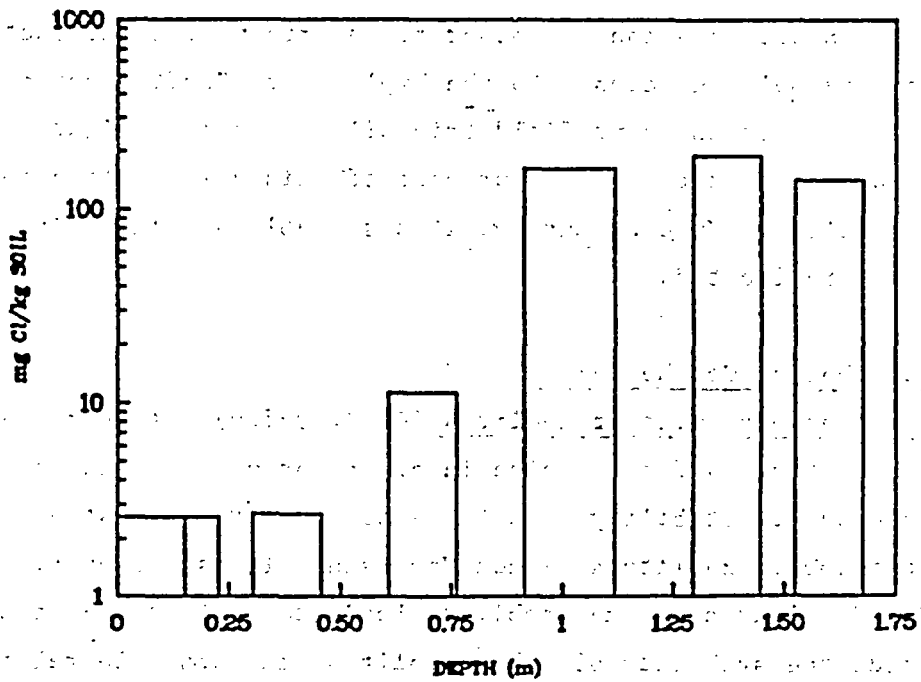


Fig. 10. Chloride distribution in Trench FW3.

The soil unit boundary at 2.5 m, shown in Fig. 8, may help to limit the downward leaching of chloride. However, the low chloride concentrations at the bottom of the bulldozer cut indicate that chloride leaching is not stopped at that point.

The highest chloride concentrations were observed in soil samples from the Yucca Wash 6 trench. Recent leaching appears to have moved the chloride down from the surface about 0.16 m, but subsequent leaching appears to be very slow.

The data from the Fortymile Canyon trench can be interpreted in terms of chloride leaching within the past 20 years that has decreased the concentrations of chloride in the top 0.8 m of the trench. This postulated flushing may have resulted from water flowing in the flood plain that includes the FW-3 trench site.

The chloride analysis results just discussed are part of the data being used to select appropriate sites to measure, by the ^{36}Cl technique, rainfall infiltration during the past 25 years. Of the four sites that were sampled, Yucca Wash 6 appears to be the only one where the ^{36}Cl infiltration should be undisturbed by water flow on the surface, which is a desirable characteristic. However, the Yucca Wash 6 trench is four kilometers from the Exploratory Shaft location. Another field trip will be conducted to see if a site can be selected closer to the Exploratory Shaft location. An additional goal of the next field trip will be to investigate whether the ^{36}Cl technique might permit measurement of rainfall infiltration into the fractured tuffs of Yucca Mountain, if a suitable sampling site for that purpose can be located.

C. Hydrothermal Geochemistry

1. Thermodynamics of Zeolites (C. J. Duffy). A thermodynamic model has been constructed for analcime in order for us to begin to understand the controls upon its stability. Analcime is neither the most abundant nor the the most sorptive zeolite at Yucca Mountain. It is, however, the most studied. Modeling analcime stability leads to insights about the parameters that affect the stability of other zeolites, the probable relative importance of kinetics versus chemical equilibrium, and the best approaches to studying the other zeolites.

Analcime does not have a fixed composition but rather is a solid solution. We have considered only that part of the solution between the end members $\text{NaAlSi}_2\text{O}_6 \cdot \text{H}_2\text{O}$ and $\text{Si}_3\text{O}_6 \cdot 1.5\text{H}_2\text{O}$. Less silica-rich analcimes exist, but they have not been considered because the way in which H_2O is involved in the solid solution may be different, and these low silica analcimes appear to only be in equilibrium with silica activities below quartz saturation. This makes them unimportant at Yucca Mountain. The compositions in the solid solution are based upon the observations of Saha.⁷ The relationship among sodium, aluminum, and silicon in the solid solution is almost certainly correct because it is constrained by charge balance. The amount of water present, however, is not constrained by charge balance and is, therefore, more uncertain. Other investigators⁸ have suggested somewhat different water contents.

An ideal solution model has been adopted to describe the analcime solid solution. In order to develop such a model, the sources of configurational entropy must be identified and evaluated. The first source of entropy is the mixing of the two end members. This mixing apparently takes place by the substitution of a $\text{Na}_2\text{Al}_2 \cdot \text{H}_2\text{O}$ unit for a $\text{Si}_2 \cdot 2\text{H}_2\text{O}$ unit. This substitution leads to the observed compositional variation and seems to be crystallographically reasonable because removal of a pair of sodium atoms makes room for an additional H_2O . Assuming that these units are randomly mixed in analcime, the configurational entropy from this source, S_{c1} is given by

$$S_{c1} = 0.5R[x \ln x + (1 - x) \ln(1 - x)] ,$$

where R is the gas constant, T is the temperature in kelvin, and x is the mole fraction of $\text{NaAlSi}_2\text{O}_6 \cdot \text{H}_2\text{O}$ (Ref. 9).

Additional configuration entropy is also present due to mixing of aluminum and silicon on the tetrahedral sites and mixing of sodium and vacancies on the sodium sites. We have adopted the basic tetragonal structure for analcime suggested by Mazzi and Galli.¹⁰ In this structure all of the aluminum is found in the T1 sites with none in the T2 sites. However, a maximum of only one-half of the T1 sites is occupied by aluminum so that there is a configurational entropy from mixing of aluminum and silicon on these sites. The statistical analogue for entropy is given by

$$S_c = -k \sum_i P_i \ln P_i ,$$

where S_c is the configurational entropy, k is Boltzmann's constant, P_i is the probability of the i th quantum state, and the summation over all accessible quantum states can be used to evaluate the entropy of aluminum-silicon mixing.

We assume that aluminum avoidance is observed in analcime; that is, no two adjacent tetrahedral sites both contain aluminum. The configurational entropy of silicon-aluminum mixing can be calculated for a unit of analcime containing four T1 sites and two T2 sites. We will choose this unit such that the T1 sites are present as a four-membered ring. This ring can contain either zero, one, or two aluminum atoms. Because of aluminum avoidance, more than two aluminums cannot be present, and there are only two ways in which two aluminums can be placed in the four-membered ring. There are four ways in which one aluminum can be placed in the ring, and one way in which no aluminums can be placed in the ring. The probability of a quantum state with two aluminums present is $x^2/2$, with one aluminum present is $x(1-x)/2$, and with no aluminum present is $(1-x)^2$. The entropy of silicon aluminum mixing (S_{cl}) is then given by

$$S_{cl} = k[(x^2 - 2x)\ln 2 + 2x\ln x + (2 - 2x)\ln(1 - x)]$$

or for a mole of analcime

$$S = 0.5R[(x^2 - 2x)\ln 2 + 2x\ln x + (2 - 2x)\ln(1 - x)].$$

The entropy of sodium vacancy mixing has been similarly evaluated assuming a tetragonal symmetry for analcime. The probability of occupancy of the two Na1 sites has been assumed to be equal. We have also assumed that

$$P_i = xP_i^0 ,$$

where P_i is the probability of a sodium being on site i of an analcime-containing mole fraction x of $\text{NaAlSi}_2\text{O}_6 \cdot \text{H}_2\text{O}$, and P_i^0 corresponds to $x = 1$.

The resultant configurational entropy for the mixing of sodium and vacancies (S_{c3}) is then given by:

$$S_{c3} = 0.5R[(2xP - 2)\ln(1 - xP) - (1 - 2x + 2xP)\ln(1 - 2x + 2xP) - 2xP\ln(xP) + (2xP - 2x)\ln(2x - 2xP)]$$

for a mole of analcime where $P = P_i^0$.

In order to calculate the stability of analcime, we must obtain the chemical potentials of the sodium and silicon end members μ_{Na} and μ_{Si} , respectively. To do this we note that

$$\mu_{Na} = G_S + (1 - x) \frac{\partial G_S}{\partial x}$$

and

$$\mu_{Si} = G_S - x \frac{\partial G_S}{\partial x}$$

where G_S is the free energy of the solid solution given by

$$G = x\mu_{Na}^0 + (1 - x)\mu_{Si}^0 - T(S_{c1} + S_{c2} + S_{c3})$$

where the μ^0 are the chemical potentials of the end members exclusive of the contributions from configurational entropy. The resulting chemical potentials of the end members are

$$\mu_{Si} = \mu_{Si}^0 + 0.5RT[5\ln x + (2x - 2P - x^2)\ln(2) + (2 - 2P)\ln(1 - xP) + (2P - 1)\ln(1 - 2x + 2xP) + 2(1 - P)\ln(1 - P) + 2P\ln(P)]$$

and

$$\mu_{Na} = \mu_{Na}^0 + 0.5RT[3\ln(1 - x) - x^2\ln(2) + 2\ln(1 - xP) + \ln(1 - 2x + 2xP)]$$

The μ^0 's in these equations are functions of temperature and pressure. They are being evaluated using a combination of calorimetric and crystallographic data in combination with information from laboratory hydrothermal experiments and field observations. Attempts to evaluate the μ^0 's have shown

that many of the data are consistent with this model for the free energy of analcime; however, few if any of the data are completely unambiguous.

2. Natural Analogues (R. M. Vidale, G. K. Bayhurst, and D. L. Bish). Construction of a repository for high-level radioactive waste has been proposed at Yucca Mountain in the southwest corner of the Nevada Test Site (NTS). Yucca Mountain was chosen because it consists of a sequence of felsic volcanic tuffs ranging from devitrified to nonwelded and zeolitized. The proposed host rock, the Topopah Spring Member of the Paintbrush Tuff, is a particularly good candidate for isolation of waste because it is in the unsaturated zone, it contains the stable minerals quartz, cristobalite, and alkali feldspar, and it is underlain by significant quantities of a clinoptilolite- and mordenite-bearing tuff that sorbs many cationic radioactive waste elements.

The presence of stored nuclear waste will produce a heat pulse in the near-field environment of the repository. Placing a heat source, such as a repository, in the tuff may accelerate and change the alteration process. In addition, groundwater moving in that temperature gradient can leach, transport, and deposit material over long periods of time. C. A. Morrow, D. E. Morre, and J. D. Byerlee¹¹⁻¹³ have studied in the laboratory the changes that may take place in Topopah Spring Member tuff with a fluid flowing through it in the presence of a temperature gradient. Warm spring systems are possible natural analogues for these processes and can be used to study their effects over the hundreds of years that may be required for isolation of waste in the presence of the thermal pulse.

a. Hot Spring Data. To find localities with rock compositions similar to those at Yucca Mountain, we chose hot spring localities in Nevada and New Mexico with a high probability of appropriate mineral alteration after studying a geothermal map of Nevada,¹⁴ other geologic maps,¹⁵⁻¹⁷ and published reports.¹⁶⁻¹⁹ Nine localities in central Nevada and New Mexico were examined for bedrock exposure and mineral alteration caused by hot springs. Water and rock from the three most promising localities were sampled to study the long-term natural alteration of felsic rock in contact with groundwater. The similarity of the water compositions to that of water near Yucca Mountain was a large part of the basis for selection. The composition of pore-water in the unsaturated zone chosen for the repository

site is not known. The procedures for collection of waters and analytical methods are described at the end of this contribution.

The first site sampled was Bailey Hot Spring in Beatty, Nevada.^{14,18} The spring is about 15 miles west of Yucca Mountain and emerges from a tuff unit that is very similar to the felsic tuffs of Yucca Mountain. The spring currently produces a bicarbonate water (Table III) that is more saline than the groundwater from Well J-13 near Yucca Mountain. The Beatty water is higher in sodium and chloride and high in sulfate. The least-altered tuff near the spring contains 50 to 60% alkali feldspar, 15 to 20% quartz, and 10 to 20% kaolinite and poorly crystallized silica. The altered tuff contains abundant quartz and alunite, traces of kaolinite and gypsum, a few per cent calcite, and a more poorly crystallized silica than that from the least-altered rock (Table IV).

The second site was Steamboat Springs, Nevada.^{16,20,21} The hot spring system underlying Steamboat Springs includes both a saturated zone with flowing hot water (Table III) and an acidic, unsaturated zone that is dominated by water vapor and gases. The older rocks are metamorphosed sediments that have been intruded by granodiorite. (Granodiorite is similar in bulk chemical composition to felsic tuff; it contains the high-temperature mineral phase assemblage found in tuff but none of the glass.) The hot spring system has been active, possibly intermittently, for over 2.5 Myr and has intensely altered the granodiorite. Analyses of the water samples obtained at Steamboat Springs are listed in Table III. The water is very hot, very saline, and alkaline. The water is depositing silica sinter as it emerges at the surface and is not now in contact with the granodiorite at the surface. The least-altered granodiorite sampled near Steamboat Springs consists of $55 \pm 10\%$ alkali feldspar, $34 \pm 5\%$ quartz, and $11 \pm 5\%$ smectite. The most-altered granodiorite contains $30 \pm 10\%$ alkali feldspar, $30 \pm 10\%$ quartz, $30 \pm 10\%$ natroalunite, and $10 \pm 5\%$ kaolinite (Table IV).

The third site sampled was Sou Hot Springs (also known as Seven Devils Hot Springs and Gilberts Hot Springs), northeast of Reno in Dixie Valley, Nevada (Tables III and IV). There are nine pools that range from 1.5 to 6 m in diameter and from 21 to 58°C. The locality was chosen because the springs rise through the Fish Creek rhyolitic tuff. Unfortunately, no tuff outcrop could be found within the present pools. Fish Creek rhyolite that appeared

TABLE III
PRESENT WATER COMPOSITIONS OF WELL J-13 AND
SIX HOT SPRINGS

Element or Compound	Well J-13 NTS ^a	Bailey Hot Spring ^b	Sou Hot Springs ^c	Steamboat Springs ^c	Spence Spring ^{b,c}	McCauley Spring ^b	San Antonio Spring ^{b,c}
Concentration (ppm)							
Na	50	143	148	670	36	18	15
K	5	7	27	80	2	1	2
Ca	14	20	80	5	6	9	2
Si	38	27	30	145	30	26	35
Mg	2	0.5	24	0.2	2	5	0.3
Mn	0.01	0.006	0.03	N.D. ^d	<0.02	<0.02	0.02
Fe	0.04	0.06	0.03	N.D.	<0.04	<0.04	0.07
Sr	0.04	0.2	15	1	0.1	0.02	0.1
Ba	0.004	0.01	0.07	0.1	N.D.	<0.03	<0.03
HCO ₃ ⁻	127	244	N.D.	N.D.	144	86	56
SO ₄ ²⁻	18	148	420	110	18	7	7
Cl ⁻	6	42	95	950	4.5	6	1.0
F ⁻	2	7	7	4	0.3	1	1
pH	8.3 ^e	8.0	7.5	8.8	6.7	6.2	6.8
Temp. (°C)	25	38	48	95	45	31	42

^aRef. 22.

^bAnalyzed by F. Goff, Los Alamos National Laboratory.

^cAnalyzed or checked by G. Bayhurst, Los Alamos National Laboratory.

^dNot determined.

^eNot measured at the site.

TABLE IV
MINERAL ASSEMBLAGES IN WATER FROM
SIX HOT SPRINGS

<u>Locality and Sample</u>	<u>Original Phases</u>	<u>Alteration Phases</u>
Bailey Hot Spring, Beatty, Nevada		
BT-6-7-1 least-altered rock	40 to 60% alkali feldspar, 15 to 25% quartz	10 to 20% kaolinite, 10 to 30% opal
BT-6-7-2 most-altered rock	30 to 50% quartz	30 to 50% quartz, 30 to 50% alunite, 10 to 30% opal, 1 to 5% calcite, trace gypsum, trace kaolinite
Steamboat Springs, Nevada		
205C least- altered granodiorite	34 ± 5% quartz, 55 ± 10% alkali feldspar	11 ± 5% smectite
205B altered granodiorite	30 ± 10% quartz, 30 ± 10% alkali feldspar	30 ± 10% natroalunite, 10 ± 5% kaolinite
205A altered granodiorite	50 ± 20% quartz	50 ± 20% quartz, 50 ± 20% amorphous silica
205D white material		100% amorphous silica
205E sinter		20 ± 10% quartz, 80 ± 20% amorphous silica
Sou Hot Springs, Dixie Valley, Nevada		
204A altered Fish Creek Tuff (white)	69 ± 10% alkali feldspar, 30 ± 5% quartz	3 ± 2% kaolinite, ~1% smectite
204B altered Fish Creek Tuff (white)	75 ± 10% alkali feldspar, 20 ± 5% quartz	3 ± 2% gypsum, 3 ± 1% calcite

TABLE IV (cont)

<u>Locality and Sample</u>	<u>Original Phases</u>	<u>Alteration Phases</u>
204D altered Fish Creek Tuff (red)	70 ± 10% alkali feldspar, 26 ± 5% quartz, ~1% mica	2 ± 1% calcite, ~1% smectite
204C altered Fish Creek Tuff (white)	42 ± 10% alkali feldspar, 16 ± 5% quartz	40 ± 5% calcite, 3 ± 2% smectite
204E natural cement in Fish Creek Tuff	25 ± 10% alkali feldspar, 11 ± 5% quartz, ~1% mica	58 ± 5% calcite, 4 ± 2% smectite
204F Fish Creek Tuff breccia	45 ± 10% alkali feldspar, 3 ± 1% quartz, ~1% mica	48 ± 5% calcite, 3 ± 2% smectite
Spence Spring, Jemez Mountains, New Mexico		
106 freshest rhyolite from area	70 ± 10% alkali feldspar, 30 ± 5% cristobalite, 2 ± 1% amphibole, 2 ± 1% mica	
107 freshest obsidian from area	70 ± 10% glass, 10 ± 5% alkali feldspar, 5 ± 3% quartz, 5 ± 3% cristobalite, 5 ± 3% amphibole, 4 ± 2% mica	
101 rhyolite near water source in main pool	70 ± 10% alkali feldspar, 30 ± 5% cristobalite, ~1% mica, ~1% amphibole	
102A rhyolite near water source in main pool	68 ± 10% alkali feldspar, 30 ± 5% cristobalite, 2 ± 1% mica, ~1% amphibole	
105 rhyolite from pool to east	70 ± 10% alkali feldspar, 30 ± 5% cristobalite, 2 ± 1% amphibole	
103 obsidian from main pool	60 ± 20% glass, 30 ± 10% alkali feldspar, 4 ± 2% cristobalite, ~1% amphibole	

TABLE IV (cont)

<u>Locality and Sample</u>	<u>Original Phases</u>	<u>Alteration Phases</u>
104 rhyolitic pumice from pool to north	60 ± 20% glass, 20 ± 10% alkali feldspar, 6 ± 3% cristobalite, 2 ± 1% amphibole 6 ± 3% quartz, 4 ± 2% mica	
McCauley Spring, Jemez Mountains, New Mexico		
108 rhyolitic pumice	60 ± 20% glass, 30 ± 10% alkali feldspar, 4 ± 2% cristobalite, 4 ± 2% quartz, 2 ± 1% mica, 3 ± 2% amphibole	
109 rhyolitic pumice	60 ± 20% glass, 30 ± 10% alkali feldspar, 5 ± 2% cristobalite, 5 ± 2% quartz, 4 ± 2% mica, 2 ± 1% amphibole	
San Antonio Spring, Jemez Mountains, New Mexico		
113 least- altered rock	70 ± 10% alkali feldspar, 20 ± 5% cristobalite, 10 ± 4% quartz, 5 ± 2% mica	
110 rhyolite from pool	60 ± 10% alkali feldspar, 20 ± 5% cristobalite, 15 ± 4% quartz, 3 ± 2% mica	~1% smectite
111 rhyolite from pool	70 ± 10% alkali feldspar, 20 ± 5% cristobalite, 10 ± 4% quartz, 4 ± 2% mica, trace amphibole	

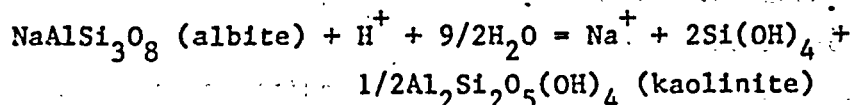
to have been exposed to earlier springs was sampled upslope, 6 to 60 m north of the present pools. The water at Sou Hot Springs is significantly more saline than that of Well J-13 at the NTS, and it contains a much higher concentration of sulfate than any of the other waters tested. The minerals in the altered rock samples are mostly the original volcanic phases (Table IV). Minor amounts of calcite and gypsum are noted. One sample contains a few per cent of kaolinite alteration.

Three hot springs (Spence, McCauley, and San Antonio) in the ring fracture zone of the Valles Caldera in the Jemez Mountains of New Mexico were sampled (Tables III and IV). The water composition from warm springs in the ring fracture zone²³ is very similar to that of Well J-13 at NTS, and the chemical composition of the rhyolitic rock is close to that of the Yucca Mountain tuff. The water temperatures of the three springs ranged from 31 to 42°C. These waters are dilute and contain predominantly sodium and calcium bicarbonate. One sample of the unaltered rock from the ring fracture zone contains 70 ± 10% alkali feldspar, 30 ± 5% cristobalite, and 2 ± 1% mica (see sample 106, Table IV). Altered rock from the San Antonio Spring appears more porous and friable, but it has the same mineralogic composition as rock from Spence Spring (see samples 101, 102A, and 105, Table IV). Loose material was collected from the rock surrounding Spence Spring and San Antonio Spring; the material was sampled approximately 0.3 m "upstream" from within the bedrock crevices where contributions from local soil, plant, or human debris would be minimized. The fine fraction of the loose material was separated by centrifugation and analyzed by x-ray diffraction (Table V). The mineral phases observed were the original phases: quartz, alkali feldspar, cristobalite, and mica and the alteration phases: smectite, kaolinite, and clinoptilolite.

b. Discussion. Mineral assemblages that include alunite (or natroalunite) and kaolinite were observed in the rock samples from Bailey Hot Spring and Steamboat Springs. Alunite- and kaolinite-bearing assemblages are considered indicators of an acid environment²⁴ and are characteristic of the vapor-dominated upper parts of active hot spring systems.^{25,26} It is believed that oxygen-bearing air circulates down into warm rock that is not water saturated. Hydrogen sulfide in the hydrothermal fluid is oxidized by the reaction:



The reaction between the acid that is produced by reaction (1) and the rock is responsible for the alunite-kaolinite alteration assemblage. For example:



Development of acid conditions in a repository environment would be a matter for concern because of the possibility of altering both metal components and rock. Hot springs commonly develop extremely acidic pore waters (pH = 1 to 3)^{21,24} in vapor-dominated zones when hydrogen sulfide oxidizes and produces sulfuric acid. A heated unsaturated zone in tuff may be analogous to the vapor-dominated zone of a hot spring in that at least some oxygen can

TABLE V
FINE-GRAINED SAMPLES CONCENTRATED BY CENTRIFUGE

<u>Locality and Sample</u>	<u>Original Phases</u>	<u>Alteration Phases</u>
Spence Spring, Jemez Mountains, New Mexico		
#1 fine fraction, loose sample from bottom of main pool	<5% quartz	~80% smectite, 10 to 20% calcite
#2 fine fraction of loose material from 0.3 m up source crevice	30 to 50% quartz, 20 to 40% alkali feldspar, ~5% cristobalite, ~2% amphibole, ~2% mica	small amount of smectite
San Antonio Spring, Jemez Mountains, New Mexico		
#3 fine fraction, loose material from source crevice	40 to 60% alkali feldspar, 5 to 10% cristobalite, 5 to 15% quartz, 2 to 5% mica	10 to 20% smectite, 2 to 10% kaolinite, 1 to 3% clinoptilolite

be supplied from the atmosphere. However, in the absence of hydrogen sulfide, the acid phase should not occur; the minor amounts of pyrite in Yucca Mountain tuffs should not produce significant quantities of acid even if they were totally oxidized.

Furthermore, hot springs do not develop acid conditions in all cases. This is illustrated by the three hot springs in the ring fracture zone of the Valles Caldera. It appears that the increased temperature, due to heat from the nuclear waste, will not result in acid conditions at the repository.

c. Analytical Procedures. Temperatures were recorded with mercury thermometers, and field pH was determined using a pH meter. (Laboratory values of pH are not considered reliable because most waters gain or lose CO₂ gas after sampling and before laboratory analysis. This loss alters the concentration of carbonic acid, which in turn changes the pH.) Two slightly different procedures were used for collecting and analysis of the water. Procedure A was used by F. Goff of Los Alamos and Procedure B by G. Bayhurst of Los Alamos. These procedures, whose results are shown in Table III, gave comparable results.

1. Procedure A. Samples of water for chemical analysis were filtered using a large syringe attached to a filter holder that contained 0.8- μ m filter paper. The filtered water was stored brimful in polyethylene bottles with Polyseal caps. Three types of samples were collected: (1) a 500-ml bottle of filtered, unacidified water for anions, (2) a 250-ml bottle of filtered, acidified water for cations, and (3) a 125-ml bottle of filtered, diluted water for silica. Dilute HCl was added by drops to the acidified sample until the pH was less than 2. The bottles used for silica analyses contained 90 ml of deionized water before 10 ml of sample was added. The dilution prevented polymerization of monomeric silica in more concentrated water samples before analysis.

Laboratory analyses were performed by the following methods: SiO₂ by a colorimetric method using a yellow molybdate complex; iron, manganese, calcium, magnesium, sodium, potassium, and lithium by atomic absorption spectroscopy; bicarbonate by sulfuric acid titration; sulfate and chloride by ion chromatography; fluoride by either selective ion electrode or ion chromatography; and boron by colorimetry using azomethine-H. Analyses of silver, barium, cadmium, chromium, copper, molybdenum, nickel, lead,

strontium, and zinc were performed by atomic absorption spectroscopy with either a graphite furnace or flame excitation.

2. Procedure B. Samples of water for chemical analysis were filtered using a large syringe attached to a filter holder that contained 0.8- μm filter paper. The filtered water was stored brimful in polyethylene bottles with Polyseal caps. Two samples were collected: (1) a 25-ml bottle of filtered, unacidified water for anions and (2) a 25-ml bottle of filtered, acidified water for cations. Dilute HCl was added by drops to the acidified sample until the pH was less than 2. The laboratory analysis for all cations was performed using Spectrametric's Spectraspan III arc emission spectrometer. The elements routinely analyzed are silicon, sodium, potassium, calcium, lithium, boron, arsenic, copper, beryllium, zinc, strontium, nickel, magnesium, manganese, cobalt, aluminum, thallium, antimony, cadmium, bismuth, molybdenum, mercury, titanium, lead, tungsten, rubidium, vanadium, gold, tin, iron, and barium. The analysis for the anions F^- , Cl^- , NO_2^- , PO_4^{3-} , Br^- , NO_3^- , and SO_4^{2-} was performed with a Dionex ion chromatograph.

d. X-Ray Powder Diffraction Analysis of the Rock. Several grams of sample were crushed in a shatterbox to homogenize the material, and approximately 100-mg of powder was crushed to -325 mesh with mortar and pestle. This powder was mounted in a cavity in a glass slide. All samples were examined with an automated Siemens D-500 x-ray powder diffractometer. Data reduction was performed with Siemens software, and semi-quantitative data were obtained using the "matrix flushing" technique of Chung.²⁷ Phases were identified using the Mineral Powder Diffraction File of the Joint Committee on Powder Diffraction Standards.

D. Solubility Determinations (D. E. Hobart, T. W. Newton, P. Palmer, V. L. Rundberg, and J. F. Kerrisk)

1. Waste-Element Solubilities. The solubilities of six waste elements (uranium, plutonium, americium, strontium, radium, and technetium) in waters from three wells from the vicinity of Yucca Mountain have been calculated with the EQ3 chemical equilibrium computer program and the current thermodynamic data base. This report consolidates a previous discussion of solubilities of some of these elements in water from two of the wells with more recent results. Table VI lists the compositions of the waters from Wells J-13, UE-25p#1 (1298 to 1792 m depth), and USW H-3 that were used in

the calculations. These three wells were chosen because they cover the range of compositions found in water from the tuffaceous aquifer under washes and canyons near Yucca Mountain (Well J-13), from the tuffaceous aquifer under Yucca Mountain (Well USW H-3), and from the carbonate aquifer (Well UE-25p#1 (1298 to 1792 m depth)).

EQ3/6 thermodynamic data files for technetium and ruthenium were recently received from Lawrence Livermore National Laboratory. The technetium data were added to the EQ3/6 data base for these calculations.

Table VII lists the solubility, the identity of the solid controlling solubility, and the primary aqueous species for the six waste elements in the three waters. The features of the water most affecting these quantities are the pH and Eh of the water, and the availability of aqueous species to complex with the waste element. Carbonate, sulfate, and fluoride are the most important complexing anions in addition to hydroxyl.

Uranium is primarily in the VI oxidation state in water from Wells J-13 and UE-25p#1. The change in the solid controlling solubility from Well UE-25p#1 to Well J-13 is caused by the increased carbonate content of Well UE-25p#1 water. The low Eh of water from Well USW H-3 results in both IV and VI oxidation states and much lower solubility than in water from the other wells.

Plutonium is primarily in the V and VI oxidation states in water from Well J-13; in water from the other two wells it is primarily in the IV oxidation state. The hydrous plutonium oxide used to control plutonium solubility results in higher solubilities than would be calculated with crystalline plutonium oxide. However, crystalline plutonium oxide may never precipitate from solution and thus may not exist as a control on solubility.

The increase in solubility in water from Well USW H-3 compared to Well UE-25p#1 is caused by the higher pH of Well USW H-3 water; this results in more complex formation with the hydroxyl anion.

Americium is only in the III oxidation state for conditions found in natural waters. The solubility is controlled mainly by the availability of complexing anions (including hydroxyl) and anions participating in the solid-forming reactions.

TABLE VI
WATER COMPOSITIONS USED FOR WASTE-ELEMENT SOLUBILITY CALCULATIONS

Species ^a	Well J-13	Well UE-25p#1 (1298 to 1792 m)	Well USW H-3
Na ⁺	45.2	110	124
K ⁺	5.47	13.4	1.49
Ca ²⁺	11.5	87.8	0.77
Mg ²⁺	1.73	31.9	0.06
Al ³⁺	0.26	0.14	0.51
SiO ₂ (aq)	64.2	37.2	36.2
Total carbonate (mol/l)	2.81×10^{-3}	1.61×10^{-2}	4.04×10^{-3}
Cl ⁻	6.4	37.0	8.3
SO ₄ ²⁻	18.1	129	31.2
F ⁻	2.1	3.5	5.4
Total phosphate (mol/l)	1.0×10^{-6}	---	1.0×10^{-6}
NO ₃ ⁻	10.1	0.5	0.2
pH	7.0	6.7	9.2
Eh (mV)	700	360	-143

^aConcentrations are in mg/l unless otherwise noted.

Both strontium and radium are particularly simple; they exist in only one oxidation state and form few complexes. Their solubility is controlled by the availability of anions that participate in the solid-forming reactions.

The solubility of technetium is controlled primarily by the redox conditions of the water. Under oxidizing conditions (Wells J-13 and UE-25p#1), technetium is very soluble. Below an Eh of about 0 mV, lower oxidation states of technetium start to become important. In Well USW H-3 water, technetium is only slightly soluble.

TABLE VII
WASTE-ELEMENT SOLUBILITIES IN WATER FROM THREE YUCCA MOUNTAIN WELLS

	Well J-13	Well UE-25p#1 (1298 to 1792 m)	Well H-3
Uranium			
Solubility (m/l)	3.65×10^{-3}	1.74×10^{-3}	4.05×10^{-8}
Solid	Schoepite ^a	Rutherfordine ^b	Uraninite ^c
Primary aqueous species	$(\text{UO}_2)_2\text{CO}_3(\text{OH})_3^-$ (98%) $\text{UO}_2(\text{CO}_3)_2^{2-}$ (1%)	$\text{UO}_2(\text{CO}_3)_2^{2-}$ (54%) $(\text{UO}_2)_2\text{CO}_3(\text{OH})_3^-$ (31%) $\text{UO}_2(\text{CO}_3)_3^{4-}$ (13%) UO_2CO_3^0 (2%)	$\text{UO}_2(\text{CO}_3)_3^{4-}$ (86%) $\text{U}(\text{OH})_5^-$ (8%) $\text{UO}_2(\text{CO}_3)_2^{2-}$ (7%)
Plutonium			
Solubility (m/l)	1.79×10^{-6}	3.11×10^{-8}	1.33×10^{-5}
Solid	$\text{Pu}(\text{OH})_4^{\text{d}}$	$\text{Pu}(\text{OH})_4^{\text{d}}$	$\text{Pu}(\text{OH})_4^{\text{d}}$
Primary aqueous species	PuO_2^+ (71%) PuO_2F_3^- (20%) $\text{Pu}(\text{OH})_5^-$ (3%) $\text{PuO}_2(\text{CO}_3)_2^{2-}$ (2%) $\text{PuO}_2\text{F}_4^{2-}$ (2%)	$\text{Pu}(\text{OH})_5^-$ (94%) $\text{Pu}(\text{OH})_4^0$ (6%)	$\text{Pu}(\text{OH})_5^-$ (100%)
Americium			
Solubility (m/l)	9.87×10^{-9}	2.16×10^{-8}	6.85×10^{-10}
Solid	$\text{Am}(\text{OH})\text{CO}_3$	$\text{Am}(\text{OH})\text{CO}_3^{\text{e}}$	$\text{Am}(\text{OH})\text{CO}_3$
Primary aqueous species	AmCO_3^+ (80%) AmOH^{2+} (8%) AmF^{2+} (4%) Am^{3+} (3%) $\text{Am}(\text{CO}_3)_2^-$ (3%)	AmCO_3^+ (83%) $\text{Am}(\text{CO}_3)_2^-$ (6%) AmF^{2+} (4%) AmSO_4^+ (2%) AmOH^{2+} (2%) Am^{3+} (2%)	$\text{Am}(\text{CO}_3)_2^-$ (46%) $\text{Am}(\text{OH})_3^0$ (36%) $\text{Am}(\text{OH})_2^+$ (12%) AmCO_3^+ (5%)

TABLE VII (cont)

	Well J-13	Well UE-25p#1 (1298 to 1792 m)	Well H-3
Strontium			
Solubility (m/l)	8.04×10^{-4}	5.27×10^{-4}	3.28×10^{-6}
Solid	Strontianite ^f	Strontianite ^f	Strontianite ^f
Primary aqueous species	Sr ²⁺ (96%) SrSO ₄ ^o (4%)	Sr ²⁺ (86%) SrSO ₄ ^o (14%)	Sr ²⁺ (94%) SrSO ₄ ^o (6%)
Radium			
Solubility (m/l)	3.39×10^{-7}	9.29×10^{-8}	2.94×10^{-7}
Solid	RaSO ₄	RaSO ₄	RaSO ₄
Primary aqueous species	Ra ²⁺ (99%)	Ra ²⁺ (99%)	Ra ²⁺ (99%)
Technetium			
Solubility (m/l)	Large ^g	Large ^g	2.06×10^{-12}
Solid	—	—	Tc ₃ O ₄
Primary aqueous species	TcO ₄ ⁻ (100%)	TcO ₄ ⁻ (100%)	TcO ₄ ⁻ (91%) TcO(OH) ₂ (9%)

^aSchoepite is UO₂(OH)₂·H₂O.

^bRutherfordine is UO₂CO₃.

^cUraninite is UO₂.

^dAlso known as hydrous PuO₂; crystalline PuO₂ would give a much lower solubility but may not control solubility.

^eAm₂(CO₃)₃ is less soluble under these conditions, but the thermodynamic data for this solid are uncertain.

^fStrontianite is SrCO₃.

^gTechnetium would be very soluble (>1 m/l) under these conditions.

2. Zeolite Formation from Water with High Calcium and Magnesium

Content. Recent analyses of water from wells other than Well J-13 have shown that water with higher calcium and magnesium contents is available near Yucca Mountain. This is particularly true of water from the carbonate aquifer that was sampled by Well UE-25p#1 (1298 to 1792 m depth). Calculations of zeolite formation from volcanic glass dissolution have been done in which it was assumed that all of the alkali metal and alkaline earth cations came from glass dissolution.²⁸ These calculations have been extended to include cases where the water that originally reacts with the glass contains dissolved calcium and magnesium carbonate. The calculations simulate dissolution of the volcanic glass in water from the carbonate aquifer.

The calculations were done using the reaction-path capabilities of the EQ3/6 chemical equilibrium computer programs.²⁹ The details of the calculation method have been reported elsewhere.²⁸ For these calculations, various concentrations of calcium and magnesium (up to 3 mmol/l) were assumed to be present in the water that reacts with the glass. Iron was considered as one of the glass constituents in the original calculations. Iron was not considered in this analysis because its disposition was not important.²⁸ Except for iron, the same pH-dependent glass dissolution rates were used in this work.²⁸ Quartz and chalcedony were not allowed to precipitate during the calculations; this restriction makes cristobalite the most stable solid silica phase and keeps the aqueous silica activity in the range observed in water from wells near Yucca Mountain.

The results from the original calculations indicated that cristobalite, zeolites (clinoptilolite and mordenite), and smectite clays were the primary products of glass dissolution. Water tended to increase in sodium, potassium, calcium, and magnesium early in the dissolution process, but potassium, calcium, and magnesium contents dropped when precipitation of the zeolites and clays started. Clinoptilolite, with sodium, potassium, calcium, and magnesium end members in its solid solution, precipitated before mordenite, which was assumed to have only sodium and potassium end members. Clinoptilolite was originally rich in calcium and potassium, but tended to become sodium rich as dissolution proceeded. The overall zeolite composition (clinoptilolite plus mordenite) also tended to become sodium rich as dissolution proceeded.

When calcium and magnesium were present in the water that originally reacted with the glass, the general trends of the results were the same as noted above. The extra magnesium precipitated in the clays and the extra calcium precipitated in clinoptilolite. Larger quantities of calcium present in the original water led to calcium-rich clinoptilolite during more of the dissolution process and to delays in the start of mordenite precipitation. Thus, the net result of calcium in the original water was to prolong the presence of calcium-rich zeolites. However, the trend toward sodium-rich zeolites with increased glass dissolution was still present.

Recent studies of zeolite compositions from drill holes UE-25b#1 and UE-25p#1 have shown that the clinoptilolite from these holes tends to remain calcium rich where ever it is found, rather than varying from calcium rich at shallower depths to sodium rich at greater depths.⁶ This observation could be an indication that these zeolites formed from dissolution of glass in calcium- and magnesium-rich water. The water from these wells is higher in calcium and magnesium than water from most other wells near Yucca Mountain, particularly the water from Well UE-25p#1, which draws from the carbonate aquifer. Thus, these zeolites may have been associated with water from the carbonate aquifer rather than water that was recharged directly into the tuffaceous aquifer.

3. Effect of Aqueous Complexes on Sorption Behavior. Sorption is expected to provide one of the primary retardation mechanisms for radionuclide transport at Yucca Mountain. One question that is just beginning to be addressed experimentally is the effect of varying water chemistry on sorption and radionuclide transport (see Section II.E.). This question is also being addressed through a modeling effort. A chemical transport computer program called CHEMTRN³⁰⁻³¹ has been used to model a very simple case of ion-exchange sorption in which the sorbing species was also allowed to form aqueous complexes. The effect of the strength of the complexes on sorption behavior was determined from a series of these transport calculations. CHEMTRN solves the one-dimensional convection, diffusion, and dispersion equations for flow in a porous media. The effects of aqueous complex formation, precipitation, sorption by ion exchange, and sorption by surface complexation are also considered. A simple problem in which strontium was sorbed by ion exchange from water containing sodium (10 mmol/l), calcium

(2 mmol/l), carbonate (10 mmol/l), chloride (3 mmol/l), and sulfate (1 mmol/l) was used to assess the effect of complex formation on sorption. The water was assumed to contain 0.001 mmol/l of natural strontium. At the start of the calculation, a boundary condition supplying radioactive strontium at a concentration of 0.001 mmol/l was imposed at $x = 0$. Water flow at a velocity of 0.01 m/yr carried the radioactive strontium over the sorbing medium. The solid sorbing material was assumed to have a density of 2.5 g/cm³ and a porosity of 20%. CHEMTRN does not have the capability to account for radioactive decay; this approximation is conservative because in reality, the amount of radioactive strontium will always be less than calculated here.

Calculations with the EQ3 chemical equilibrium program and data base have indicated that strontium forms significant quantities of aqueous complexes with only one anion, sulfate, in water from Yucca Mountain. The largest amount of strontium that was complexed was seen with water from Well UE-25p#1, where 14% of the aqueous strontium existed as the sulfate complex; the remainder of the aqueous strontium was as the uncomplex Sr²⁺ ion. For the CHEMTRN calculations, strontium was assumed to complex with only sulfate. The formation constant of the strontium-sulfate complex was varied during the series of calculations to produce different amounts of strontium in the complexed state, up to 25% of the aqueous strontium. Only uncomplexed strontium was assumed to sorb; this assumption is conservative because it should show the maximum effect of complex formation on sorption. In addition to the strength of the strontium-sulfate complex, the cation exchange capacity (CEC), the strontium sorption coefficient (K_d), and the run time were also varied. Values of CEC from 0.001 to 1.0 meq/g and of K_d from 1.5 to 1500 ml/g were used. Most calculations were run for a 30-yr time, with a few run to 160 yr. Figure 11 shows the results of one set of three calculations with CEC of 0.1 meq/g, K_d of 150 ml/g, and run time of 30 yr. The location of the radioactive strontium front with 25% strontium complexed is at most about 15% ahead of the front with no strontium complexes; the location of the radioactive strontium front with 11% strontium complexed is at most about 7% ahead of the front with no complexes. Calculations under other conditions gave similar results.

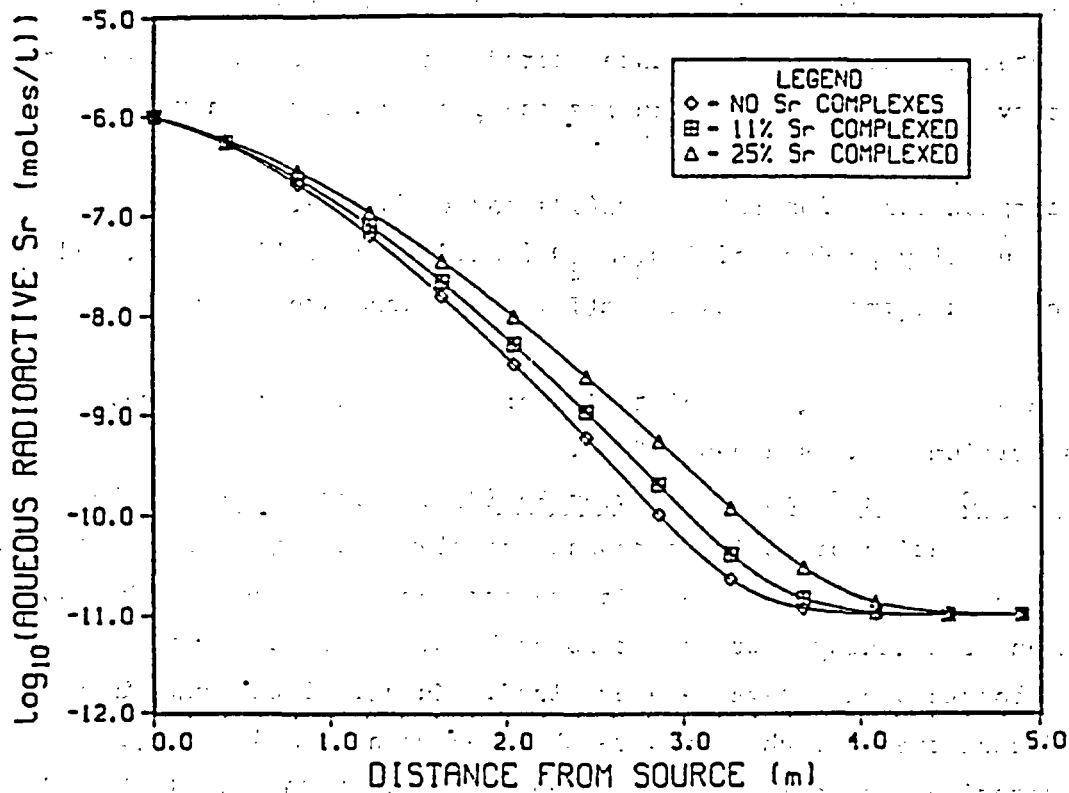


Fig. 11. Radioactive strontium concentration as a function of distance from the source at 30 yr; CEC = 1.0 meq/g, K_d , 150 ml/g, water velocity = 0.01 m/g.

The primary result of this analysis is that changes in aqueous complexation should not have significant effect on strontium transport. This same conclusion should hold for radium and cesium, because these elements only form a few weak complexes. The effect of reducing CEC or K_d was to increase the distance that radioactive strontium migrated in a given time. However, the difference between the location of the migration front of complexed strontium and strontium without complex formation was still in the same relative range indicated above.

4. Actinide Chemistry in Near-Neutral Solutions. The chemistry of actinides in the near-neutral waters found in the vicinity of Yucca Mountain will have a significant impact on actinide solubility and transport in water that interacts with nuclear waste stored there. Three aspects of actinide chemistry have been examined during the past quarter. They are

- complex formation between Pu(IV) and carbonate,
- solubility product of $\text{PuO}_2 \cdot n\text{H}_2\text{O}$ (solid or colloidal sol), and
- complex formation between Am(III) and carbonate.

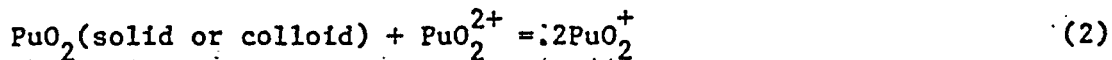
The two areas dealing with plutonium are a continuation of previous work. The americium work is a new effort.

a. Complex Formation Between Pu(IV) and Carbonate. We have continued our investigation of Pu(IV)-carbonate complexes using spectrophotometry to study the competition between citrate and carbonate ions for Pu(IV). Sets of solutions containing citrate but no carbonate, both citrate and carbonate, and carbonate alone, have been examined. In all of the experiments, significant spectral changes were observed when pH and/or ligand concentration was varied. To fix the activity of CO_2 and H_2CO_3 , all the carbonate-containing solutions were swept with definite CO_2 -argon mixtures. Several tentative conclusions are drawn from the current experiments.

- The effect of pH on Pu(IV)-citrate mixtures indicates three complexes, which are probably $\text{Pu}(\text{Cit})^+$, $\text{Pu}(\text{Cit})_2^{2-}$, and $\text{Pu}(\text{Cit})_3^{5-}$. "Cit" stands for $[\text{C}_3\text{H}_5\text{O}(\text{CO}_2)_3]^{3-}$.
- Experiments at constant total citrate concentration but varying pH and CO_2 pressure suggest the formation of a mixed citrate-carbonate complex as well as one or more carbonate complexes.
- Experiments in the absence of citrate but with varying total carbonate and pH indicate the presence of at least three different complexes.

A computer program has been written for calculating the composition of solutions containing given concentrations of Pu(IV) and total citrate, pH and CO_2 pressure, and for given values for the association quotients. This is being coupled to a least-squares program so that we can determine the best speciation scheme and the values for the associated equilibrium quotients.

b. Solubility Product of $\text{PuO}_2 \cdot n\text{H}_2\text{O}$. The reaction



is important because its equilibrium quotient is directly related to the solubility product of PuO_2 and because it typifies the solubility reactions that occur under mildly oxidizing conditions where Pu(V) is the principal soluble species. For these reactions we are continuing our study of reaction (2).

A measure of the extent of reaction (2) is the quantity $Q' = [\text{Pu(VI)}]/[\text{Pu(V)}]^2$. If the reaction reaches equilibrium, Q' will be the equilibrium quotient and will be independent of concentrations, independent of how the mixture was prepared, and independent of the Eh and the pH, for values of the pH less than about 3, where neither PuO_2^+ nor PuO_2^{2+} hydrolyze appreciably.

We have studied reaction (2) by preparing mixtures of Pu(IV) colloid, Pu(V), and Pu(VI) in a variety of ways shown below and by following the concentrations of Pu(V) and Pu(VI) spectrophotometrically.

- (1) Allowing Pu(V) to disproportionate in solutions initially containing only that oxidation state.
- (2) Mixing colloidal Pu(IV) with Pu(V) and/or Pu(VI).
- (3) Allowing colloidal sols of Pu(IV) to stand long enough for Pu(V) and Pu(VI) to form by oxidation (probably alpha induced).

Mixtures made by disproportionation of Pu(V) gave $\log Q'$ values close to 2.3 after standing at room temperature for 3 months. These mixtures were at unit ionic strength (LiClO_4), pH values 1.4 to 1.8, and the total Pu was $(1 \text{ to } 4) \times 10^{-2}$ M. Similarly, $\log Q'$ was found to be about 2.7 in an experiment in which Pu(V) was added to colloidal Pu(IV) to give a total Pu concentration of 1.6×10^{-3} M.

However, when attempts were made to establish equilibrium starting with colloidal Pu(IV) without Pu(V) present initially, very much higher $\log Q'$ values were obtained. When the initial colloid concentration was 6×10^{-3} M, $\log Q'$ was found to be about 4.8 after 6 months. In a similar experiment

using 0.014 M colloid, log Q' was about 5.2 after three months. In these experiments the average oxidation state increased by about $0.14 \pm 0.07\%$ per day.

At present it is not at all clear why observed values for log Q' are far smaller when colloidal Pu(IV) is formed from Pu(V) than when Pu(V) and Pu(VI) are formed by oxidation. It should be noted, however, that the relative amounts of colloid are much greater in the latter experiments. The conclusions to be drawn at present are that further work will be required before the system is understood and that solubility products determined from experiments such as these must all be viewed with caution.

c. Complex Formation Between Am(III) and Carbonate. A recent review of thermodynamic data for americium has indicated that there is considerable uncertainty in the identity and formation constants of Am(III) with carbonate.³² Because americium is an important waste element, this information will be needed to calculate americium solubility in water from Yucca Mountain. We have found that the citrate and carbonate ligands compete effectively in complexing Am(III). The solution absorption spectrum of Am(III) containing equal molar concentrations of citrate and carbonate was observed to be quite different from the spectra of solutions containing the individual ligands. Further study should yield the carbonate complexation quotients for Am(III) and indicate if mixed species are present.

5. Determination of Solubilities and Complexation of Waste Radio-nuclides Pertinent to Geologic Disposal at the Nevada Test Site (H. Nitsche and N. Edelstein). Work continued on the measurement of the solubilities of $^{237}\text{NpO}_2^+$, $^{237}\text{NpO}_2^{2+}$, $^{242}\text{Pu}^{4+}$, $^{242}\text{PuO}_2^+$, $^{242}\text{PuO}_2^{2+}$, and $^{243}\text{Am}^{3+}$, individually, in groundwater from the Nevada site and in aqueous NaClO_4 solutions of similar pH and ionic strength.³³ The NpO_2^{2+} , NpO_2^+ , and Am^{3+} solutions have reached equilibrium. The actinide concentration in the supernates was determined with a solid-state x-ray counting system utilizing the 29.4-keV decay line for ^{237}Np and 74.7-keV energy peak for ^{243}Am .³⁴ Oxidation state distribution analysis of these solutions was performed as adsorption spectrophotometry on a Cary 17 double beam recording spectrophotometer with 1-cm cuvettes and 0.1 M NaClO_4 at pH 7 as reference solution. Separation of solid and solution phases was made by centrifugal filtration with Centricon Microconcentrators (Amicon Corporation), molecular weight cutoff 30 000, pore size approximately 2 nm. Possible absorption of soluble material on the filters was minimized

by first filtering an aliquot of the sample and discarding the filtrate before filtering a second sample for analysis. Table VIII lists the analytical results.

No absorption band was found at 1223 nm that would indicate the presence of NpO_2^{2+} . The initially hexavalent neptunium solution underwent complete conversion to NpO_2^+ , whereas no change in oxidation state occurred for the NpO_2^+ and Am^{3+} solutions. The slight difference in concentration for the Am^{3+} solution between the results for gamma pulse height analysis (γ -PHA) and absorption spectroscopy can be attributed to variation in molar absorptivity. The value used ($\epsilon = 378 \text{ M}^{-1} \text{ cm}^{-1}$) has been determined in 0.1 M HClO_4 solution and not at pH 7, where a hydrolysis contribution might change the value.³⁵ The Pu^{4+} , PuO_2^+ , and PuO_2^{2+} solutions are near steady state; approximate numbers for supernate concentration determined by α -liquid scintillation counting are given in Table IX. Characterization of the solids by X-ray powder diffraction is currently being performed.

Because the presence of plutonium polymer can be expected in the supernates of these plutonium solutions, we wanted to familiarize ourselves with its solution properties.

TABLE VIII
ANALYTICAL RESULTS OF SOLUTIONS IN EQUILIBRIUM WITH THEIR
SOLID PHASE (SUPERSATURATED STARTING CONDITIONS)
IN 0.1 M NaClO_4 AT $\text{pH} = 7.0 \pm 0.1$, $25 \pm 1^\circ\text{C}$, AFTER 78 DAYS

	Initial Species	Concentration (mol/l) ^a	Concentration (mol/l) ^b	Final Species
1	NpO_2^{2+}	3.41×10^{-4}	3.47×10^{-4}	NpO_2^+
2	NpO_2^+	4.35×10^{-4}	4.49×10^{-4}	NpO_2^+
3	Am^{3+}	2.90×10^{-4}	2.35×10^{-4}	Am^{3+}

^a γ -PHA.

^b Absorption spectrophotometry

NpO_2^+ : 980 nm, $\epsilon = 395 \text{ M}^{-1} \text{ cm}^{-1}$

Am^{3+} : 503 nm, $\epsilon = 378 \text{ M}^{-1} \text{ cm}^{-1}$.

TABLE IX
PLUTONIUM CONCENTRATIONS IN EQUILIBRIUM WITH A SOLID PHASE

	<u>Initial Species</u>	<u>Mol/l</u>	<u>Time (Days)</u>
4	Pu ⁴⁺	~2 x 10 ⁻⁸	69
5	PuO ₂ ²⁺	~8 x 10 ⁻⁸	62
6	PuO ₂ ⁺	~3 x 10 ⁻⁹	61

The Pu(IV) polymer was prepared from ²⁴²Pu⁴⁺ stock by hydroxide precipitation and redissolution of the precipitate in a small amount of concentrated HCl. Dilution with CO₂-free H₂O gave a solution with 1.9 x 10⁻³ M total plutonium concentration and 0.05 M [H⁺]. All manipulations were done in a inert box. After 7 days, approximately 28% of the plutonium was converted to Pu(IV) polymer. The plutonium polymer concentration was determined by absorption spectrophotometry utilizing the band at 613 nm. The remaining plutonium in solution was PuO₂⁺ (~50%) and Pu³⁺ (~22%). A part of this solution underwent a cation-exchange column separation on Dowex AG 50 x 8 resin (200 to 400 mesh) in order to obtain pure Pu(IV) polymer. The absorption spectra of the polymer agreed well with published data, although our molar absorptivity value of 11 to 12 M⁻¹ cm⁻¹ for the 613-nm line was lower than reported.³⁶

After 7, 21, and 27 days, no change was noticeable in oxidation-state distribution for both the polymer mixture before the ion exchange and the Pu(IV)-polymer solution. The fate of the oxidation-state distribution in these solutions will continue to be monitored. Separations of the Pu(IV) polymer with an Eppendorf Microcentrifuge (12 000 x g, ~100 nm sizing) and with an Amicon Microconcentrator (sizing ~2 nm) showed that 65.5% of the polymer had a size of <100 nm, and 0.4% a size of <2 nm, respectively.

The rather low concentrations of our plutonium supernate solutions require also a different method than absorption spectrophotometry for the determination of oxidation-state distribution of solution species. The most commonly used method utilizes a combination of coprecipitation with rare earth fluorides and both thenoyltrifluoroacetone (TTA) and hexone (methyl

isobutyl ketone) extractions.³⁷ The methods used and their selectivity for specific oxidation states are given in Table X.

The TTA-extraction method was tested individually on Pu^{4+} , Pu^{3+} - Pu^{4+} , and Pu^{4+} - PuO_2^{2+} mixtures of known concentration at the 10^{-4} M level in air. Oxidation-state distribution was verified by absorption spectrophotometry.

Extraction of Pu^{4+} - Pu^{3+} mixtures was performed in 0.5 M TTA/xylene in acetate buffered solution at pH 4; $92 \pm 2\%$ of total plutonium was recovered. TTA-extractions at pH 0 always yielded $98 \pm 2\% \text{ Pu}^{4+}$. Several hexone extractions on Pu^{4+} - PuO_2^{2+} led to irreproducible results; PuO_2^{2+} - Pu^{4+} recovery was between 60 and 100%. This can be due to the fact that the phase boundaries are not very distinct since they are formed by two colorless solutions.

Our study also showed that the plutonium-state measurements are more reliable and reproducible if fewer extraction steps are involved. For example, a TTA-extraction of the Pu^{4+} at pH 0 followed by an additional TTA-extraction of the Pu^{3+} at pH 4 gave an erroneous value for the Pu^{3+} , whereas the determination as the difference of the results for the two extractions performed separately agreed well with the Pu^{3+} value determined by spectrophotometry.

TABLE-X
OXIDATION STATE DISTRIBUTION

Method	Organic Phase	Aqueous Phase
TTA-extraction ³⁸ at pH 0	IV	III, V, VI, polymer
TTA-extraction ^{38,39} at pH 4	III and IV	IV, VI, polymer
Hexone-extraction	IV and VI	III, V, polymer
LaF_3 -precipitation method with holding- oxidant	III, IV, polymer in precipitate	V, VI in supernate

Finally, Pu^{3+} , Pu^{4+} , Pu(IV) polymer, and PuO_2^{2+} mixtures were analyzed by the above-described methods at the 10^{-4} M and 10^{-7} M levels in an argon-atmosphere glove box. First, the concentrations of the Pu^{4+} - PuO_2^{2+} mixture and Pu(IV) -polymer were determined by spectrophotometry at 10^{-4} M and 10^{-3} M, respectively. Second, the two solutions were mixed to yield a total plutonium concentration of 1.844×10^{-4} M. And third, this solution was diluted with 1 M HCl to a total plutonium concentration of 9.67×10^{-8} M. Then both solutions underwent the oxidation-state analysis. Each extraction and coprecipitation was done in parallel at both concentrations to exclude possible changes of the solution composition with time. Results are given in Table XI.

All samples were assayed by α -liquid scintillation counting and corrected for background. Quenching effects in the TTA-samples were considered by setting the energy window of the Packard A 460C Scintillation Counter appropriately. A modification of the instrument enables us to monitor the α -liquid-scintillation spectrum on a multichannel analyzer.

Because the ^{242}Pu test solutions contain a small amount of ^{241}Pu , corrections for the daughter nuclide ^{241}Am of the liquid scintillation counting results were also made. All samples were analyzed by counting the 59.5 keV ^{241}Am γ -ray with a solid-state x-ray counting system.

The values for the 10^{-4} M starting concentration agree to within $\pm 5\%$ with the findings by absorption spectroscopy. Agreement between 10^{-8} M and 10^{-4} M mixtures is within $\pm 5\%$ for Pu^{3+} and the sum of PuO_2^+ and PuO_2^{2+} . However, for Pu^{4+} the value is 20% higher at the lower concentration, and no Pu(IV) polymer was recovered.

One could conclude that either the polymer extracted into TTA at pH = 0 at low concentration or that the 10^{-7} M plutonium-stock solution was depolymerized with 1 M HCl solution to yield Pu^{4+} . Therefore, we repeated the TTA extraction at pH 0 as a function of time. Extractions were performed 15, 45, 90, and 180 minutes after preparation of a 10^{-8} M solution by dilution. The results showed that no polymer extracted into the TTA phase; however, not all of the polymer could be found in the aqueous phase. Experiments are being considered to ascertain the source of this discrepancy.

TABLE XI
RESULTS OF OXIDATION-STATE DISTRIBUTION DETERMINATION ON PLUTONIUM OXIDATION-STATE MIXTURES
25 ± 1°C, ARGON ATMOSPHERE

Method	Oxidation State	Total Pu 1.844×10^{-4} Concentration (M) (% Total)	Total Pu 9.67×10^{-8} Concentration (M) (% Total)	Total Pu 1.844×10^{-4} Concentration (M) (% Total)
TAA, pH = 0 (direct)	Pu ⁴⁺	9.45×10^{-5} (53.3)	7.65×10^{-8} (74.4)	8.69×10^{-5} (47.1)
TTT, pH = 4 (indirect)	Pu ³⁺	1.77×10^{-5} (9.8)	1.53×10^{-8} (14.9)	below detection
LaF ₃ , pcpt. (indirect)	Pu(IV)- polymer	4.30×10^{-5} (23.8)	8×10^{-10} (0.9)	5.6×10^{-5} (30.4)
LaF ₃ , supernate (direct)	PuO ₂ ⁺ + PuO ₂ ²⁺	2.54×10^{-5} (14.1)	1.02×10^{-8} (9.9)	1.23×10^{-5} (6.7) (only PuO ₂ ²⁺) PuO ₂ ⁺ , below detection
Total Yield		1.806×10^{-4} (97.9)	1.028×10^{-7} (106.3)	1.552×10^{-4} (84.2)

^aResults from absorption spectroscopy.

E. Sorption and Precipitation

1. Batch Sorption Experiments of Uranium, Tin, and Thorium (B. P. Bayhurst, S. D. Knight, and K. W. Thomas). Batch desorption measurements have been completed for uranium and tin with water from Well J-13 on tuff samples described in the last quarterly report⁴⁰ and are reported in Table XII. The uranium desorption values measured do not follow the trend observed previously where desorption values had been up to 2.5 times higher than sorption values. However, there may be very large errors in the experiments due to the very small degree of uranium sorption initially, and these results are not disturbing. The tin desorption ratios were as expected.

Although not specifically listed by the Environmental Protection Agency (EPA) in 40CFR191 as a primary hazardous waste element, thorium is important because ^{230}Th is the long-lived parent of ^{226}Ra , which is considered a hazardous nuclide. Because of the long half-life of ^{230}Th ($t_{1/2} = 7.5 \times 10^4$ yr), radium may be transported in the form of the parent thorium isotope. Therefore, it is important to characterize the sorption properties of thorium as well as radium. Initial studies of thorium solubility and sorption were described previously.⁴¹ Table XIII lists sorption ratios measured this quarter on four tuff samples. USW G-1-1292 and USW G-1-2233 are described by Daniels et al.;²² USW G-1-2289 contains 37% mordenite, 5% clinoptilolite, 7% quartz, 4% cristobalite, and 45% alkali feldspar; USW G-1-2363 contains 33% quartz and 62% alkali feldspar.

The thorium sorption ratios do not correlate with either pH or mineralogy. The thorium tracer feed solution was adjusted to pH 5.6 to 5.8 with NH_4OH prior to filtering, yet the yield through the 0.5- μm filter was only 12 to 24%. Previous experiments had shown thorium solubility to be much higher at this pH. It is suspected that the neutralization process might have caused some precipitation of thorium prior to filtering. Once the sorption experiments were under way, the pH was measured every other day. At 12 days the pH reached 7, the experiments were halted and the sorption ratios measured. Experiments are just beginning in the controlled CO_2 atmosphere box to be compared with these ambient atmosphere conditions.

2. Long-Term Sorption Experiments on Technetium and Neptunium (S. D. Knight, F. O. Lawrence, M. R. Cisneros, and K. W. Thomas). The long-term sorption experiments for technetium and neptunium were started 9 months ago to determine whether the measured sorption ratios for these two elements

TABLE XII
DESORPTION RATIOS FOR URANIUM AND TIN IN J-13 GROUNDWATER

Core ^a	Element	Traced Feed pH	Traced Feed Concentration (M)	Desorption Ratios ^b (ml/g)		
				Experimental (pH)	Value	Average ^c
G-1-1982	Uranium	8.72	2.7×10^{-6}	0 (8.05)	4.1 (8.06)	2.1(1.4) ^d
G-1-2233	Uranium	8.72	2.7×10^{-6}	9.1 (8.28)	6.6 (8.27)	7.9(0.9) ^d
G-1-2698	Uranium	8.62	2.7×10^{-6}	1.3 (8.13)	1.7 (8.10)	1.5(0.1) ^d
G-1-2840	Uranium	8.59	2.7×10^{-6}	0 (8.23)	0 (8.39)	0 ^d
G-1-3116	Uranium	8.78	2.7×10^{-6}	1.4 (8.31)	1.9 (8.33)	1.7(0.2) ^d
GU-3-1937	Uranium	8.68	2.7×10^{-6}	7.2 (8.31)	9.8 (8.31)	8.5(0.8) ^d
G-1-2840	Tin	8.41	2×10^{-8}	910	650	780(130)
G-1-2901	Tin	8.38	1×10^{-7}	30 100	45 700	38 000(8000)
GU-3-1301	Tin	8.47	2×10^{-8}	1100 (8.52)	1460 (8.45)	1280(180)
G-4-1502	Tin	8.48	3×10^{-8}	503	492	500(8)

^aFraction size is 75 to 500 μm .

^bAll desorption times were 6 weeks.

^cNumbers in parentheses are standard deviations of the mean.

^dDesorption measurements are subject to larger errors than sorption measurements when the initial sorption ratios are low.

TABLE XIII
SORPTION RATIOS FOR THORIUM IN J-13 GROUNDWATER

Core ^a	Traced Feed pH	Traced Feed Concentration (M)	Sorption Time (days)	Sorption Ratios (ml/g)		
				Experimental (pH)	Value	Average ^b
USW G-1-1292	5.61	5.39×10^{-8}	12	566 (7.52)	389 (7.52)	478(63)
USW G-1-2233	5.75	1.07×10^{-7}	12	266 (7.00)	421 (6.93)	344(55)
USW G-1-2289	5.76	5.86×10^{-8}	12	140 (6.89)	146 (6.86)	143(2)
USW G-1-2363	5.60	6.52×10^{-8}	12	940 (6.83)	1484 (6.82)	1213(193)

^aFraction size was 75 to 500 μm .

^bNumbers in parentheses are standard deviations of the mean.

change over long-time periods. As seen from the data in Table XIV, there have been no changes in the measured sorption ratios for these two elements over a 9-month period. The studies will be completed after 15 months. The tuff samples being investigated are described in Bryant and Vaniman.⁴¹

3. Neptunium Sorption Isotherm Measurements (F. O. Lawrence, M. R. Cisneros, and K. W. Thomas). An investigation is under way to determine the effect of radionuclide concentration on the measured sorption ratio. Such studies are referred to as isotherm measurements. Isotherm measurements are nearly complete for neptunium on tuff sample USW G-4-1608, a zeolitized tuff. The data are given in Table XV. These experiments were performed in a CO₂-controlled atmosphere box in order to maintain the pH close to 7, the general pH value for groundwaters found at Yucca Mountain.

TABLE XIV
 LONG-TERM NEPTUNIUM AND TECHNETIUM SORPTION
 RATIOS IN Well J-13 GROUNDWATER

Core ^a	Element	Traced Feed pH	Traced Feed Concentration (M)	Sorpton Time	Sorpton Ratios (ml/g)		
					Experimental Values (pH)		Average ^b
GU-3-916	Neptunium	Not avail- able	6×10^{-11}	6 weeks	4.8 (8.76)	4.9 (8.65)	4.8(1)
				3 months	5.1 (8.69)	5.4 (8.68)	5.3(1)
				6 months	5.6 (8.48)	5.2 (8.54)	5.4(1)
				9 months	5.1 (8.24)	5.1 (8.08)	5.1(1)
0.72(0.2)	Technetium	8.57	6×10^{-10}	6 weeks	0.50 (8.51)	0.94 (8.57)	
				13 weeks	0.33 (8.75)	1.3 (8.70)	
				6 months	0.81 (8.61)	0.44 (8.66)	
				9 months	0.14 (8.81)	0.11 (8.83)	
0.81(0.5)							
0.62(0.2)							
0.13(0.02)							

TABLE XIV (cont)

Core ^a	Element	Traced Feed pH	Traced Feed Concentration (M)	Sorption Time	Sorption Ratios (mg/g)		
					Experimental Values (pH)		Average ^b
GU-3-1301	Neptunium	8.4	2×10^{-11}	6 weeks	1.8 (8.53)	1.7 (8.54)	1.7(1)
				3 months	2.3 (8.63)	2.1 (8.65)	2.2(1)
		3 months	2.1 (8.65)	1.9 (8.67)	2.0(1)		
		6 months	2.2 (8.55)	2.3 (8.62)	2.2(1)		
		9 months	1.9 (8.46)	1.8 (8.47)	1.9(1)		
		6 weeks	0.058 (8.41)	0.022 (8.47)	0.04(0.02)		
	Technetium	8.67	7×10^{-10}	13 weeks	0.065 (8.63)	0.002 (8.69)	0.03(0.03)
				6 months	-0.003 (8.60)	0.004 (8.61)	0
				9 months	0.013 (8.70)	0.031 (8.72)	0.02(0.01)

TABLE XIV (cont)

Core ^a	Element	Traced Feed pH	Traced Feed Concentration (M)	Sorption Time	Sorption Ratios (ml/g)		Average ^b
					Experimental	Values (pH)	
G-4-1502	Neptunium	8.72	1×10^{-10}	6 weeks	4.6 (8.33)	3.5 (8.32)	4.0(1)
				3 months	5.1 (8.66)	3.4 (8.70)	4.3(1)
				6 months	4.7 (8.44)	5.0 (8.49)	4.8(1)
				9 months	5.2 (8.37)	5.0 (8.53)	5.1(1)
	Technetium	8.74	8×10^{-10}	6 weeks	0.042 (8.60)	-0.003 (8.60)	0.02(0.02)
				13 weeks	0.06 (9.00)	-0.038 (8.81)	0.01(0.05)
				6 months	-0.085 (8.65)	-0.09 (8.65)	0
				9 months	-0.06 (8.71)	-0.05 (8.75)	0

^aFraction size is 75 to 500 μ m.

^bNumbers in parentheses are standard deviations of the mean.

The measured sorption ratios are independent of the neptunium concentration at concentrations less than 10^{-5} M and show little variation at greater concentrations. Comparisons of sorption ratios measured in a CO_2 -controlled atmosphere and under ambient conditions are shown in Table XVI. With the exception of tuff USW GU-3-433, the ratios are unaffected by the atmospheric conditions studied. The USW GU-3-433 experiment will be repeated. Data were also obtained for ^{233}Pa , the daughter nuclide of the tracer, ^{237}Np . These are reported in Table XVII.

4. Effect of Goundwater Composition on the Sorptive Properties of Tuff (S. D. Knight, and K. W. Thomas). Because groundwater composition may vary between the repository and the accessible environment, studies are being conducted to determine what effect various groundwater compositions have on the measured sorption ratio. Comparisons are being made between sorption measurements performed using water from Well J-13 and those using water from the 1298- to 1782-m zone of Well UE-25p#1. Well UE-25p#1 water has a much higher concentration of calcium, magnesium, strontium, barium, sodium, bicarbonate, and sulfate than does Well J-13 water. The detailed compositions of these two waters are discussed in the previous quarterly report.³⁴

Table XVIII gives the results obtained for tin using Well UE-25p#1 water, and Table XIX compares results of sorption in Well J-13 groundwater with sorption in this water. In general, tin sorption ratios are higher for Well UE-25p#1 water than for Well J-13 water, the same effect observed for europium previously. It is suspected that precipitation of tin occurs in the higher ionic strength water. While the sorption ratios measured cover a wide range, none of the ratios was less than 100 ml/g. The sorption ratios for tin do not appear to be related to mineralogic composition of the tuff. However, USW G-1-2901, a devitrified tuff with a small amount of calcite, had very high sorption and desorption ratios in both groundwaters. The highly zeolized tuff, USW G-4-1502, had low sorption ratios in both groundwaters; thus tin sorption ratios seem to be independent of zeolitic content. This is not unexpected for a tetravalent species.

These studies continue to show that groundwater composition can have a significant effect on the sorptive behavior of elements. Future work will include additional tuff samples and water from Well USW H-3.

TABLE XV
NEPTUNIUM ISOTHERM SORPTION RATIOS UNDER
CO₂-CONTROLLED ATMOSPHERIC CONDITIONS^a

Traced Feed Concentration (M)	Traced Feed pH	Isotope(s) of Np Present	Sorption Ratios (ml/g)		
			Experimental Values (pH)		Average Value ^b
6 x 10 ⁻⁴	7.0	²³⁷ Np, ²³⁵ Np	2.0 (6.4)	2.7 (6.3)	2.4(1)
3 x 10 ⁻⁴	7.2	²³⁷ Np, ²³⁵ Np	1.3 (6.4)	0.57 (6.5)	0.94(1)
7 x 10 ⁻⁵	7.3	²³⁷ Np, ²³⁵ Np	3.5 (6.7)	3.2 (6.7)	3.4(1)
3 x 10 ⁻⁵	7.2	²³⁷ Np, ²³⁵ Np	3.4 (6.7)	3.1 (6.7)	3.3(1)
8 x 10 ⁻⁶	7.3	²³⁷ Np, ²³⁵ Np	4.7 (6.7)	5.1 (6.7)	4.9(1)
3 x 10 ⁻⁶	7.3	²³⁷ Np, ²³⁵ Np	4.5 (6.7)	5.4 (6.7)	5.0(1)
7 x 10 ⁻⁷	7.3	²³⁷ Np, ²³⁵ Np	5.2 (6.7)	4.7 (6.7)	5.0(1)
4 x 10 ⁻⁷	7.3	²³⁷ Np, ²³⁵ Np	4.4 (6.7)	5.9 (6.7)	5.2(1)
2 x 10 ⁻¹¹	7.2	²³⁵ Np	5.2 (6.7)	5.6 (6.8)	5.4(1)

^aCore was G-4-1608, 75 to 500 μm. Atmosphere was enriched in CO₂ to ~5%. Sorption was for 6 weeks.

^bNumbers in parentheses are standard deviations of the mean.

TABLE XVI
COMPARISON OF NEPTUNIUM SORPTION RATIOS UNDER AMBIENT
AND CONTROLLED ATMOSPHERIC CONDITIONS

Core ^a	Atmospheric ^b Conditions	Traced Feed pH	Traced Feed Concentration (M)	Sorption ^c or Desorption	Sorption Ratio (mg/g)		
					Experimental Value (pH)	Average Value ^d	
GU3-433	Ambient	8.6	3×10^{-11}	Sorption	13 (8.4)	14 (8.4)	13.5(1)
	CO ₂	6.8	8×10^{-12}	Sorption	0.82 (6.6)	0.68 (6.7)	0.75(1)
GU3-1203	Ambient	8.6	3×10^{-11}	Sorption	0.5 (8.4)	0.49 (8.5)	0.49(1)
	CO ₂	7.1	6×10^{-11}	Sorption	0.36 (6.8)	0.35 (6.8)	0.35(1)
GU3-1301	Ambient	8.4	2×10^{-11}	Sorption	1.8 (8.53)	1.7 (8.54)	1.7(1)
				Desorption	18 (---)	18 (8.42)	18(1)
	CO ₂	---	2.5×10^{-11}	Sorption	2.1 (6.65)	2.1 (6.63)	2.1(1)
				Desorption	31 (6.15)	26 (6.14)	29(3)
G4-1608	Ambient	8.7	3.5×10^{-11}	Sorption	6.1 (8.3)	6.6 (8.4)	6.3(1)
	CO ₂	7.2	2×10^{-11}	Sorption	5.2 (6.7)	5.6 (6.8)	5.4(1)

^aFraction size was 75 to 500 μ m.

^bCO₂-atmosphere was controlled to be enriched to ~5% in CO₂.

^cSorption and desorption times were 6 weeks.

^dNumbers in parentheses are standard deviations of the mean.

TABLE XVII
 PROTACTINIUM ISOTHERM SORPTION RATIOS UNDER
 CO₂-CONTROLLED ATMOSPHERIC CONDITIONS^a

Traced Feed Concentration (M)	Traced Feed pH	Experimental Value (pH)		Average Value ^b
1×10^{-11}	7.0	3.4 (6.4)	5.3 (6.3)	4.4(1)
5×10^{-12}	7.2	5.0 (6.4)	5.0 (6.5)	5.0(1)
1×10^{-12}	7.3	3.8 (6.7)	4.1 (6.7)	4.0(1)
5×10^{-13}	7.2	5.3 (6.7)	10.1 (6.7)	7.7(2.4)
1×10^{-13}	7.3	8.4 (6.7)	8.0 (6.7)	8.2(1)
5×10^{-14}	7.3	3.3 (6.7)	4.1 (6.7)	3.7(1)

^aCore was G-4-1608, 75 to 500 μ m. Atmosphere was enriched in CO₂ to ~5%. Sorption was for 6 weeks.

^bNumbers in parentheses are standard deviations of the mean.

TABLE XVIII
TIN SORPTION RATIOS IN WELL UE-25p#1 GROUNDWATER^a

Core ^b	Traced Feed pH	Traced Feed Concentration (M)	Sorption ^c or Desorption	Sorption Ratios (mg/g)		
				Experimental Values (pH)		Average Value ^d
G1-2840	8.86	6×10^{-8}	Sorption	18 000 (8.84)	22 700 (8.89)	20 000(2700)
			Desorption	25 300 (9.00)	11 600 (9.02)	18 400(6900)
GU3-1301	8.88	9×10^{-8}	Sorption	3480 (8.99)	4420 (8.99)	4000(520)
			Desorption	X	6750 (9.10)	6750
G4-1502	9.01	7×10^{-8}	Sorption	706 (9.05)	910 (9.06)	800(110)
			Desorption	428 (9.16)	182 (9.18)	300(130)
G1-2901	8.75	1×10^{-7}	Sorption	35 000 (8.82)	36 700 (8.94)	35 800(900)
			Desorption	54 400 (8.97)	50 700 (8.98)	52 500(1900)

^aWater taken from a depth of 1298 to 1792 m.

^bFraction size was 75 to 500 μ m.

^cSorption and desorption times were 6 weeks.

^dNumbers in parentheses are standard deviations of the mean.

TABLE XIX

COMPARISON OF TIN SORPTION RATIOS IN J-13 AND UE-25#1^a GROUNDWATERS

Core	Sorption Ratios (m ℓ /g)		Desorption Ratios (m ℓ /g)	
	Well J-13	Well UE-25#1	Well J-13	Well UE-25#1
USW G-1-2840	283	20 000	780	18 400
USW GU-3-1301	168	4000	1280	6750
USW G-4-1502	215	800	500	300
USW G-1-2901	22 000	35 800	38 000	52 500

^aWater from depth 1298 to 1792 m.F.. Dynamic Transport Processes

A Kinetic Effect in Actinide Sorption (J. L. Thompson, P. Q. Oliver, W. R. Daniels, and R. S. Rundberg). In a previous report⁴² we have described a kinetic effect for plutonium and americium sorption on crushed tuff columns run at moderate flow rates (about 100 m/yr). Our purpose in writing this section is to summarize the experimental data relative to this kinetic effect which, to our knowledge, has not been discussed in the literature. While we have not identified the underlying causes for the slow sorption of the actinides studied to date, we believe this to be related to the sorption process itself, and not to be an artifact of the experimental design or mode of construction and operation of the columns. Furthermore, the kinetic effect appears to be present for a variety of sorption substrates and may prove to be a significant factor in modeling actinide retardation.

The columns with which the kinetic studies have been performed are constructed from acrylic tubing. They are 5 cm long, about 1 cm³ in volume, and fitted with polyethylene frits and polypropylene Leur fittings. Typical column parameters for a filled column are column density (ρ) = 1.7 g/ml, column porosity (ϵ) = 0.6, and free column volume of 0.5 ml. The experiments are carried out at constant flow rate and constant feed concentration.

The volume at which the solvent (water) from the feed solution first appears in the effluent is determined using tritium. When an actinide is present in the feed solution, the volume at which the actinide first appears in the effluent is compared to the volume at which the solvent first appears. This ratio is called the retention factor, R_f . It can be related to the sorption ratio, R_d , by $R_f = 1 + (\rho/\epsilon)R_d$ (Ref. 43). [The conventional formulation is $R_f = 1 + (\rho/\epsilon)K_d$, where K_d is the distribution coefficient. In the geochemical research conducted at Los Alamos in support of the NNWSI, the term "sorption ratio" is used rather than "distribution coefficient" to emphasize the fact that equilibrium conditions have not necessarily been obtained.⁴⁴] The tuffs with which we have been working typically have sorption ratios of a hundred or greater for plutonium and americium, so it was anticipated that a column with the parameters given above would yield R_f values of at least several hundred. This was found to be in sharp contrast with our observation that a portion of the activity moved through the column with the solvent front (that is, R_f approximately = 1). The tuffs studied to date in our flow column experiments with plutonium and americium are specified in Table XX, along with R_d values as determined by the batch technique and as calculated from the column R_f values. Also included are some preliminary data on neptunium sorption. Here the contrast is not quite so striking, since neptunium has rather low sorption ratios. Nevertheless, the R_d values as calculated from the column elutions are significantly lower than those determined by batch techniques. Note that in both batch and column experiments the amounts of actinide involved are small. Solutions are generally about 10^{-8} M in the actinide; sorbed actinides on the crushed tuff are about 10 ppb. Because the elution pattern of the actinides from these columns was so different from what was expected on the basis of the batch R_d values, numerous experiments were performed to check the column behavior. It was found that similar replicate results were obtained from duplicate columns and from the same columns on repeat runs. Also, column elutions of tritiated water and of ^{85}Sr indicated that the column performance was normal. Slowing the flow rate of feed solution from 0.15 ml/h to 0.025 ml/h made only a slight difference in the volume at which the activity broke through. We came to the conclusion that for these columns 10 to 50% of the input radionuclide concentration activity will appear with the solvent front, or quite close to it. We then did an experiment using our usual batch

TABLE XX
KINETIC STUDIES OF SORPTION COLUMNS

Experiment	Tuff	Type	Constituents	R _d Values	
				Batch	Column
Plutonium	JA-37	Welded	Glass, feldspar, cristobolite	4 E2	4
	YM-49	Partially welded			
	USW G-1-1883	Partially welded	Feldspar, quartz, cristobolite	8 E1	0.3
	UI2G	Zeolitized	Clinoptilolite, feldspar	3 E2	0.5
USW G-1-1292	Welded	Glass, feldspar, cristobolite	6 E2 ^a	<1	
Americium	USW G-1-1292	Welded	Glass, feldspar, cristobolite	3 E4 ^a	<1
	USW G-1-1436	Zeolitized	Clinoptilolite, quartz, cristobolite, feldspar	2 E3	<1
	USW GU-3-1301	Vitric	Glass, feldspar, cristobolite, quartz		<1
Neptunium	JA-37	Welded	Glass, feldspar, cristobolite	2 E1	4
	YM-49	Partially welded	Glass, feldspar, clinoptilolite	8 E0	2
	USW G-1-1883	Partially welded	Feldspar, quartz, cristobolite	6 E0	0.5

^aEstimated value.

methodology, but for short contact times. We used USW GU-3-1301 tuff, which had previously yielded R_d values of 1500 to 2000 ml/g for 6-week contact periods. Our results for contact times of 6 hours, 24 hours, and 8 days were 54, 84, and 2000 ml/g, respectively. A number of experiments are now under way which will yield data on short term versus long term R_d values for plutonium and americium with a variety of tuffs.

Several explanations may be advanced to account for the appearance of actinides in the effluent with the solvent front. (1) A contact time longer than a few hours may be required for sorption of all the input species to occur. (2) The species originally present in the feed solution may not sorb completely, but may change slowly (in a period of days) to a more sorbable species. (3) The activity appearing with the solvent front may be due to colloid-sized particles (carrying sorbed radioactivity) that have washed from the column.

The idea that our observed kinetic effect is due to speciation changes has some appeal. The feed solutions are prepared by our standard method, which involves air drying an acid solution of the actinide, taking the residue up in groundwater, and filtering through a 0.05- μ m Nuclepore filter. In the case of plutonium, we have experimental evidence that suggests that several oxidation states are represented in the final solution. These might well have differing sorption properties, so that some plutonium would be sorbed while some passed through the column with the solvent. Also, in a matter of a few days, equilibria conditions might lead to conversion of nearly all of the plutonium to a strongly sorbed species, thus accounting for the long-term batch experiment results. However, these arguments become very tenuous when applied to americium, which presumably exists in only one oxidation state. Furthermore, in one experiment some of the americium feed solution was held in a polycarbonate tube for 7 days prior to being used. This fraction of the solution gave the same elution pattern as the portion used immediately after preparation. Thus, while an explanation invoking speciation may seem useful when applied to the plutonium data, it appears inadequate as an aid to rationalizing the americium data.

The idea that colloidal material could cause the observed activity breakthrough was discredited by the following experiment. Duplicate columns of tuff were prepared and washed with special care to remove as many of the fine particulates as possible. One column was run with the feed solution

filtered through a 0.05- μ m Nuclepore filter, as usual; the other column, with a feed solution of groundwater that had only been centrifuged enough to remove larger, visible particulates. Both columns showed similar elution behavior, with somewhat less activity being eluted from the column having colloidal material in the feed solution. We conclude from this that because flooding a column with colloids does not appreciably affect its elution behavior, the presence of relatively small amounts of colloidal material could not cause the breakthrough of any large fraction of the input activity.

The evidence accumulated so far, then, leads us to believe that the sorption process itself must involve one or more time-dependent steps. It may be, for example, that some sorption must be preceded by diffusion and that a few hours' contact time is insufficient for enough diffusion to take place to allow all the feed material to reach sorption sites. Obviously, more experimental work should be directed toward resolving the uncertainties surrounding this interesting kinetic effect. We believe this kinetic effect may have significance for waste management. For example, models of actinide transport may have to be modified to account for the observation that the source material can move over short time periods much farther than would be predicted on the basis of R_d values determined by long-range batch measurements.

A program to numerically invert autocorrelated photon spectroscopy data was developed. The code, which uses regularization and a positivity constraint, will enable a detailed study of particle size distributions. This advance will greatly enhance the ability of NNWSI to address the question of colloid or particulate transport.

Two additional 2-m crushed-tuff columns have been prepared each containing USW G-2-339 tuff, a montmorillonite-containing tuff, for use in anion exclusion studies and actinide transport studies. These long columns will provide long residence times to access actinide adsorption kinetics in a dynamic system.

The fractured tuff columns are continuing to be eluted with cationic tracers, and the results are in the process of being interpreted with matrix diffusion models. New solid rock core columns are being prepared in an effort to find cores permeable enough to enable transport experiments in a reasonable time frame.

G. Retardation Sensitivity Analysis (B. J. Travis, S. Hodson, E. Nutall, and L. Brown)

1. Field Studies. We summarize the details of two field studies of heavy element radionuclide migration and assess their relevance to the NNWSI project. One of these studies is described in the draft report by Polzer et al.⁴⁶ That report investigates the mobility of plutonium and americium species in Mortandad Canyon. Treated waste effluents from the Central Waste Treatment Plant, TA-50, at the Los Alamos National Laboratory have been released to the environment in Mortandad Canyon since 1963. Analysis of water and sediment samples as well as deeper well water samples provided information on the mobility of the discharged plutonium and americium nuclides. Water samples were collected from as far as 3400 m downstream of the effluent, from the channel, and from access wells at depths of 2 to 20 m below the channel surface. The desert canyon stream has rather complex hydrology with episodic recharge from spring snow melt and from summer rains.

Analysis of samples indicated that 99% of the released radioactivity associated with the runoff was captured by suspended sediments of 0.45 μm and greater. The nature and location of the remaining 1% radioactivity was the focus of that report. Reported maximum concentrations of plutonium and americium were about 15 pCi/g. There was indication that colloid size may be important to nuclide mobility. The exact chemical nature of the colloids was not fully investigated nor was the source of the colloids identified; that is, did the colloids originate with the effluent or were they pseudocolloids and if so what was their composition.

In summary, that report and the associated investigations at Mortandad Canyon clearly indicate the presence and enhanced migration of radiocolloids; however, the experiments were not controlled as in a laboratory environment and, therefore, the data are quite limited in terms of their usefulness in system modeling. The study is not suitable for code or model verification. However, an analysis of the data and system could identify the types of data needed for modeling and perhaps add to our general understanding of colloid migration.

The second field study⁴⁶ involves radionuclide migration from four gravel/cobble rock liquid waste disposal beds located at Los Alamos in Area T. These disposal beds, which received radioactive liquid wastes discharged from the DP West plutonium purification and liquid waste treatment

facility, were completed in 1945. Liquid waste in varying amounts and types was discharged into these beds between 1945 and 1967. Plutonium and ^{241}Am were the primary radionuclides. This site has been extensively studied (over 17 reports) beginning with a study of soil samples taken from the site in 1946 and continuing to the present with the most recent report. This is a highly studied and well-characterized site.

The most recent report/paper by Nyhan et al.⁴⁷ provides a well documented history of the site and presents study findings that include the analysis of about 800 tuff samples taken from drill cores. Sampling holes were drilled to a depth of 30 m below two of the disposal beds.

The significant implications for nuclear waste management are that plutonium and ^{241}Am migrated (at this site) much faster and farther than indicated by earlier laboratory experiments. Plutonium was measured at depths of 30 m below the disposal beds while laboratory column/core studies reported in 1959 showed essentially complete adsorption and retention of plutonium in the top few millimeters of the tested cores.

The DP West site and the proposed Yucca Mountain site have many similar characteristics that could aid in the evaluation of Yucca Mountain. These similarities are (a) welded volcanic tuff, (b) fractured flow regions, (c) partially saturated flow, (d) episodic recharge, and (e) migration in a vertically downward direction. There are important differences also. The tuff at DP site is not the same as found at Yucca Mountain. Also, the recharge was considerably greater than expected at the NTS. There is a strong possibility that the accelerated transport observed at the DP West site was due to presence and migration of radionuclides down fractures in the Bandelier tuff and/or to dependence of sorption on pH.

We are currently enhancing the TRACR3D transport code to include radiocolloid migration. The new version of TRACR3D can quantitatively analyze the experimental data and test various flow and transport scenarios that may have contributed to the rapid migration of plutonium and ^{241}Am .

2. Analysis of Laboratory Measurements of Colloids. A sophisticated laser system is being used to study colloid size distributions under laboratory conditions. The laser scattering process can be described mathematically as a Fredholm integral equation of the first kind:

$$g(t) = \int_a^b K(x, \sigma) f(\sigma) d\sigma, f(\sigma) > 0, \quad (3)$$

where $K(x, \sigma)$ is called a kernel function and represents the physical process, $g(t)$ represents the observations and $f(\sigma)$ is the unknown particle size distribution. Strictly speaking, the true $f(\sigma)$ cannot be recovered uniquely because of the presence of error in measurements. The effect of error must be "smoothed" out.

Equation (3) does not have a unique classical solution. One solution to this difficulty is to convert Eq. 3 to a Fredholm integral equation of the second kind that is well-behaved mathematically. This is done by adding a small smoothing term to give

$$\int_c^d K(t, \sigma)g(t)dt = \int_a^b \int_c^d K(t, \sigma)K(t, z) f(z)dzdt + \alpha f(\sigma), f(\sigma) > 0 \quad (4)$$

Here α is a small parameter that is related to the size of the error in the data. When α is small, Eq. (4) is close in a sense to Eq. (3).

Stated simply, the only way to get a solution to Eq. (3) is to add assumptions such as a certain degree of smoothness in the distribution functions. The degree of resolution that can be obtained in $f(\sigma)$ depends on the amount of data, the magnitude of error in the data, the nature of the kernel function, and the accuracy of the numerical integration.

A computer code called INVPOS has been written that solves Eq. (4) for the general case. An example of how the model works can be found in J. R. Britten et al.⁴⁸ Figures 12 and 13 are from Britten et al.⁴⁹ and show how well the code can retrieve a bimodal distribution when data error is extremely small and when data error is 1%, respectively. The model is being adapted to the colloid-laser scattering system and is just about operational for application. It will allow us to extract colloid size distributions from the laser observations.

3. Comparisons of TRACR3D With Analytic Solutions. An analytic solution is available for one-dimensional transport of natural colloids in a steady flow field.⁴⁸ The colloids can have a log normal size distribution. The colloids are inert except for filtration effects. In this case, the concentration of the colloids is given by

$$c(x) = C^0 \int_0^{\infty} f(\lambda)e^{-\lambda x} d\lambda \quad (5)$$

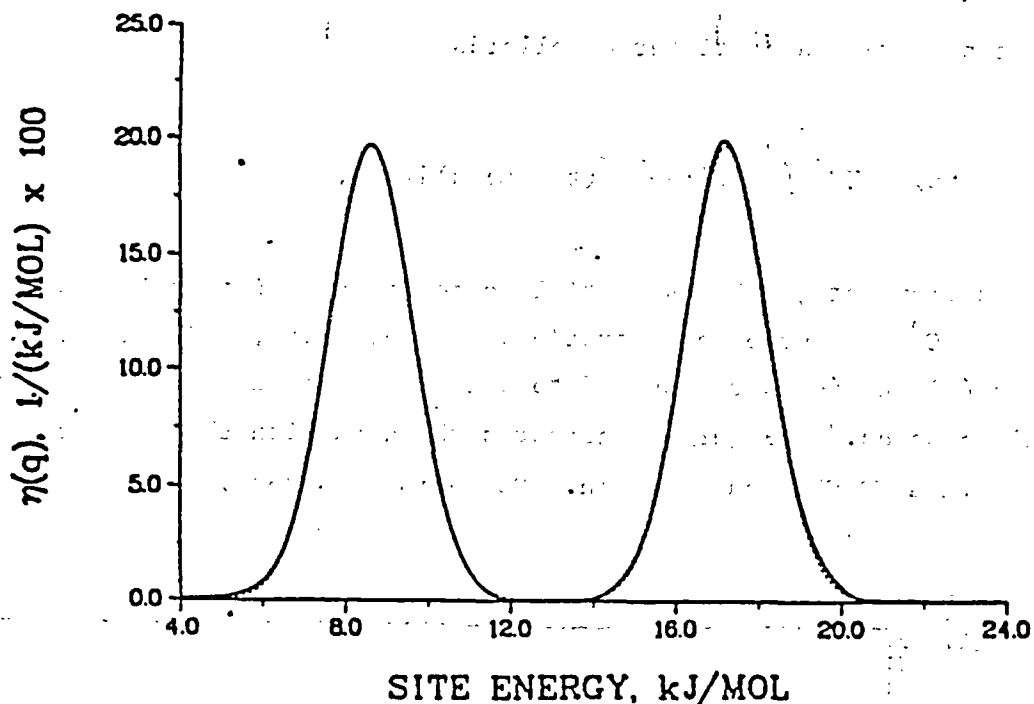


Fig. 12. Site Energy Distribution (SED) by regularization from calculated adsorption isotherm; bimodal SED, Langmuir-isotherm kernel, data with 4-figure accuracy.

.....SED postulated to obtain overall adsorption isotherm.
 -----SED calculated from isotherm by regularization.

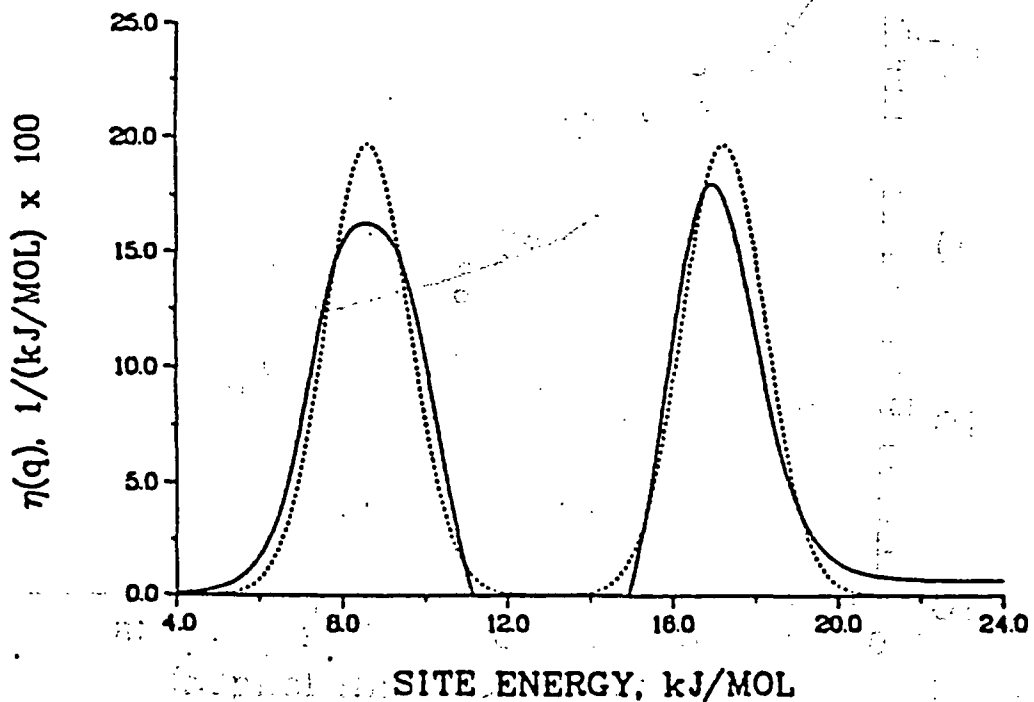


Fig. 13. SED by regularization from calculated isotherm with error; bimodal SED, Langmuir-isotherm kernel, 1% random error in isotherm data.

.....SED postulated to obtain overall adsorption isotherm.
 -----SED calculated from isotherm by regularization.

and the concentration of filtered colloids

$$\sigma(x) = UC^0 \int_0^{\infty} \lambda f(\lambda) e^{-\lambda x} (t - xw/u) d\lambda \quad , \quad (6)$$

where U is flow rate, $f(\lambda)$ is particle size distribution, x is position from the source, C^0 is source concentration, w is porosity, and t is time.

Equations (5) and (6) were applied to data on americium percolation through glauconitic sands.⁴⁹ Figure 14 compares the data with the solution of Eq. (5) and with a TRACR3D calculation. Comparison is good.

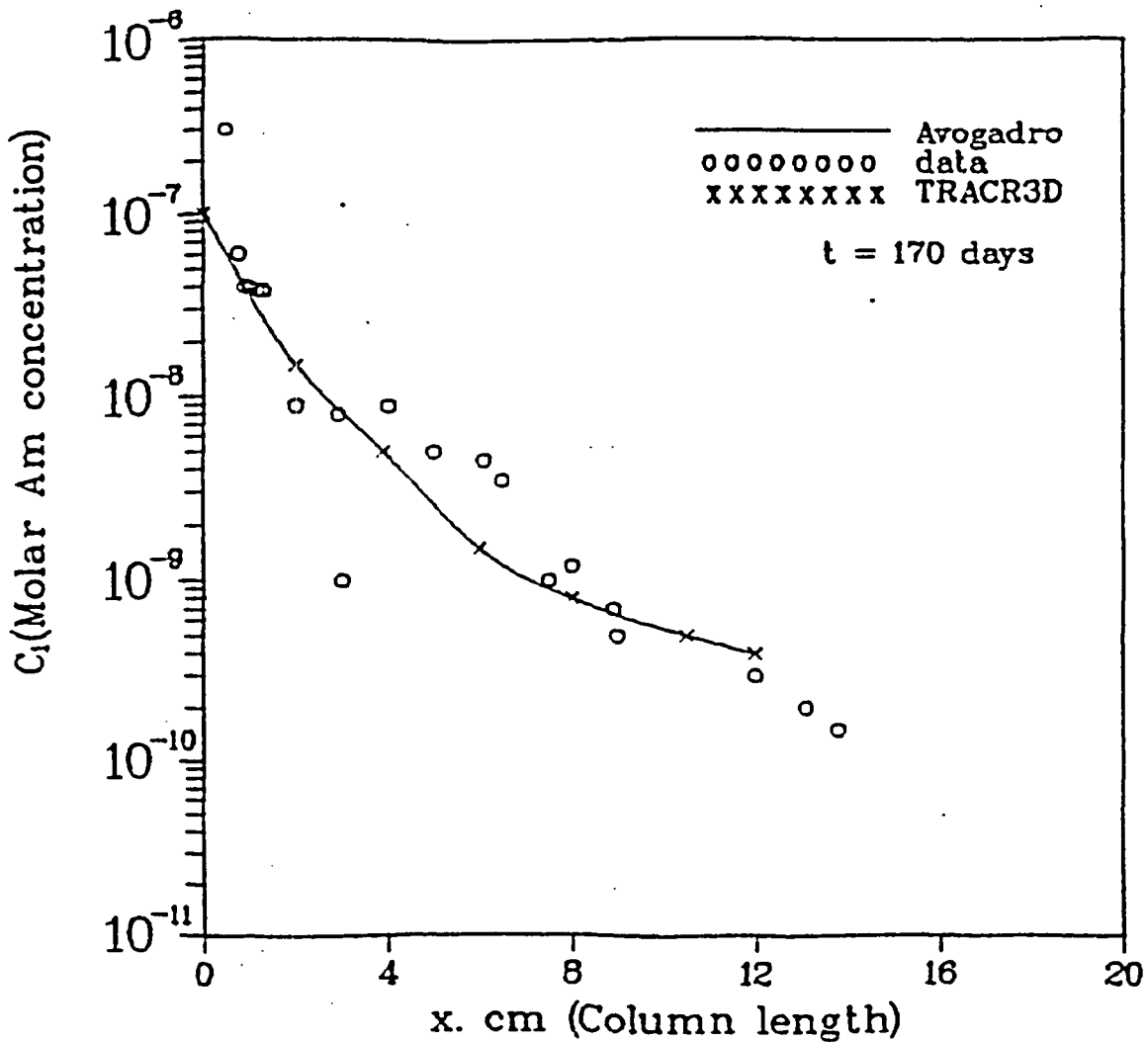


Fig. 14. Americium filtration pattern, comparison between experimental and theoretical data.

H. Applied Diffusion (A. E. Norris, P. L. Wanek, and K. Wolfsberg)

The purpose of this task is to measure diffusivity under field conditions at Yucca Mountain to ensure that the diffusivity values determined in laboratory experiments are reliable when used to calculate the retardation of nonsorbing radioactive wastes in water that might flow through the repository block. The work this quarter involved the development of analytical techniques for the detection of low levels of bromide ions in groundwater and the use of bromide as a tracer on a crushed tuff column in experiments to demonstrate that bromide can be used as a nonsorbing tracer. The development of bromide analysis techniques will be important, too, if bromide is chosen as the water tracer for the Exploratory Shaft mining operations.

Three analytical techniques have been investigated for use in routine analyses of low-level bromide ion concentrations in groundwater. Two of these techniques used ion chromatography columns to separate bromide ions from other anions in the water. Detection of bromide with an ultraviolet detector at 205 nm resulted in consistently reproducible data with a sensitivity of 50 $\mu\text{g}/\text{l}$. The use of an anion chromatography column and a potentiostatic detection system with a silver working electrode and a silver chloride reference electrode permitted the detection of bromide ions at lower concentrations than with the ultraviolet detector. However, the potentiostatic detector yielded poor peak shapes, which made quantitative analyses difficult. The third technique investigated for routine use in bromide determinations was neutron activation analysis. Five-minute irradiations of aqueous samples in a flux of 3.4×10^{12} neutrons/cm².s showed that ⁸²Br ($t_{1/2} = 35$ h) could be detected with 200 minutes of counting in a Ge(Li) system when the bromide concentration was 100 $\mu\text{g}/\text{l}$. A 20-minute count was insufficient to detect the ⁸²Br activity. Well J-13 water was irradiated and counted for 200 minutes, but no ⁸²Br activity could be detected. The bromide concentration in Well J-13 water must be less than 100 $\mu\text{g}/\text{l}$.

We conclude that bromide analyses on a routine basis appear to be most convenient with an ion chromatography technique that uses an ultraviolet detector.

One experiment was performed to measure the extent of bromide retention on a column of crushed Topopah Spring tuff. Dilution of the bromide tracer was less than anticipated. Additional experiments will be performed to measure bromide migration relative to tritium.

III. MINERALOGY-PETROLOGY OF TUFF (D. L. Bish, D. E. Broxton, F. M. Byers, Jr., B. A. Carlos, S. S. Levy, and D. T. Vaniman)

A. Petrographic Stratigraphy of the Topopah Spring Member

During this quarter, the petrographic stratigraphy of the Topopah Spring Member from hole USW G-4, near the proposed exploratory shaft, has been extensively studied. These studies combined petrographic modal counts, electron microprobe analysis, and scanning electron microscope analysis. Comparison of the petrographic microstratigraphy within the Topopah Spring Member is being extended to drill hole USW GU-3 to the south and will be extended to other cored drill holes within the proposed repository block, as well to drill hole USW G-2 in which the internal Topopah Spring stratigraphy consists largely of one thick lithophysal zone.⁵⁰ Our work on petrographic stratigraphy is guided by the stratigraphic framework provided by R. W. Spengler and R. B. Scott of the US Geological Survey.

The importance of being able to determine stratigraphic position within the Topopah Spring Member arises because of the need to identify which level of the Topopah Spring is being worked during repository construction. For example, if a fault is crossed during construction, should the drift be driven in a new direction in order to stay within the most favorable rock type? The data on petrographic stratigraphy obtained during this quarter reveal several features that may provide new stratigraphic subdivisions of the lower Topopah Spring Member in rock that previously seemed very homogeneous.

Figure 15 illustrates the petrography of different stratigraphic levels within the Topopah Spring Member in drill hole USW G-4. For cross-reference, the lithologic zones in drill hole USW G-4 outlined by R. W. Spengler (written communication, May 1983) of the US Geological Survey are shown in the stratigraphic column at the left. The elongate bar graphs in the central part of Fig. 15 compare coarse to fine textures between the different stratigraphic levels, starting with the coarsest (crystals and lithic fragments) at the left and ranging to the finest (cryptocrystalline, glass, and voids) at the right. The granophyric intergrowths (alkali feldspars and silica minerals) and the silica-filled microvesicles (cristobalite and/or tridymite) both range from 0.05 mm to approximately 0.5 mm and are most abundant in the lithophysal zones where crystallization may have been enhanced by a vapor phase. Feldspar-silica intergrowths may also produce a

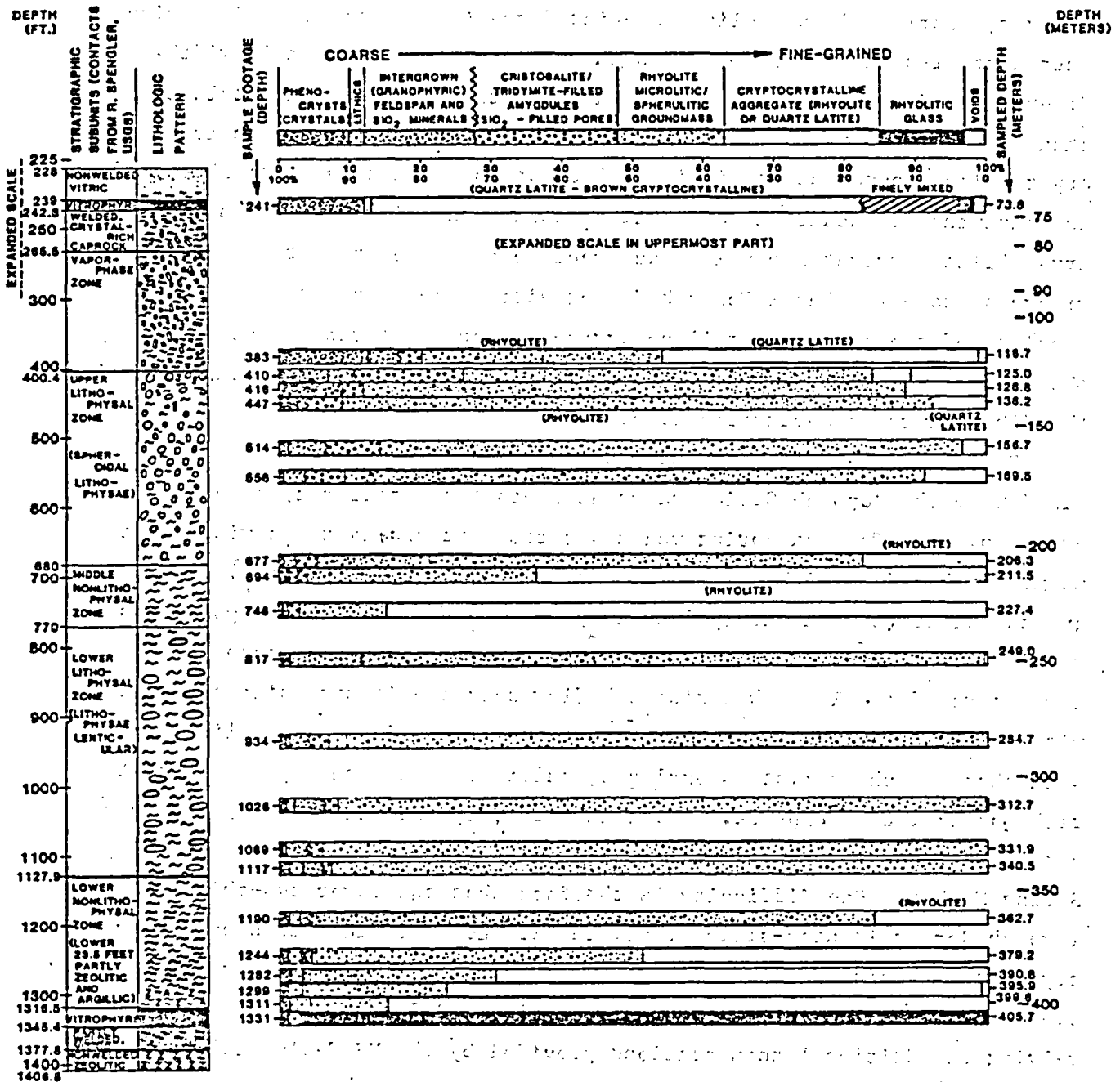


Fig. 15. Petrographic textural percentages of selected matrix samples, Topopah Spring Member, Drill Hole USW G-4. Lithology and stratigraphy were provided by R. W. Spengler, US Geological Survey (May 1983). Further subdivision of some minerals (for example, the upper lithophysal zone) may be required in future studies, but the divisions shown are current.

microlitic or spherulitic aggregate in which it is difficult to identify individual minerals. Spherulitic crystals are elongate, radiate from a common center, and in some rocks may attain several millimeters in length. However, nearly all spherulite-associated crystals in the Topopah Spring matrix are less than 0.5 mm in length and less than 0.005 mm in width. Finer-grained groundmass textures, in which the individual crystals are less than 0.005 mm in size, are referred to as cryptocrystalline. In cryptocrystalline groundmass the individual crystals can not be seen; XRD studies indicate that in addition to alkali feldspars and silica minerals the cryptocrystalline aggregates may include smectite and other hydrated secondary minerals above the basal Topopah Spring vitrophyre. In appearance, thin sections of the cryptocrystalline aggregates are semitranslucent to nearly opaque. The cryptocrystalline aggregates represent quickly chilled rock in the first stage of devitrification.

Figure 16 shows the percentages of phenocrysts or crystals that crystallized from the Topopah Spring magma at depth (intratelluric) prior to eruption. The Topopah Spring magma was compositionally zoned within the magma chamber from high-silica rhyolite (approximately 77% SiO_2) downward to quartz latite (approximately 70% SiO_2) or even less silicic compositions at greater depth. This sequence was inverted during eruption, such that the lower part of the Topopah Spring ash-flow sequence is high-silica rhyolite, with its sparse crystal assemblages, followed upward by less silicic magma with changing phenocryst assemblages, culminating in the uppermost crystal-rich quartz latite caprock.⁵¹ The changing, upward-increasing phenocryst assemblage may then be a guide to stratigraphic position within the Topopah Spring Member. One difficulty is the fact that the lower two-thirds of the Topopah Spring is high-silica rhyolite with commonly less than one per cent crystals, yielding poor data on crystal abundances. This difficulty is being overcome by counting phenocrysts separately on 0.5-mm traverses and by relying on additional thin sections provided by the US Geological Survey for drill holes USW G-1 and USW GU-3.

From Figs. 15 and 16, based on study of drill hole USW G-4, the following preliminary conclusions on petrographic stratigraphy within the Topopah Spring Member are suggested.

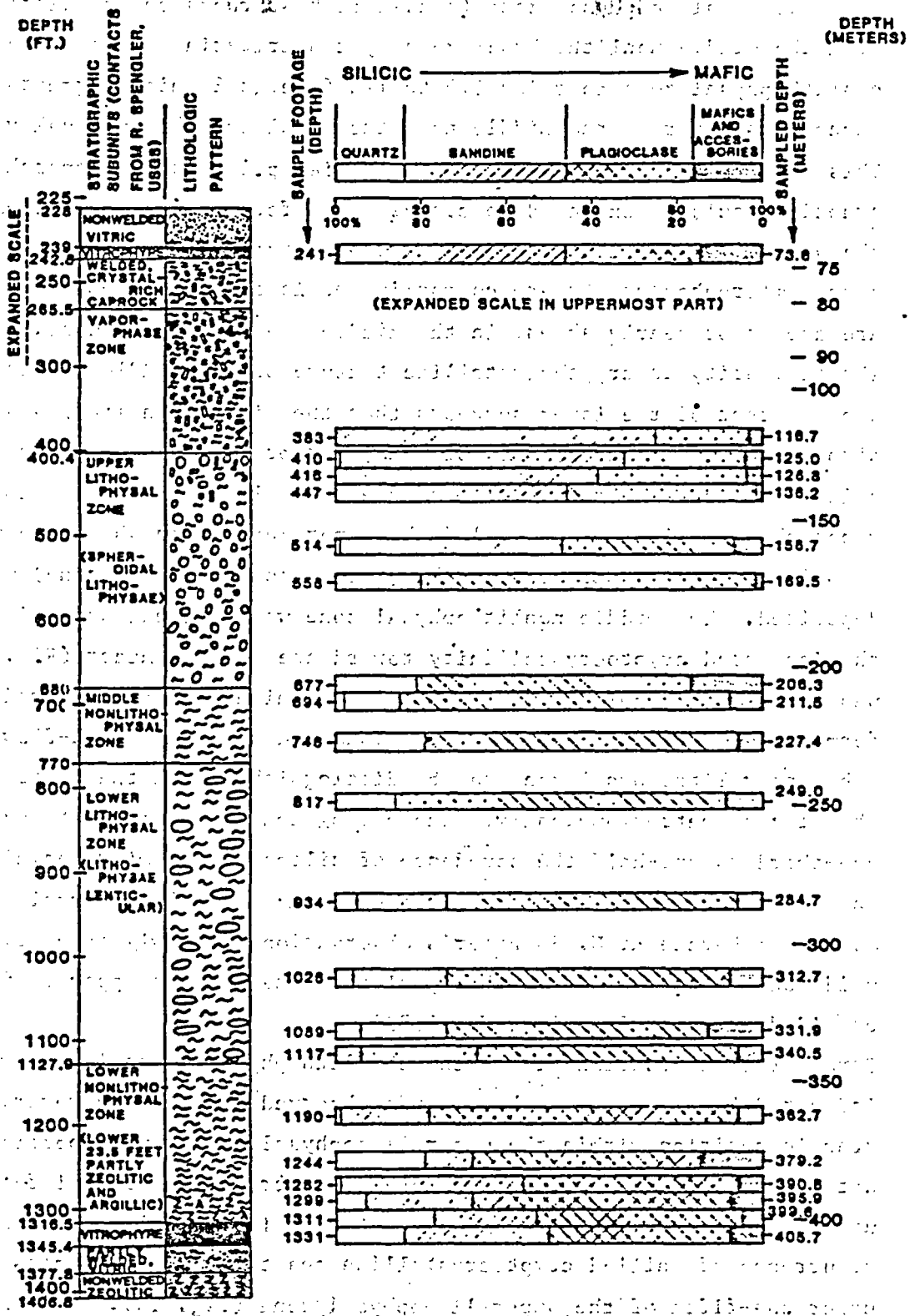


Fig. 16. Phenocryst percentages in selected samples, Topopah Spring Member, Drill Hole USW G-4. Lithology and stratigraphy were provided by R. W. Spengler, US Geological Survey (May 1983).

- (1) The lower nonlithophysal zone (candidate host rock) can be distinguished from the middle nonlithophysal zone by two criteria. First, the lower nonlithophysal zone contains 1.5 to 17% foreign lithic fragments (xenoliths) whereas the middle nonlithophysal zone has virtually none. This is understandable, because the earlier pulse of the Topopah Spring eruption would be expected to contain more foreign fragments from both the vent walls and the ground surface over which it traveled. Second, quartz microphenocrysts are common in the lower nonlithophysal zone but are absent or nearly absent in the middle nonlithophysal zone.
- (2) The similarity in cryptocrystalline texture of the middle nonlithophysal zone to that of the lower suggests that the middle nonlithophysal zone also formed by chilling, probably due to a brief hiatus between eruption pulses. This brief hiatus allowed the lower lithophysal zone to form by vapor phase action, which cooled the upper surface on which the next eruptive pulse (represented by the middle nonlithophysal zone) was deposited. The middle nonlithophysal zone was chilled, as indicated by the increased cryptocrystallinity toward the lower contact (Fig. 15) but was not strongly chilled by a sufficiently high temperature gradient to form a medial vitrophyre, as may be found in some thick ash-flow tuffs.
- (3) The upper lithophysal zone can be distinguished from the lower lithophysal zone petrographically. The petrographic data indicate only one-third to one-half the abundance of silica-filled microvesicles in the lower lithophysal zone compared with the upper lithophysal. These data corroborate R. W. Spengler's observations that significantly fewer voids occur in the lower lithophysal zone than in the upper (information provided by R. W. Spengler, May 1983).
- (4) Stratigraphic position within the two lithophysal zones is not well indicated by any petrographic trends observed to date. However, stratigraphic position within the upper lithophysal zone can be partially determined from the increase of total phenocrysts and alkali feldspar upward in the upper half of the zone (Figs. 15 and 16) and by the occurrence of chilled cryptocrystalline quartz-latitude lenticles in the upper one-fifth of the upper lithophysal zone (Fig. 15).

These modal petrographic distinctions are being supplemented by electron microprobe data on feldspar phenocrysts, on oxide minerals, and on bulk rock

groundmasses in samples having glassy or cryptocrystalline texture. Visual recognition of differences between cryptocrystalline groundmass areas, that is, high-silica rhyolite (about 77% SiO₂) or quartz latite (about 70% SiO₂), has been confirmed by bulk-rock electron microprobe analyses using a 20-micron raster. During these analyses, it was found that slight chemical differences occur between the cryptocrystalline groundmass near the base of the middle nonlithophysal zone and that near the base of the lower nonlithophysal zone just above the basal vitrophyre. Part of the cryptocrystalline groundmass above the basal vitrophyre has lost potassium and contains smectite and zeolite secondary minerals that are probably attributable to the increased water abundance due to devitrification of former vitrophyre. These minerals are not found at the base of the middle nonlithophysal zone where no vitrophyre is present and where none probably ever formed, owing to the much smaller thermal gradient within the Topopah Spring compound cooling unit.

Differing chemical compositions of feldspar phenocrysts and of secondary granophyric alkali feldspars may provide a further means of subdividing the petrographic stratigraphy of the Topopah Spring Member. Over one thousand microprobe analyses of feldspars from drill hole USW-G-4 thin sections at 16 different stratigraphic levels have been done. All oxide minerals in eight of these thin sections have also been analyzed for the same purpose. These data are currently being analyzed. Whether or not these data will provide an additional description of stratigraphic position within dominantly rhyolitic portions of the Topopah Spring Member remains to be seen.

B. Studies of Natural Alteration at Yucca Mountain

Continuing studies of the lower Topopah Spring vitrophyre are furnishing further evidence that hydrous minerals in this interval--heulandite and smectite--are alteration products related to late-stage devitrification in the upper part of the vitrophyre. The temperature of formation has not been determined directly for the hydrous minerals, but oxygen isotope geothermometry of a contemporary quartz fracture filling gives a temperature of about 91 to 95°C. The water that promoted alteration and deposited quartz, heulandite, and smectite was meteoric water presumably heated during passage through still-hot portions of the Topopah Spring Member tuff. Recognition of this alteration episode provides an opportunity to study the effects of hot

water percolating through the glassy rock immediately below the candidate host rock. In particular, differences in style and intensity of alteration can be studied in relation to fracture abundance and its influence on the movement of water through the host rock.

C. Sulfur Analyses within the Topopah Spring Member

The report on the use of hot spring systems as natural analogues to a repository in tuff was completed this quarter (Section II.C.2). Apparent increases in permeability were noted at several localities, and evidence for the development of acid sulfate systems in some springs was seen. To determine the possibility for development of an acid sulfate system in the unsaturated zone in Yucca Mountain, we have analyzed ten samples of Topopah Spring tuff from drill holes USW GU-3 and G-4 for total sulfur (using x-ray fluorescence). Total sulfur in the samples ranged from 46 to 137 ppm with a mean value of 66 ppm. Work next quarter will place limits and bounds on the total amount of H_2SO_4 that can be produced in the repository environment, assuming that all of the sulfur is present as sulfide.

D. Mineralogy/Petrology along Transport Pathways away from the Host Rock

Petrologic data on rock types both within and away from the repository block are needed to evaluate the retardation along transport pathways, since the degree of retardation is in part a function of rock type. During this quarter, x-ray diffraction studies of samples from drill holes USW WT-1, WT-2, and Well J-12 were completed to add to our understanding of the diverse vitric, devitrified, and zeolitized rock zones within the exploration block at Yucca Mountain and along potential pathways away from the exploration block. These data will be summarized in a forthcoming report, but some of the preliminary findings can be summarized here. Drill hole USW WT-2 is within the southeastern margin of the exploration block at a location between one drill hole where the Calico Hills tuff is thoroughly zeolitized (USW H-4) and another drill hole where the Calico Hills tuff is nonzeolitized (USW GU-3). Samples from drill hole USW WT-2 bridge the gap between these two very different drill holes: the zeolitized Calico section in drill hole USW WT-2 contains about 40 m of clinoptilolite and is at an appropriate elevation to be intermediate between Well USW H-4 (about 100 m of clinoptilolite) and USW H-3 (no clinoptilolite in this interval). These new data will

allow a more accurate mapping of the zeolitized intervals below the exploration block at Yucca Mountain. Drill hole USW WT-1, just southeast of the exploration block at Yucca Mountain, is unique among the drill hole samples so far studied in that alteration near the water table here has been so complete that the basal vitrophyre of the Topopah Spring Member is completely altered. In the USW WT-1 samples, none of the vitrophyre glass remains, and the vitrophyre interval now consists mostly of clinoptilolite. Drill hole J-12 is about nine kilometers from the exploration block and provides our most distant samples along the possible flow paths beneath Fortymile Canyon. Although this core did not penetrate far below the water table, the samples studied indicate that the zeolitization of the lower Topopah Spring Member and upper Calico Hills tuff is comparable to the other drill holes examined closer to the eastern margin of the exploration block.

Study of zeolite compositions within drill hole USW G-4 was also completed this quarter, showing that alkalic zeolites occur in the major zeolitized interval from 436 to 537 m depth, but calcium-rich zeolites begin to appear at 650 m in a compositional series similar to the calcium-rich zeolites that occur throughout the zeolitized intervals to the east in Well UE-25p#1. There is a major difference in calcium, sodium, and potassium contents between those clinoptilolites beneath the Yucca Mountain crest (alkalic clinoptilolites) and those to the east (calcic clinoptilolites). As part of our studies, the silicon-to-aluminum ratios of zeolites from these two areas have been compiled for comparison with the new data from drill hole USW G-4 (Fig. 17). This ratio can significantly affect zeolite ion exchange capacities and selectivities, and it is important to compare this property within the major zeolite intervals that may behave as sorptive barriers beneath Yucca Mountain. Figure 17 shows that the silicon-to-aluminum ratios for clinoptilolites throughout Yucca Mountain are generally similar. However, the silicon-to-aluminum ratios of the eastern group of clinoptilolites are bimodal with a main population having ratios falling between 4.0 and 5.2 and a second, smaller population with ratios between 2.8 and 3.6. The smaller population of low silicon-to-aluminum ratios is confined to the deepest, most calcic clinoptilolites in Wells UE-25b#1 and UE-25p#1. As shown in Fig. 17, no silicon-to-aluminum ratios less than 4.2 were found in any of the clinoptilolites from drill hole USW G-4. Therefore, in general, this parameter of clinoptilolite composition does not vary significantly

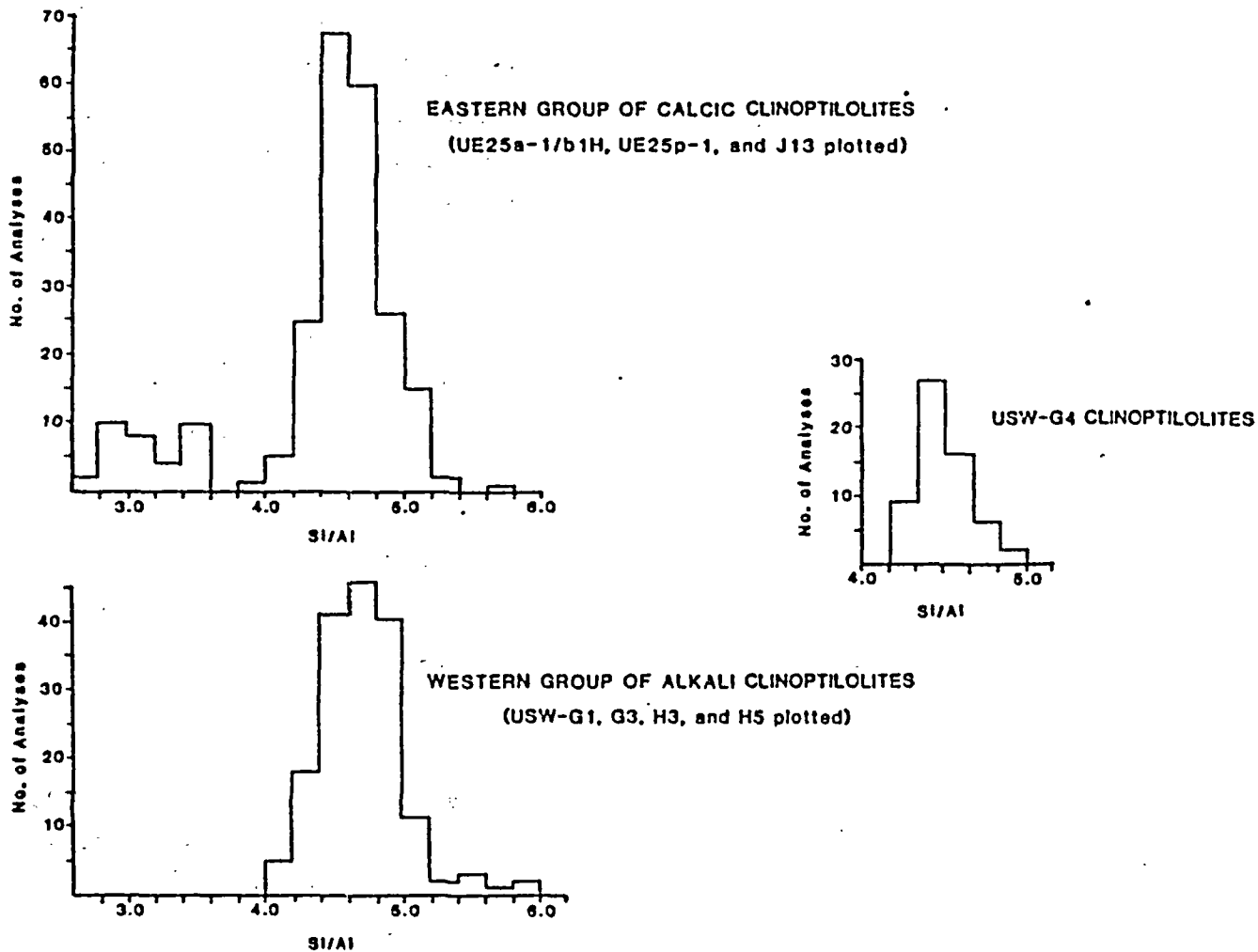


Fig. 17. Comparison of silicon/aluminum ratios of clinoptilolite in Drill Hole USW G-4 to clinoptilolites in other drill holes at Yucca Mountain.

throughout Yucca Mountain except for a few samples well below the water table and along the eastern margin of the exploration block. Future work will summarize the more variable exchangeable cation compositions of the Yucca Mountain clinoptilolites.

During this quarter, work was also initiated with the Statistical Analysis Division at Los Alamos to determine what level of sampling is necessary to predict the lateral extent of the various vitric, devitrified, and zeolitized tuffs that occur both within and away from the exploration block at Yucca Mountain.

E. Reports

Fracture-lining minerals within tuff may be very different from minerals in the surrounding rock matrix. Waste transport studies must be concerned with the differences between fracture and matrix transport, particularly in rocks where fracture permeability may greatly exceed matrix permeability. In order to develop an understanding of how fracture mineralogy varies within the Topopah Spring Member and underlying rocks, we have studied fracture samples from drill hole USW G-4. The unsaturated-zone part of this study was completed this quarter, and a technical report is in first-draft stage. We will study fractures in the saturated zone down to the transmissive interval in the Tram Member of the Crater Flat Tuff, next quarter. Future studies will be extended to other cores in the vicinity of the exploration block. Two other technical reports went to press this quarter: "Variations in Authigenic Mineralogy and Sorptive Zeolite Abundance at Yucca Mountain, Nevada, Based on Studies of Drill Cores USW GU-3 and G-3" (LA-9707-MS) and "Petrology of Samples from Drill Holes USW H-3, H-4, and H-5, Yucca Mountain, Nevada" (LA-9706-MS).

IV. TECTONICS AND VOLCANISM (B. Crowe, D. Curtis, D. Vaniman, and N. Bower)

Volcanism studies are being conducted for the NNWSI to evaluate the relative hazards of future volcanism with respect to storage of high-level radioactive waste. Work during the quarter included field studies in southern Death Valley to investigate the structural setting of Quaternary volcanism and continued refinement of the major and trace-element geochemical data base for the NTS region.

Sites of Quaternary volcanism in southern Death Valley were examined in the field as a part of studies of the regional tectonic setting of basaltic volcanism in the Death Valley-Pancake Range volcanic zone. These sites include a 0.7 Myr scoria cone that is offset by the southern branch of the southern Death Valley fault zone and 1.7 Myr sequence of basaltic andesite lavas (basaltic andesites of Shoreline Butte) largely buried by alluvial fill. Local pyroclastic surge deposits mantle older alluvium to the east and west of the outcrop area of the two Quaternary centers. These deposits could have been derived from either of the centers. Structurally, the basalt centers are located at the intersection of the inferred northeast-trending Windgate Wash fault with the southern Death Valley fault zone.

Additional data entry and editing were completed for the trace element data base using DATATRIEVE on the VAX 11/780. Data for 22 elements encompassing 109 samples from the NTS area have been entered in the data base. This data base was cross-checked with the major element data base and five samples were located which had trace element data but no major element data. These samples were analyzed by X-Ray Fluorescence (XRF) for their major-element compositions. Neutron activation data from the automated data system was cross-calibrated with the more rigorous neutron activation data. Relatively good agreement was obtained for the rare earth elements and for uranium, hafnium, vanadium, and scandium.

A manuscript entitled "Volcanic Hazard Assessment for Disposal of High-Level Radioactive Waste" was accepted by the National Research Council for publication in a special volume on recent tectonics and their impact on society.

V. TUFF LABORATORY PROPERTIES (J. D. Blacic)

The purpose of this work is to investigate the time-dependence of mechanical properties of Yucca Mountain tuffs. Knowledge of how tuff mechanical properties can be expected to vary over the lifetime of a repository is necessary for design and for performance assessment. Laboratory investigation of physical and chemical processes responsible for time-dependence of properties is the first step in an attempt to quantify and predict the consequences of slow changes in key engineering properties of the geologic barrier. The results of laboratory investigations will be used to formulate preliminary predictive models which will then be used to design

Exploratory Shaft and additional laboratory experiments needed to fully quantify the time-dependent phenomena.

The approach in this investigation is to perform long-term creep deformation experiments on Calico Hills and Topopah Spring tuff samples over a range of temperatures and stresses at simulated repository confining and pore pressure conditions. This quarter, creep experiments were completed on Calico Hills zeolitized tuff samples from drill hole USW G-4, and work was initiated on Topopah Spring welded tuff samples from a surface block collected at Busted Butte. Analysis of recovered samples and data from experiments on Calico Hills tuff is continuing, but some preliminary conclusions can be stated at this time for this tuff type.

- o Hydration/dehydration strains are large and strongly time-dependent. Hydration-state changes appear capable of generating compressive stresses of 20 to 60 MPa (hydration) and tensile stresses in excess of the tensile strength of any rock within the thermal field of a repository (dehydration).
- o Creep deformation of Calico Hills zeolitized tuff appears to be characterized by a "steady state" strain rate component as low as $1 \times 10^{-10} \text{ s}^{-1}$. This result offers hope that a predictive model of mechanical strength can be formulated that will be valid over the long time extrapolation required for performance assessment, although the complicated coupling of hydration strain, microcracking, and water transport phenomena needs to be sorted out before the hope can be realized. The experimental basis for these preliminary conclusions is discussed below.

Test samples are normally oven dried at 75°C in the process of attaching strain gauges to the surfaces of the samples. Consequently, experiments begin with a pore-saturation phase before final test conditions are applied and deformation begins. This saturation phase was found to require a much longer time than originally anticipated, varying from 2 to 5 weeks during which large dilational strains were recorded; an example is shown in Fig. 18. Volume strains upon saturation average about -5×10^{-3} , which together with an average bulk modulus of 4 GPa imply an elastic swelling stress of about 20 MPa at room temperature. The long saturation times are the result of the combination of large porosity (about 25%) and low permeability (about

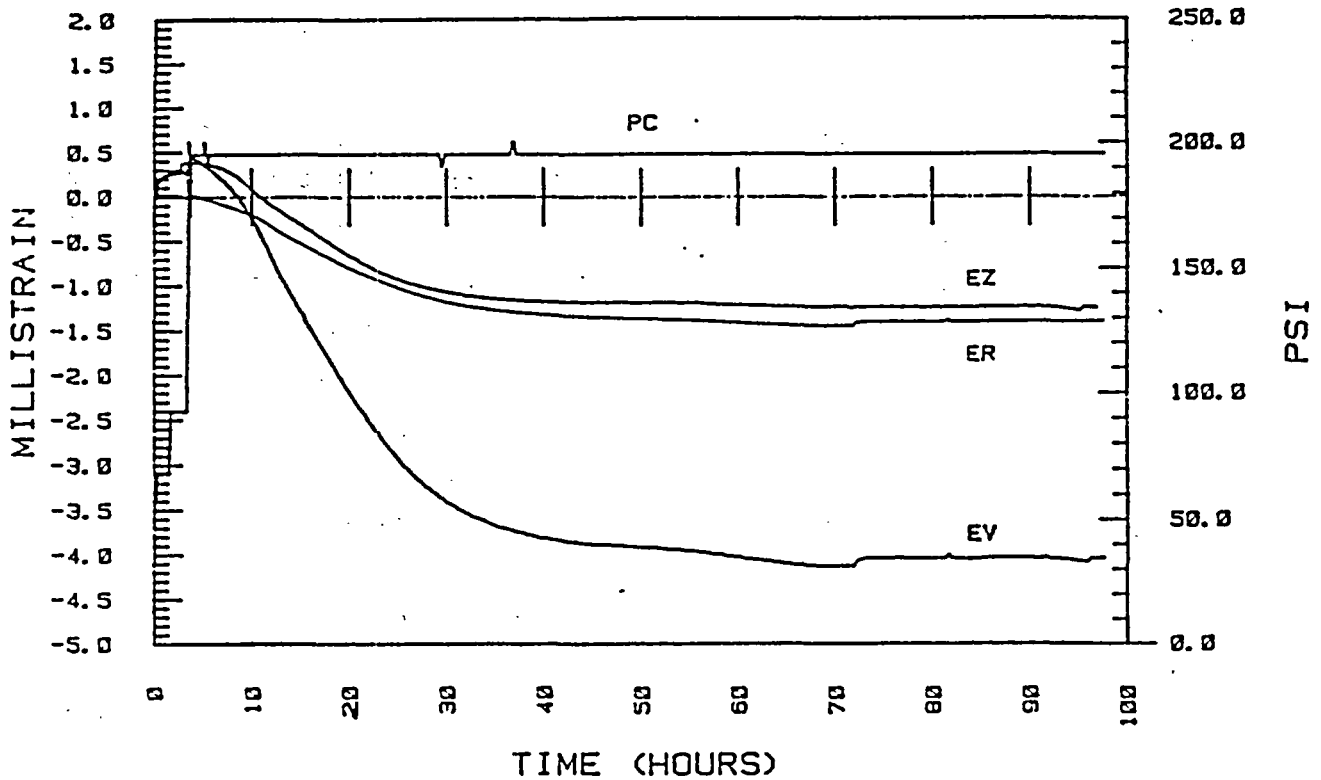


Fig. 18. A portion of the saturation phase for experiment #TC8 shows axial strain (EZ), circumferential strain (ER), volume strain (EV), and confining pressure (PC) as a function of time. The externally controlled water pressure (not shown) was held constant at 100 PSI. After an initial hydrostatic compression, the sample strongly dilates until saturation is nominally complete (about 1 week in this case). All tests on Calico Hills tuffs have exhibited a saturation phase similar to the one shown here.

1 microDarcy). Saturation is assumed to be nominally complete when pore pressure in the valved-off sample does not fall over a 1-hour time period. However, this does not mean that the sample is 100% saturated, as will be discussed below. After several additional days of saturation during which the final test pressures and temperature are established, a constant axial differential stress is applied to the sample, and sample strains are monitored over time. At stresses below about 85% of the ultimate failure stress, samples first exhibit primary creep at nearly logarithmically decreasing rates, but then the sense of axial strain reverses, and the samples elongate against the applied axial stress. This appears to

be due to very slow swelling resulting from incomplete saturation and hydration of zeolite and clay minerals. The maximum rate of swelling coincides with the onset of dilational microcracking in tests in which the axial stress is increased in steps (Fig. 19). This implies that microcracking produces additional pathways for water to penetrate the innermost regions of the sample and produce an increased rate of hydration swelling. In other words, brittle microcracking, water permeation, and mineral hydration strain are coupled phenomena in this rock.

Although it will ultimately be necessary to separately quantify the strain contribution due to hydration, we have begun to formulate a constitutive equation to express the time-dependent deformation of Calico Hills tuff. Primary creep appears to be best represented by a power law of the form: $e(t) = At^b$, where e is axial strain, t is time, and A and b are empirical constants. A is about $3 \times 10^{-3} \text{ s}^{-1}$ and b is approximately 0.02, based on preliminary test data. Most tests exhibited a region of constant, "steady state" strain rate ranging from about $1 \times 10^{-10} \text{ s}^{-1}$ (which is detection limit in our experiments) to about $3 \times 10^{-6} \text{ s}^{-1}$, depending on stress level. Test temperatures have only varied from 35 to 75°C, so it is difficult to quantify any thermal activation with certainty in the presence of large sample variability. Nevertheless, if the raw data are taken at face value, a steady state activation energy of about 160 kJ/mol is indicated. The most consistent parameter observed in the experiments is the strain at the onset of tertiary creep failure. Average axial failure strain is approximately 6×10^{-3} and volume strain about -1×10^{-3} . These values represent good approximate strain limits for planning and predictive purposes at present.

The phenomena we have discussed above are of sufficiently large magnitude that important consequences for long-term bore hole and tunnel stability may be involved. It is clear that these phenomena are complex, coupled, thermal-mechanical-chemical processes that are poorly understood in detail but warrant further investigation.

TEMP = 50 C PC = 5.0 MPA PP = 0.1 MPA

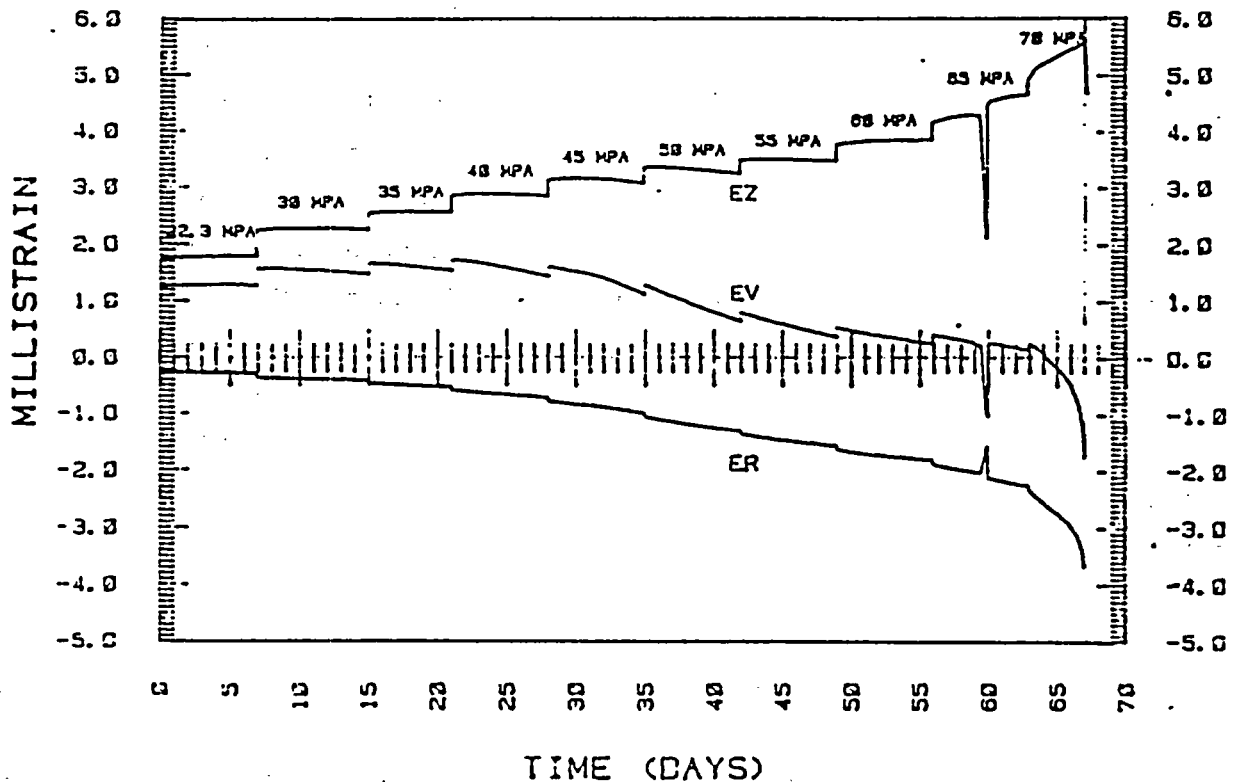


Fig. 19. Stepped-stress creep curve for experiment #TC9. Axial strain (EZ), circumferential strain (ER), and volume strain (EV) are shown as a function of time. The constant stress level for each creep stress level is shown above the axial creep curve. Note that the maximum rate of negative axial strain occurs at about 45 to 50 MPa, which is also the onset of dilational microcracking indicated by the volume strain curve.

VI. SEALING MATERIALS EVALUATION (D. M. Roy and C. J. Duffy)

A. Objectives

Cementitious materials (grouts, mortars, and concretes) are being proposed as one major type of potential sealing material for a nuclear waste repository sited in the felsic tuffs of Yucca Mountain. Introduction of any sealing materials will, in general, cause reactions between the host rock and the sealant because of chemical differences and the reactive nature of fine minerals and glasses in the tuff.

Different concrete-type sealing materials are being evaluated for their potential chemical compatibility with the tuff chemistry. Two approaches to sealant/host rock compatibility were examined. The first concrete utilized

indigenous sands and gravel in the formulation of the sealant. The second approach utilized more conventional concrete materials, but controlled the 'bulk' chemical composition of the concrete to make it more closely approach the tuff composition.

The purpose of this work is to evaluate the chemical stability of potential sealing materials based upon laboratory studies conducted with a series of conditions that represent a range of credible temperature conditions. These studies are being supplemented by other evaluations based upon thermodynamic considerations and durable analogues from other sources.

B. Elevated-Temperature Reaction Experiments

A number of different experimental designs are being used to evaluate the chemical compatibility of the host tuff with the concretes. Current experimental efforts are being applied to the latter approach in which the bulk chemical composition of the sealant is adjusted by the addition of reactive admixtures, largely silica or silica-rich components that are added in the appropriate proportions to minimize the formation of calcium hydroxide during the hydration of the cementitious phases. The additions were carefully selected to provide the maximum formation of the calcium silicate minerals tobermorite and gyrolite, resulting in a less porous, less permeable material.

The cementitious mixture 82-22 has been exposed to a potentially reactive vapor phase and to Well J-13 groundwater for extended time periods. The concretes exposed to the vapor phase at 200°C exhibited extensive growth of euhedral crystals on the surface of the cementitious matrix. The tuff appeared lightly etched, and the surfaces in contact with the cementitious matrix appeared to be altered to a depth of about 500 μm .

The 200°C grout/rock experiments were completed, the solids were characterized by XRD, and detailed microstructural studies are in progress. X-ray diffraction characterization of the surfaces of the 200°C grout/tuff discs revealed the dominant presence of tobermorite, which decreased in relative quantity with time of exposure to the hydrothermal solution. Some gyrolite was also present.

The solutions in contact with the solids were collected and chemical analyses completed. Solution analyses are given in Table XXI for reactions

TABLE XXI
 ANALYSES OF AQUEOUS PHASE FROM TREATMENT OF
 82-22/TOPOPAH SPRING TUFF DISCS AT 300°C, SATURATED
 CONDITIONS FOR 1 TO 4 WEEKS, STATIC CONDITIONS^a

	<u>($\mu\text{mol/g}$)</u>				<u>mg/g (ppm)</u>		
	<u>1 wk</u>	<u>2 wk</u>	<u>4 wk</u>		<u>1 wk</u>	<u>2 wk</u>	<u>4 wk</u>
Al ₂ O ₃	52	48	41	Al	1.4	1.3	1.1
CaO	3625	4000	3750	Ca	145	160	150
Fe ₂ O ₃	3	33	15	Fe	0.2	2.2	1.0
K ₂ O	177	277	433	K	6.9	10.8	16.9
MgO	8	25	25	Mg	0.2	0.6	0.6
MnO	BDL ^b	BDL ^b	BDL ^b	Mn	<0.05	<0.1	<0.1
Na ₂ O	1435	2214	2565	Na	33	51	59
SiO ₂	964	5893	3214	Si	27	165	90
TiO ₂	BDL ^b	BDL ^b	BDL ^b	Ti	<0.05	<0.1	<0.1
F ⁻	BDL ^b	NA ^c	NA ^c	F ⁻	<0.05	NA ^c	NA ^c
NO ₃ ⁻	225	BDL ^b	BDL ^b	NO ₃ ⁻	9	<2	<2
SO ₄ ²⁻	521	5521	5313	SO ₄ ²⁻	50	530	510
pH	7.14	7.6	7.6				

^aSampled at room temperature.

^bbelow detection limits.

^cNot analyzed.

at 300°C. A complete evaluation of all of the solution analyses has not yet been completed, because they have only recently become available from the analytical laboratory.

Table XXII gives solution data for rocking autoclave reactions at 200°C, contrasting the solutions sampled at temperature with the solutions after cooling to room temperature.

C. Intermediate-Temperature Reaction Experiments

Following the 200 and 300°C tests, a test matrix of samples composed of Topopah Spring tuff prisms cast into 82-22 mortar cylinders was prepared. Tests have been made at 150 and 90°C. Fluids in contact with the concrete specimens are sampled at temperature and pressure in the rocking autoclave apparatus, at room temperature (after a furnace quench) in all of the vessels, and at temperature and ambient pressure in the 90°C experiments. Analyses of the solutions in contact with the grout/tuff samples are only completed to the 2-month interval at 150°C and the one-month interval at 90°C. The results are presented in Table XXIII.

Preliminary surface characterization of the solids removed from the reaction vessels has been completed. X-Ray Diffraction (XRD) examination of grout/tuff discs showed the presence of poorly developed tobermorite and extensive calcite on discs hydrothermally treated at 150 and at 90°C. Scanning Electron Microscope (SEM) characterization of these samples supports the XRD observations.

D. Discussion

Preliminary observations of the solution data for the saturated disc experiments at 90, 150, 200, and 300°C show that a significant difference is observed in the concentrations of calcium, SO_4^{2-} , and silicon between samples that were obtained at temperature and those that were obtained after the reaction vessel was allowed to equilibrate to room temperature. Solution concentrations at temperature are more informative because they appear to be unaffected by precipitation or by retrograde solubility. Comparison with the calcium concentration data for 200°C as a function of time in the hydrothermal environment reveals a steadily increasing concentration; in contrast, the 300°C experiments exhibit a slight decrease in concentration with increasing time suggesting that equilibrium between the solid and fluid

TABLE XXII
 ANALYSES OF AQUEOUS PHASE FROM TREATMENT OF 82-22/TOPOPAH
 SPRING TUFF DISCS AT 200°C, SATURATED CONDITIONS
 FOR 1 TO 7.1 MONTHS, ROCKING AUTOCLAVE
 ($\mu\text{mol}/\ell$)

	1 Month		2 Months		4 Months		7.1 Months	
	@T ^a	@RT ^b	@T ^a	@RT ^b	@T ^a	@RT ^b	@T ^a	@RT ^b
Al ₂ O ₃	215	11	278	19	BDL ^c	7	BDL	7
CaO	1400	900	2375	2000	10 500	6500	12 250	3500
Fe ₂ O ₃	388	7	121	11	BDL ^c	BDL ^c	71	5
K ₂ O	1359	1924	1333	871	924	398	1795	375
MgO	874	BDL ^c	200	37	83	21	125	12
MnO	11	BDL ^c	4	BDL ^c				
Na ₂ O	3261	3478	5870	6304	12 609	7826	7391	7174
SiO ₂	2321	2500	6083	6534	1723	1585	1723	1862
TiO ₂	BDL ^c	BDL ^c	9	BDL ^c				
F ⁻	495	147	211	89	NA ^d	NA ^d	NA ^d	NA ^d
NO ₃ ⁻	1452	129	177	145	BDL	65	BDL ^c	48
SO ₄ ²⁻	938	2083	2500	2917	21 875	11 875	30 208	7500
CO ₂	884	925	--	--	--	--	--	--
pH							7.50	8.30

^aSampled at 200°C.

^bSampled at room temperature.

^cBelow detection limits.

^dNot analyzed.

TABLE XXXIII.
 ANALYSES OF AQUEOUS PHASE FROM TREATMENT OF
 82-22/TOPOPAH SPRING TUFF DISCS AT 150 AND 90°C,
 SATURATED CONDITIONS
 ($\mu\text{mol}/\ell$)

	(150°C) 2 Month ^a		(90°C) 1 Month ^b
	@T ^c	@RT ^d	@T ^c
Al ₂ O ₃	19	7	44
CaO	1875	1625	155
Fe ₂ O ₃	BDL ^e	BDL ^e	BDL ^e
K ₂ O	5756	2308	2051
MgO	553	12	17
MnO	BDL ^e	BDL ^e	BDL ^e
Na ₂ O	7813	5425	3039
SiO ₂	2036	789	2218
TiO ₂	BDL ^e	BDL ^e	BDL ^e
NO ₃ ⁻	97	161	161
SO ₄ ²⁻	7604	5938	1771
pH	11.13	10.42	10.04

^a Rocking autoclave.

^b Static conditions, 1 atm.

^c Sampled at 200°C.

^d Sampled at room temperature.

^e Below detection limits.

phases was closely approached and that formation of alteration phases continued to take place.

Solution concentrations of calcium for the 90°C samples are lower, by an order of magnitude, than for the higher temperature experiments; whereas the 150°C experiment (rocking autoclave) produced a calcium concentration comparable to the 200°C experiment at a comparable time. The lower calcium concentrations in the 90°C experiment may be due to the formation of calcite.

The data obtained to date suggest that stable reaction products are produced by the end of 7 months at 200°C and the solutions reach 'saturation' or near equilibrium with the mineral phases. These data will be used in calculations that have been initiated to estimate the dissolution rates of cementitious plugs and fracture seals.

REFERENCES

1. W. R. Daniels, B. R. Erdal, and D. T. Vaniman, Comps., "Research and Development Related to the Nevada Nuclear Waste Storage Investigations, July 1--September 30, 1982," Los Alamos National Laboratory report LA-9577-PR (March 1983).
2. W. Stumm and J. J. Morgan; Aquatic Chemistry (John Wiley and Sons, New York, 1981).
3. O. P. Bricker, "Redox Potential: Its Measurement and Importance in Water Systems," Water Analysis, Vol. 1, Inorganic Species, Part 1, R. A. Minear and L. H. Keith (Eds.) (Academic Press, New York, 1982), pp. 55-83.
4. R. M. Garrels and C. L. Christ, Solutions, Minerals, and Equilibria, Freeman, Cooper, and Co., San Francisco (1965).
5. F. Caporuscio, D. Vaniman, D. Bish, D. Broxton, B. Arney, G. Heiken, F. Byers, R. Gooley, and E. Semarge, "Petrologic Studies of Drill Cores USW G-2 and UE-25b#1H, Yucca Mountain, Nevada," Los Alamos National Laboratory report LA-9255-MS (July 1982).
6. K. Wolfsberg and D. T. Vaniman, Comps., "Research and Development Related to the Nevada Nuclear Waste Storage Investigations, October 1--December 31, 1983," Los Alamos National Laboratory report LA-10032-PR (August 1984).
7. P. Saha, "Geochemical and X-Ray Investigation of Natural and Synthetic Analcites," *Am. Mineral.* 44, 300-313 (1959).
8. Ki-Tae Kim and B. J. Burley, "The Solubility of Water in Melts in the System $\text{NaAlSi}_3\text{O}_8 - \text{NaAlSiO}_4 - \text{H}_2\text{O}$," *Canadian J. Earth Sci.* 8, 558-571 (1971).

9. K. Denbigh, The Principles of Chemical Equilibrium, Cambridge University Press, pp. 429-435 (1966).
10. F. Mazzi and E. Galli, "Is Each Analcime Different?" *Am. Mineral.* 63, pp. 448-460 (1978).
11. C. A. Morrow, D. E. Moore, and J. D. Byerlee, "Permeability and Pore-Fluid Chemistry of the Topopah Spring Member of the Paintbrush Tuff, Nevada Test Site, in a Temperature Gradient," *Application to Nuclear Waste Storage, Materials Research Society Symposium Proceedings, Vol. 26*, 883-890 (1984).
12. D. E. Moore, C. A. Morrow, and J. D. Byerlee, "Chemical Reactions Accompanying Fluid Flow through Granite Held in a Temperature Gradient," *Geochem. Cosmo. Acta* 47, 445-453 (1983).
13. J. Byerlee, C. Morrow, and D. Moore, "Permeability and Pore-Fluid Chemistry of the Bullfrog Tuff in a Temperature Gradient: Summary of Results," US Geological Survey open file report 83-475 (1983).
14. D. T. Trexler, B. A. Koenig, and T. Flynn, "Geothermal Resources of Nevada and Their Potential for Direct Utilization," Nevada Bureau of Mines and Geology, Reno, Nevada (1980).
15. D. H. Stewart and J. E. Carlson, "Geologic Map of Nevada," US Geological Survey (1978).
16. L. J. Garside, "Field Trip #4, Moana Hot Springs, Steamboat Springs, and Brady's Hot Springs," Geothermal Resources Council Annual Meeting (1979).
17. R. K. Hose and B. E. Taylor, "Geothermal Systems of Northern Nevada," US Geological Survey open file report 74-271 (1974).
18. L. J. Garside and J. H. Schilling, "Thermal Waters of Nevada," Nevada Bureau of Mines and Geology, Bulletin 91, Mackay School of Mines, Univ. Nevada at Reno (1979).
19. L. J. Garside, "Geothermal Exploration and Development in Nevada Through 1973," Nevada Bureau of Mines and Geology, Report 21, Mackay School of Mines, Univ. Nevada at Reno (1974).
20. M. L. Silberman, D. E. White, T. E. C. Keith, and R. D. Dockter, "Duration of Hydrothermal Activity at Steamboat Springs, Nevada, from Ages of Spatially Associated Volcanic Rocks," US Geological Survey professional paper 458-D (1979).
21. R. Schoen and D. E. White, "Hydrothermal Alteration in GS-3 and GS-4 Drill Holes, Main Terrace, Steamboat Springs, Nevada," *Econ. Geol.* 60, 1411-1421 (1965).

22. W. R. Daniels, K. Wolfsberg, R. S. Rundberg, A. E. Ogard, J. F. Kerrisk, C. J. Duffy et al., "Summary Report on the Geochemistry of Yucca Mountain and Environs," Los Alamos National Laboratory report LA-9328-MS (December 1982).
23. F. Goff, T. McCormick, P. E. Trujillo, D. Counce, and C. O. Grigsby, "Geochemical Data for 95 Thermal and Nonthermal Waters of the Valles Caldera--Southern Jemez Mountains Region, New Mexico," Los Alamos National Laboratory report LA-9367-OBES (May 1982).
24. J. J. Henley, P. B. Hostetler, A. J. Gude, and W. T. Mountjoy, "Some Stability Relations of Alunite," *Econ. Geol.* 64, 599-612 (1969).
25. R. W. Hemley and A. J. Ellis, "Geothermal Systems Ancient and Modern: A Geochemical Review," *Earth-Sci. Rev.* 19, 1-50 (1983).
26. D. E. White, L. P. J. Muffler, and A. H. Truesdell, "Vapor-Dominated Hydrothermal Systems Compared with Hot Water Systems," *Econ. Geol.* 66, 75-97 (1971).
27. F. H. Chung, "Quantitative Interpretation of X-Ray Diffraction Patterns of Mixtures I. Matrix-Fluxing Method for Quantitative Multicomponent Analysis," *J. Appl. Crystallogr.* 7, 519-525 (1974).
28. J. F. Kerrisk, "Reaction-Path Calculations of Groundwater Chemistry and Mineral Formation at Rainier Mesa, Nevada," Los Alamos National Laboratory report LA-9912-MS (December 1983).
29. T. J. Wolery, "Calculation of Chemical Equilibrium between Aqueous Solution and Minerals: The EQ3/6 Software Package," Lawrence Livermore Laboratory report UCRL-52658 (February 1979).
30. Constance W. Miller, "Toward a Comprehensive Model of Chemical Transport in Porous Media," in Scientific Basis for Nuclear Waste Management VI, D. G. Brookins, (Ed.) (North-Holland Publishing Company, New York-Amsterdam-Oxford), pp. 481-488 (1983).
31. C. W. Miller and L. V. Benson, "Simulation of Solute Transport in a Chemically Reactive Heterogeneous System: Model Development and Application," submitted to *Water Resources Research*.
32. J. F. Kerrisk, "Americium Thermodynamic Data for the EQ3/6 Data Base," Los Alamos National Laboratory report (in preparation).
33. B. M. Crowe and D. T. Vaniman, "Research and Development Related to the Nevada Nuclear Waste Storage Investigations, January 1--March 31, 1984," Los Alamos National Laboratory report LA-10154-PR (1985).
34. D. Ertel and D. Dressler, "Gammaspktrometrische Bestimmung von Neptunium-237 in PUREX-Prozessloesungen," KFK-2725 (1977).
35. R. J. Silva, "The Solubilities of Crystalline Neodymium and Americium Trihydroxides," ONWI Topical report LBL-15055 (1982).

36. D. A. Constanzo, R. E. Biggers, and J. T. Bell, "Plutonium Polymerization-I A Spectrophotometric Study of the Polymerization of Plutonium (IV)," *J. Inorg. Nucl. Chem.* 35, 609-622 (1973).
37. E. A. Bondietti and S. A. Reynolds, Proceedings Actinide-Sediment Reactions Working Meeting, Seattle, Washington, February 10-11, 1976, BNWL-2117, 505-530, L. L. Ames, Ed., Pacific Northwest Laboratory (1976).
38. S. C. Foti and E. C. Freiling, "The Determination of the Oxidation States of Tracer Uranium, Neptunium and Plutonium in Aqueous Media," *Talanta* 11, 385-393 (1964).
39. P. A. Bertrand and G. R. Choppin, "Separation of Actinides in Different Oxidation States by Solvent Extraction," *Radiochimica Acta* 31, 3/4, 135-137 (1982).
40. A. C. Walters and P. R. Carroll, Eds., "Preliminary Stratigraphic and Petrologic Characterization of Core Samples from USW-G1, Yucca Mountain, Nevada," Los Alamos National Laboratory report LA-8840-MS (November 1981).
41. E. A. Bryant and D. T. Vaniman, Comps., "Research and Development Related to the Nevada Nuclear Waste Storage Investigations, July 1--September 30, 1983," Los Alamos National Laboratory report LA-10006-PR (February 1984).
42. K. Wolfsberg, D. T. Vaniman, and A. E. Ogard, Comps., "Research and Development Related to the Nevada Nuclear Waste Storage Investigations, January 1--March 31, 1983," Los Alamos National Laboratory report LA-9793-PR (June 1983).
43. E. N. Treher and N. A. Raybold, "The Elution of Radionuclides Through Columns of Crushed Rock From the Nevada Test Site," Los Alamos National Laboratory report LA-9329-MS (October 1982).
44. W. R. Daniels, K. Wolfsberg, R. S. Rundberg, A. E. Ogard, et al., "Summary Report on the Geochemistry of Yucca Mountain and Environs," Los Alamos National Laboratory report LA-9328-MS, p. 19 (December 1982).
45. W. L. Polzer, E. H. Essington, and D. M. Nelson, "Mobility of Waste Actinides in the Shallow Aquifer of Mortandad Canyon, Los Alamos, New Mexico."
46. J. W. Nyhan, B. J. Drennon, W. V. Abeele, M. L. Wheeler, W. D. Putymum, T. Trujillo, W. J. Herrera, and J. W. Booth, "Distribution of Radionuclides and Water in Bandelier Tuff Beneath a Former Los Alamos Liquid Waste Disposal Site After 33 Years," Los Alamos National Laboratory document LA-UR-83-1199 (1983).
47. J. W. Nyhan, B. J. Drennon, W. V. Abeele, M. L. Wheeler, W. D. Putymum, T. Trujillo, W. J. Herrera, and J. W. Booth, "Distribution of Radionuclides and Water in Bandelier Tuff Beneath a Former Los Alamos Liquid Waste Disposal Site After 33 Years," Los Alamos National Laboratory report LA-10159-LLWM (July 1984).

48. J. R. Britten, B. J. Travis, and L. F. Brown, "The Calculation of Site-Energy Distribution from Adsorption Isotherms and Temperature-Programmed Desorption Data," A.I.C.H.E. Symposium Series #230, 79, 7-17 (1983).
49. J. R. Britten, B. J. Travis, and L. F. Brown, "The Calculation of Site-Energy Distribution from Adsorption Isotherms and Temperature-Programmed Desorption Data," Los Alamos National Laboratory document LA-UR-83-1654.
50. F. Maldonado and S. L. Koether, "Stratigraphy, Structure, and Some Petrographic Features of Tertiary Volcanic Rocks at the USW G-2 Drill Hole, Yucca Mountain, Nye County, Nevada," US Geological Survey open file report 83-732 (1983).
51. P. W. Lipman, R. L. Christiansen, and J. T. O'Connor, "A Compositionally Zoned Ash-Flow Sheet in Southern Nevada," US Geological Survey professional paper 524-F, F-1 - F-47 (1966).

Printed in the United States of America
Available from
National Technical Information Service
US Department of Commerce
5285 Port Royal Road
Springfield, VA 22161

Microfiche (A01)

Page Range	NTIS Price Code						
001-025	A02	151-175	A08	301-325	A14	451-475	A20
026-050	A03	176-200	A09	326-350	A15	476-500	A21
051-075	A04	201-225	A10	351-375	A16	501-525	A22
076-100	A05	226-250	A11	376-400	A17	526-550	A23
101-125	A06	251-275	A12	401-425	A18	551-575	A24
126-150	A07	276-300	A13	426-450	A19	576-600	A25
						601-up*	A99

*Contact NTIS for a price quote.

Los Alamos